Lappeenrannan teknillinen yliopisto
Lappeenranta University of Technology

Christine Sarrette

Effect of Noncondensable Gases on Circulation of Primary Coolant in Nuclear Power Plants in Abnormal Situations

Thesis for the degree of Doctor of Science (Technology) to be presented with due permission for public examination and criticism in the Auditorium of the Student Union House at Lappeenranta University of Technology, Lappeenranta, Finland, on the 14th of February 2003, at 12 o'clock noon.

**Acta Universitatis
Lappeenrantaensis
144**

Supervisor Professor Heikki Kalli
Department of Energy Technology
Lappeenranta University of Technology
Finland

Reviewers Docent, D. Sc. (Tech.) Juhani Hyvärinen
Säteilyturvakeskus - Finnish Radiation and Nuclear Safety Authority (STUK)
Helsinki
Finland

D. Sc. Alain Porracchia
Commissariat à l'Énergie Atomique (CEA)
France

Opponent Professor Michel Giot
Université catholique de Louvain (UCL)
Belgium

ISBN 951-764-717-4
ISSN 1456-4491

Lappeenrannan teknillinen yliopisto
Digipaino 2003

Abstract

Christine Sarrette
Effect of Noncondensable Gases on Circulation of Primary Coolant in Nuclear Power Plants in Abnormal Situations
Lappeenranta 2003
114 p.
Acta Universitatis Lappeenrantaensis 144
Diss. Lappeenranta University of Technology
ISBN 951-764-717-4, ISSN 1456-4491

The present study focuses on two effects of the presence of a noncondensable gas on the thermal-hydraulic behavior of the coolant of the primary circuit of a nuclear reactor in the VVER-440 geometry in abnormal situations.

First, steam condensation with the presence of air was studied in the horizontal tubes of the steam generator (SG) of the PACTEL test facility. The French thermal-hydraulic CATHARE code was used to study the heat transfer between the primary and secondary side in conditions derived from preliminary experiments performed by VTT using PACTEL. In natural circulation and single-phase vapor conditions, the injection of a volume of air, equivalent to the total volume of the primary side of the SG at the entrance of the hot collector, did not stop the heat transfer from the primary to the secondary side. The calculated results indicate that air is located in the second half-length (from the mid-length of the tubes to the cold collector) in all the tubes of the steam generator The hot collector remained full of steam during the transient.

Secondly, the potential release of the nitrogen gas dissolved in the water of the accumulators of the emergency core coolant system of the Loviisa nuclear power plant (NPP) was investigated. The author implemented a model of the dissolution and release of nitrogen gas in the CATHARE code; the model created by the CATHARE developers. In collaboration with VTT, an analytical experiment was performed with some components of PACTEL to determine, in particular, the value of the release time constant of the nitrogen gas in the depressurization conditions representative of the small and intermediate break transients postulated for the Loviisa NPP. Such transients, with simplified operating procedures, were calculated using the modified CATHARE code for various values of the release time constant used in the dissolution and release model. For the small breaks, nitrogen gas is trapped in the collectors of the SGs in rather large proportions. There, the levels oscillate until the actuation of the low-pressure injection pumps (LPIS) that refill the primary circuit. In the case of the intermediate breaks, most of the nitrogen gas is expelled at the break and almost no nitrogen gas is trapped in the SGs. In comparison with the cases calculated without taking into account the release of nitrogen gas, the start of the LPIS is delayed by between 1 and 1.75 h. Applicability of the obtained results to the real safety conditions must take into account the real operating procedures used in the nuclear power plant.

Keywords: thermalhydraulics, nuclear safety, noncondensable gas, gas dissolution-release
UDC 621.039.534 : 621.039.58

Preface

I performed this study between 1994 and 2002 while working as a researcher in the Laboratory of Nuclear Engineering at Lappeenranta University of Technology (LUT).

I would like to express my gratitude to my supervisor, Prof. Heikki Kalli: the inventive and stimulating co-operation he initiated with France was decisive for my work. I am also indebted to our colleagues from the 'REWET team' at LUT for their concrete support in the various phases of this study.

I have not forgotten the collaboration with the CATHARE team at CEA Grenoble either, and particularly with Dominique Bestion without whom this work would not have been possible.

Very special thanks go out to Prof. Rainer Salomaa, head of the Laboratory of Advanced Energy Systems at Helsinki University of Technology (HUT), who offered me the possibility to work near the domicile of my family. I would like to thank the members of the laboratory for the assistance they provided.

I also acknowledge the different reviewers who gave penetrating insights into my work.

Thanks are also due to Minna Tuomainen and Ismo Karppinen, from VTT Processes, who kindly helped me to find the missing bibliographical references.

Financial support for this research was provided by various Finnish organizations: the Guerillot foundation, Etelä-Karjalan Suomen Kulttuurirahasto, LTKK:n Tutkimus Apuraha, LTKK:n Tukisäätiö, Tekniikan Edistämissäätiö, the Jenny and Antti Wihuri foundation and Imatran Voiman Säätiö. The important financial support of the Academy of Finland, which was provided within the framework of the Computational Fluid Dynamics Graduate School coordinated by Prof. Timo Siikonen at HUT, is acknowledged. Part of the work presented in reference (Sarrette 1996) was financed by the Finnish Radiation and Nuclear Safety Authority (STUK).

To Timo, Sophie and Matias who gave me reasons to live so far in the North.

Espoo, October 28, 2002

Contents

Nomenclature

ACRONYMS

APROS	Advanced PROcess Simulation Software (Finnish multifunctional simulator)
ATHLET	Analysis of THermal-hydraulics LEaks and Transients (German thermal-hydraulic computer code)
BETHSY	French Integral Test Facility for PWR Safety Studies
BWR	Boiling Water Reactor
CATHARE	Code Avancé de THermohydraulique pour Accidents de Réacteur à Eau (French nuclear safety analaysis code for PWR)
CEA	Commissariat à l'Énergie Atomique
COSI	French test facility investigating direct condensation at ECCS injections
COTURNE	French test facility investigating film condensation in vertical SG U-tubes of the PWR
CSNI	Committee on the Safety of Nuclear Installations
DC	Downcomer
EC	Emergency Condenser
ECCS	Emergency Core Cooling System
EDF	Électricité de France
FINNUS	Finnish Research Programme on Nuclear Power Plant Safety
HORUS-II	German test facility of HORizontal U-tube Steam generators
HPIS	High Pressure Injection System
HSG	Horizontal Steam Generator
HTC	Heat Transfer Coefficient
HUT	Helsinki University of Technology (English acronym)
IBLOCA	Intermediate Break LOCA
IC	Isolation Condenser
IET	Integral Effects Tests
IPSN	Institut de Protection et de Sûreté Nucléaire
LOCA	Loss-of-Coolant Accident
LPIS	Low Pressure Injection System
LTKK	Lappeenranta University of Technology (Finnish acronym)
LUT	Lappeenranta University of Technology (English acronym)
MIT	Massachusetts Institute of Technology
NC	NonCondensable
NCg-x	Series of tests carried out on PACTEL facility studying NC gas effect
NOKO	German test facility investigating the effectiveness of the emergency condenser
OECD	Organization for Economic Co-operation and Development
PACTEL	Parallel Channel Test Loop
PWR	Pressurized Water Reactor
Revision	name given to the set of the physical laws of the CATHARE code
RCP	Reactor Coolant Pump
RELAP	Reactor Excursion and Leak Analysis Program (US reactor safety code)

RPV	Reactor Pressure Vessel
RUN-x	Series of analytical tests carried out with some components of the PACTEL facility studying the nitrogen gas release from the water
SBLOCA	Small Break LOCA
SBWR	Simplified Boiling Water Reactor
SET	Separate Effects Tests
SG	Steam Generator
SGTR	Steam Generator Tube Rupture
STUK	Säteilyturvakeskus - Finnish Radiation and Nuclear Safety Authority
SWR 1000	Innovative BWR developed by Siemens (now Framatome-ANP)
TOKE	Thermal-hydraulic experiments and code validation project (in FINNUS) (Termohydrauliset kokeet ja Ohjelmistojen KElpoistus in Finnish)
UP	Upper Plenum
VTT	Technical Research Centre of Finland
VVER	Vodo Vodjanyi Energetitseskij Reaktor
volume	two-node volume module used to model large capacities with one or several connections in CATHARE code
1D axial	one-dimensional module used to model pipes with two connections in CATHARE code

PHYSICAL PARAMETERS

a_I	volumetric interfacial area	$[m^{-1}]$
A	flow section	$[m^2]$
A_C	area of separation surface between the two sub-volumes of a *volume*	$[m^2]$
C_D	drag coefficient	
Cp_a	NC gas specific heat capacity at constant pressure (=1056. $J.kg^{-1}.{}^oK^{-1}$)	
d	NC gas bubble diameter	[m]
D_H	mean hydraulic diameter of a *volume*	[m]
DP	differential pressure in a section	[Pa]
DV2	square of velocity difference $\lvert V_v - V_l \rvert \cdot (V_v - V_l)$	$[m^2.s^{-2}]$
f_I	friction coefficient	
g	gravity	$[m/s^2]$
H	enthalpy	$[J.kg^{-1}]$
H_{ao}	reference enthalpy for NC gas in CATHARE code	$[J.kg^{-1}]$
H_{sat7}	steam saturation enthalpy at 0.7 MPa (=2766.43 10^3 $J.kg^{-1}$)	
$K(T_I)$	Henry´s law constant	[Pa]
L	length of a section	[m]
m	mass	[kg]
M_a	NC molar mass	[kg]
M_{air}	air molar mass	[kg]
M_{H2O}	water molar mass	[kg]
N_{aeq}	NC gas mole fraction in solution at equilibrium	
N_b	volumetric number of bubbles	$[m^{-3}]$
P	pressure	[Pa]
P_a	NC gas partial pressure	[Pa]
P_v	steam partial pressure	[Pa]
Q	Mass flow rate	[kg/s]
R	universal gas constant (= 8.32 $J.mole^{-1}.{}^oK^{-1}$)	
Re	Reynolds number	
S_{aI}	interfacial NC gas mass flux per unit of volume	$[kg.m^{-3}.s^{-1}]$
$S_{aI}\,H_a$*	interfacial NC gas enthalpy flux per unit of volume	$[J.m^{-3}.s^{-1}]$
T_k	temperature of phase k	$[^oC]$
T_{sat7}	steam saturation temperature at 0.7 MPa (=164.94°C)	$[^oC]$
V_k	velocity of phase k	$[m.s^{-1}]$
X_{ag}	NC gas mass fraction in gas phase	
X_{al}	NC gas mass fraction dissolved in liquid phase	
X_{aleq}	NC gas mass fraction dissolved in liquid phase at equilibrium	
Z_C	separation level between the two sub-volumes of a *volume*	[m]
Z_{max}	height of a *volume*	[m]
α	void fraction	
$\Delta\rho$	absolute value of density difference	$[kg.m^{-3}]$
$\Delta T_{out\text{-}core,sat}$	saturation margin at core outlet	$[^oC]$
μ_k	viscosity at P and T_k	[Pa.s]
ρ_k	density at P and T_k	$[kg.m^{-3}]$

σ	interfacial tension	$[W.m^{-1}]$
τ	time constant of NC gas transfer between liquid and gas	[s]
τ_{dis}	time constant of NC gas transfer associated to gas dissolution	[s]
τ_{gr}	gas rising time	[s]
τ_{rel}	time constant of NC gas transfer associated to gas release	[s]
τ_I	interfacial friction	$[N.m^{-3}=kg.m^{-2}s^{-2}]$
Φ	heat flux	$[W/m^2]$
Ω	a *volume* of CATHARE is divided into two sub-volumes a lower sub-volume: Ω^-, and a upper sub-volume: Ω^+	

Superscript:

-	related to lower sub-volume Ω^-
+	related to upper sub-volume Ω^+

Subscript:

a	NC
air	air
g	gaseous
I	interfacial
k	phase
l	liquid
mean	mean value in the set of sections 1,2, and 3
NC	noncondensable
prim	primary circuit
sat	at saturation
sec	secondary circuit
v	steam
w	wall
x	related to section x

1 Introduction

The effect of noncondensable (NC) gases on the thermal-hydraulic behavior of the nuclear power plants is a topic of ever increasing interest. The covered spectrum of situations in which an NC gas could interfere with the dynamics of the coolant, goes from mid-loop operations in shutdown conditions at ambient temperature and atmospheric pressure where air is the NC gas, to severe accidents where hydrogen gas is produced by the oxidation of the fuel cladding. One should not forget accidents that involve the loss of the coolant (LOCA), during which nitrogen gas that pressurizes the accumulators could escape into the primary circuit.

Moreover, it has been largely recognized that the designs of new generations of nuclear reactors in the medium or long-term future will include passive safety systems. Analyses of such advanced safety systems were initiated during the last decade, inducing extensive international co-operation. Passive systems are self-actuating and rely only on fluid dynamics phenomena (gravity, natural flow circulation…) to perform all the required safety functions. Their purpose is to increase the operational safety of the nuclear reactor and to simplify plant systems and operation. Nevertheless, in the failure mode, the characteristics of passive systems make them vulnerable to the NC gas effect. This is particularly because condensation phenomena are more significant in the natural circulation mode than in forced circulation and condensation is, as is explained below, very sensitive to the presence of a NC gas.

The aim of the present study is to investigate some of these NC effects in the Soviet-designed VVER-440 pressurized water reactors (PWR) under various conditions.

- The well-known inhibition of the heat transfer in presence of NC gas. The heat transfer coefficients decrease significantly with the increased mass fraction of the NC gas. The steam generator (SG) tubes, where the heat transfer between the primary and secondary circuits takes place, are, in this respect, a sensitive location.

  Impact of the presence of an NC gas on the heat transfer of the SG heat transfer has been extensively studied in vertical steam generators of western-designed reactors, whereas very few studies have been carried out on the horizontal steam generators (HSG) of the VVER-440 PWR. Experiments and existing film condensation models in the thermal-hydraulic codes are reviewed briefly in Chapter 2.

  Horizontal steam generator calculations performed with the thermal-hydraulic code CATHARE are presented in Chapter 3. More specifically, the effect of the injection of air as an NC gas on the heat transfer between the primary and secondary circuits in the HSG, has been studied at low pressures (0.1-0.3 MPa). The geometry used and the boundary conditions were derived from the very first tests (‘feasibility tests’), carried out on NC gas by VTT in the PACTEL facility (VVER-440). Chapter 3 contains a description of the experiment, authored by VTT.

- The release of a NC gas, which is potentially dissolved in water of the primary circuit, according to Henry’s law. As previously mentioned, the NC gas could be air, nitrogen gas

or hydrogen gas. The bubbles of the degassed NC gas may degrade the heat transfer between the primary and secondary circuits and may also interrupt the natural circulation of the coolant in the primary circuit by lowering the level below the junctions between neighboring components. This question was raised by Hyvärinen at STUK (1991) and initiated, in practice, in this study.

As far as the author knows, very few studies have been conducted to investigate this gas release phenomenon in nuclear reactors. Aumiller (1997) studied and implemented a mass equation in the WCOBRA/TRAC code for dissolved hydrogen. Aumiller used a release time constant equivalent to 0.1 s for this model. More recently, Yeung and Sundaram (2002) implemented a nitrogen release model in the RELAP5/MOD3 code, using it to analyze the discharge from a typical PWR accumulator. Yeung and Sundaram used an empirical release coefficient for dissolved nitrogen, several orders of magnitude larger than the corresponding value that was obtained experimentally and is presented in Chapter 4.

Chapter 4 presents a dissolution-release of the NC gas model that was developed by CEA Grenoble and implemented by the author in the CATHARE code. This model includes a release time constant to account for the degassing of NC gas from water. An analytical experiment for the degassing of nitrogen gas was designed and carried out with some components of PACTEL in collaboration with CEA Grenoble and VTT. The chosen pressure conditions were, representative of the depressurization observed during the LOCA transients, in a sub-cooled regime. The reduction of the obtained data provided estimations of the diameter of the nitrogen gas bubbles and the release time constant attached to the degassing. According to the nitrogen gas bubble diameter, a specific interfacial friction coefficient for the nitrogen gas bubbles in the water was developed for CATHARE and used to perform this analytical experiment.

The rigorous implementation of such a dissolution-release model in thermal-hydraulic codes is not easy. In the present state-of-the-art thermal-hydraulic codes, the physical laws (including, in particular, the interfacial friction coefficient) are assessed for steam bubbles only and are not validated for NC gas bubbles whose diameter differs from that of steam bubbles by an order magnitude. At present, it would be extremely difficult to simultaneously take into account the two types of bubbles in the physical laws. The above-mentioned difficulty is the reason why, involving a gaseous mixture of steam and nitrogen gas (the latter originating from accumulators), the LOCA calculations presented in Chapter 5 were performed using the CATHARE code which included the dissolution-release model and standard physical laws (validated for steam bubbles and not for nitrogen gas bubbles). These calculations aim to study if the release of the nitrogen gas, dissolved in the water of accumulators, in the primary circuit would endanger the integrity of the core in the postulated small and intermediate break LOCAs. It is assumed that the accumulators close immediately after all the water they contain has been injected, and so only the nitrogen gas dissolved in accumulator water, and not the nitrogen gas originating from the nitrogen cover above the water level in the accumulators, is taken into account. The study was carried out for the Finnish nuclear power plant of Loviisa (VVER-440) using the nominal and set-point values in use before the modernization and other more recent modifications of the plant.

2 Film Condensation Models in Thermal-Hydraulic Codes and the Related Experimental Assessment

Film condensation occurs on a wall when the wall temperature is lower than the saturation temperature at the partial pressure of steam:

$$T_w < T_{sat}(P_v)$$

Starting from the saturation state, film condensation can be caused either by a decrease in the wall temperature or by an increase in the content of steam in atmosphere.

The presence of a NC gas in a gaseous mixture, such as an NC-steam mixture, is prejudicial to thermal exchanges. When steam is condensed on a wall, the partial pressure of the steam decreases locally. To restore equilibrium, NC molecules replace the condensed steam and introduce a thermal resistance that degrades the heat transfer on the wall (Figure 2.1).

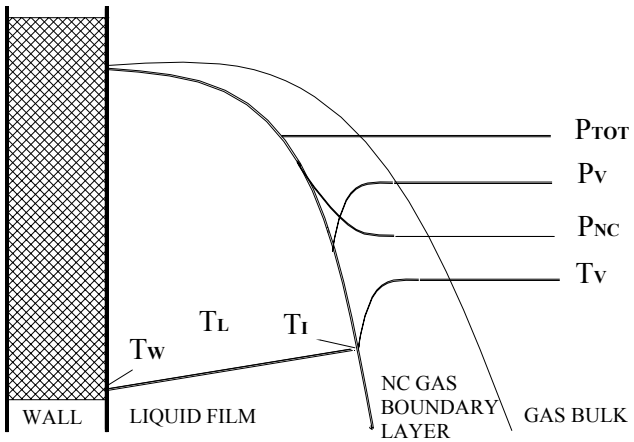

Figure 2.1. The NC gas boundary layer at wall.

The film condensation models, currently included in the commonly used thermal-hydraulic system codes for nuclear safety, will be briefly reviewed below. All these models were developed in the late 80s and early 90s, when the need arose for the more accurate representation of the influence of NC gases on heat transfer phenomena (low pressure transients, advanced design including passive safety systems sensitive to the presence of NC gases). Since it is used in the present study, special emphasis will be placed on the CATHARE code.

2.1 Condensation Models in CATHARE

The French thermal-hydraulic code for nuclear safety analysis, CATHARE, is developed at the CEA Grenoble as a joint effort of IPSN, EDF and FRAMATOME-ANP in order to carry out the best estimate calculations for PWRs (Barré and Bestion 1995) (Micaëlli et al. 1995). CATHARE is based on the two-fluid, six-equation model and includes two mass-balance equations, two momentum-balance equations, two energy-balance equations and transport equations for one or two NC gases (Bestion 1994).

2.1.1 Pure Steam Conditions

In the versions of CATHARE, which include the set of physical laws named Revision 5 (V1.3E Rev 5 or V1.4 Rev 5), and previous versions, the model for film condensation was derived from the Shah correlation (1979). This correlation is used for all void fraction values, but, according to their author, validated only for a steam quality $X < 0.85$.
A comparison of the predictions obtained using these code versions with experimental results shows an underestimation of the heat exchange coefficient.

This was the case, for example, for the separate effects tests (SET) calculated by Sorjonen et al. (1997) for the PO-IC-02 experiment performed on the PIPER-ONE facility. The performance of the isolation condenser (IC), the main passive safety component used in Simplified Boiling Water Reactor (SBWR), was evaluated. The IC consisted of 12 vertical pipes with an outer diameter of 22 mm and length 0.4 m and which were immersed in a tank of volume 1 m^3.

Also, the film condensation in horizontal tubes was found to be underestimated by the CATHARE participants in the OECD/NEA/CSNI International Standard Problem N°33. The ISP33, consisted of a natural circulation stepwise coolant inventory reduction experiment and was carried out on the Integral Effects Tests (IET) PACTEL facility. It aimed at studying natural circulation in a VVER plant in single and two-phase regimes (Purhonen et al. 1994). At low pressure and a high void fraction, CATHARE2 V13.E Revision 5 underpredicted the heat transfer in the horizontal steam generator.

An improved model, based on the Chen correlation (1993), was developed and implemented in CATHARE version V1.5 Revision 6. This model is used at a void fraction higher than the limit value consistent with $X = 0.85$. It includes three terms: one to initiate film condensation as soon as the wall temperature is lower than saturation (necessary for initiating condensation in superheated conditions), one for established film condensation and one term for direct contact condensation in the absence of a wall (Bestion et al. 1994).

Pilon et al. (1998) extended the range of validation of the CATHARE steam film condensation model using the results of the COTURNE experiment. This experiment is designed to investigate the film condensation of steam in vertical PWR SG-U tubes during the reflux condenser mode in pure steam conditions or in the presence of NC gases. Based on COTURNE and bibliographic data for a downward condensing film, Chataing et al. (1999) proposed a new correlation for steam condensation in the case of a wavy laminar regime.

With this new model, the calculated values agreed better with the experimental results in the film condensation regime (Geffraye et al. 2002). Still, the model requires improvement for direct contact condensation in pure steam conditions. The predictability of the COSI separate-effects tests (Janicot 1993), which study direct contact condensation at ECC injection in the cold leg of a Western PWR, was not improved (Serre 1998).

2.1.2 Condensation with a NC Gas

The potential existence of a boundary gas layer near the liquid-gas interface with a higher NC gas mass fraction due to vapor condensation is not taken into account in Revision 5. The NC NC effect is simply taken into account via an interface at saturation temperature which corresponds to the partial pressure of the steam. For an increasing NC gas mass fraction, this model underpredicts the heat transfer degradation caused by the presence of this gas layer.

To overcome these shortcomings, Coste and Bestion developed and introduced, in Revision 6 of CATHARE, a model based on the heat mass transfer analogy using the 'diffusion layer theory' (1995). A semi-empirical method is used to avoid interface temperature calculation (Bestion et al 1994). The heat flux between the liquid and the interface, Φ_{Il}, is expressed as

$$\Phi_{Il} = \frac{H_{Il}}{1 + F_{COR}\dfrac{H_{Il}}{\Phi'}}\left(T_{sat}(P_v) - T_l\right) \qquad (2.1)$$

where

Φ' is obtained by linearization of the condensation heat flux Φ_{cond} using

$$\Phi_{cond} \approx \Phi'\left[T_{sat}(P_v) - T_l\right] \qquad \text{and} \qquad \Phi' = \frac{\partial \Phi}{\partial T_{sat}(P_v)}$$

F_{COR} is an empirical nonlinearity correction function, which takes into account the reduction of condensation due to vapor diffusion through the NC gas near the interface.

H_{Il} stands either for Chen's heat transfer coefficient (HTC) or the stratified HTC.

Coste and Bestion (1995) reported a satisfactoring assessment for film condensation with a NC gas in vertical tubes typical of the isolation condenser in SBWR design. The NC gas was air and helium in the Massachusetts Institute of Technology's (MIT) experiments performed by Siddique et al. (1992), and nitrogen in those performed by Nagasaka et al. 1991. Serre (1998) also reported a strong improvement in the results in the case of direct condensation in horizontal tubes in the presence of nitrogen in the COSI experiment.

2.2 Condensation Models in ATHLET

The German 1-D thermal-hydraulic code ATHLET was developed by the Gesellschaft für Anlagen-und Reaktorsicherheit (GRS) mbH for the analysis of anticipated and abnormal transients in light water reactors (LWR) (Teschendorff et al. 1988).

In the standard version of the ATHLET code, condensation models were developed for vertical tubes. The correlation used can be the Nusselt (laminar films), Chen or Carpenter and Colburn (turbulent films) correlation. The inhibiting effect of the NC gas is not taken into account by any specific correlation. A homogeneous mixture of steam and NC gas is assumed, and the saturation temperature of the steam is a function of its partial pressure.

The extended use of the ATHLET code for the analysis of transients in VVER reactors and innovative nuclear power plants led to development of appropriate condensation models in horizontal tubes.

Schaffrath et al. (2001) originally developed the KONWAR ("Condensation in Horizontal Tubes" in German) model to analyze the experimental results obtained from the Separate Effects Test (SET) facility NOKO-EC. NOKO-EC was designed to investigate, in particular, the effectiveness of the emergency condenser (EC) of SWR 1000. KONWAR determines the flow regime using the flow pattern map of Tandon and calculates the heat transfer coefficient according to this flow regime using a semi-empirical correlation. Schaffrath compared the calculated values with the experimental results obtained from NOKO-EC (Schaffrath et al. 1997).

Fjodorow used a different approach, HOTCON, to analyze SBLOCA in VVER geometry based on Huhn's film condensation theory, his work is presented in (Schaffrath et al. 1997). Both models use an empirical sump coefficient adjusted to the geometrical parameters and flow conditions (co- or counter-current regimes).

A comparative assessment of these two models, which were implemented in the ATHLET code, was carried out in pure steam conditions using the experimental results of the SET HORUS facility. The HORUS-II rig consists of a single U-tube of the SG of a VVER (Alt et al. 1997). NOKO-EC and HORUS-II operate at very different heat flux densities and temperature differences across the tube wall, among other parameters. This assessment shows an improvement of both models compared to the standard version of the film condensation of ATHLET. The next step will be the development of a mechanistic model for the elimination of the empirical coefficients.

To account for the inhibiting effect of NC gases, Fjodorow incorporated the correlation of Schrader (including gas concentration) in the ATHLET code (Lischke and Fjodorow 1996). Alt et al. (1997) used this model to calculate the PCHN.6 test performed with nitrogen gas injection in the HORUS-II facility. The conditions were representative of the late phase of a postulated SBLOCA in the VVER geometry after accumulators start to inject. Alt et al. (1997) reported good agreement between the calculated and measured values.

2.3 Condensation Models in APROS

The Finnish APROS code, Advanced PROcess Simulation Software, is being jointly developed by VTT and Fortum Engineering. This multifunctional environment is used, in particular, to analyze and simulate nuclear power plants. APROS Nuclear applications include five- and six-equation thermal-hydraulic models (Hänninen et al. 1992).

The standard APROS six-equation model uses Shah's model for interfacial heat transfer. A new model was developed using Chen's correlation. NC gases are taken in account using the Vierow and Schrock model (1991).

Karppinen et al. (2000) qualified the new condensation models in pure steam conditions and in the presence of air against the SET PANDA and IET PANTHERS experiments results. The PANDA experiments simulate the behavior of the SBWR Passive Containment Condenser (PCC) in a reduced scale (Dreier et al. 1998). The PANDA PCC heat exchanger includes 20 full length tubes. PANTHERS-PCC is a full-scale prototype of the PCCs of the General Electric SBWR.

Karppinen also used the new model to calculate NOKO Emergency Condenser tests in pure steam in a pressure range of between 1 and 7 MPa (in Hicken and Verfondern 2000, p 91) within the framework of the EU BWR R&D Cluster project. The global heat transfer was correctly predicted, but the local power profiles calculated along the EC tubes were unexpected. In the complementary project, BWR Physics and Thermal-hydraulics Complementary Actions (BWR/CA), Schaffrath and Dumaz (1998) observed similar trends for the NOKO-EC calculations performed using the ATHLET and CATHARE codes. The authors concluded that a deeper analysis would require the more detailed measurement of the local parameters (FISA-99).

2.4 Condensation Models in RELAP

The US thermal-hydraulic code RELAP5/MOD3 code is developed at the Idaho National Engineering Laboratory and sponsored by the US Nuclear Regulatory Commission (RELAP5 1995). This transient analysis code uses a six-equation model.

In the standard version MOD3.3 of the code (RELAP5/MOD3.3 Code Manual), the wall heat transfer coefficient is degraded to account for the effect of NC gas. A diffusion method based on the work of Colburn-Hougen (1934) is used as the default model. An alternative model uses modification factors of the Vierow-Schrock correlation (1991); neither of these two models is fully satisfactory. To extend the capabilities of the RELAP5/MOD3 code to simulate the passive systems included in the next generation of nuclear reactors (General Electric SBWR, Westinghouse AP600), an improvement of the film condensation model in the presence of NC gases is necessary.

For future versions, the developers of the code announced a new condensation model using the diffusion method for both wall and steam-water interfacial heat transfer rates (RELAP5/MOD3.3 Code Manual).

For a previous version of the code RELAP5/MOD3, Hassan and Banerjee (1996) proposed an iterative approach to calculate the interface temperature and the degraded heat transfer coefficient. Based on the heat and mass transfer analogy proposed by Peterson et al. (1993), this model replaced the original reduction factor approach. Using this new model, the results of the simulation of four separate effect experiments in the vertical tube geometry were significantly improved. These were the MIT Pressurizer Experiment (Kang et al. 1984), the MIT Steam Condensation Experiment (Dehbi et al. 1990), the MIT Single Tube Experiment (Siddique 1992) and the University of California, Berkeley (UCB) Steam Condensation Experiment (Vierow and Schrock 1990).

2.5 Conclusion

So far, NC gases accounting in the present system codes has been done in an empirical manner. For advanced design of NPP, including in particular passive safety systems where the effect of the NC gas is predominant, such approach will not be accurate enough.

3 Horizontal Steam Generator Calculations with CATHARE2 V1.5a: NC Gas Effect on SG Heat Transfer

3.1 Introduction

In order to study the behavior of NC gases in the VVER geometry, LUT and VTT Energy carried out a series of preliminary tests on the Finnish Integral Effects Tests (IET) loop PACTEL (Tuunanen et al. 1998). This study is a part of the Thermal-Hydraulic Experiments and Code Validation project (TOKE). The purpose of the TOKE program is to investigate safety-related thermal-hydraulics during VVER accidents and transients and is part of the Finnish Research Program on Nuclear Power Plant Safety (FINNUS) (Vanttola 2000).

The aim of this series of three tests was to study the effect of NC gases on system thermal-hydraulics and heat transfer in a horizontal steam generator (SG). Altogether, three tests (NCg-1, NCg-2 and NCg-3) were carried out. Detailed descriptions of these tests can be found in (Purhonen and Puustinen 2001).

In Western PWR geometry, the effect of NC gases on condensation heat transfer has been studied in SG vertical tubes: Noël et al. have reported tests carried out on the French IET facility BETHSY, test 7.2C with nitrogen (1994) and test 10.2 with helium (May 1997). NC gas is injected in the hot leg, near the SG entrance. This creates a passive zone mainly located in the downflowside of SG tubes, with a high concentration of NC gas where no condensation takes place. In a similar geometry, Schoen and Umminger (1999) studied the influence of nitrogen gas dissolved in the water of the primary circuit on the German PKL III facility. Their results confirm those obtained for BETHSY.

Steam condensation in horizontal tubes with the presence of NC gases has been studied in Separate Effect Tests (SET). In the single-U tube German HORUS-II test facility, Alt et al. (1997) investigated condensation phenomena in pure steam flow or with NC gas, in a range of parameters typical of the behavior of horizontal SG tubes for VVER. Dedicated to the study of the emergency condenser of the SWR 1000, the German NOKO test facility operates at higher pressure (up to 10 MPa) and at a higher maximum heat flux density (up to 1000 kW/m^2) (Schaffrath et al. 2001).

In the VVER geometry, system scale studies with NC gases are rare. In the Hungarian PMK-2 facility, Perneczky et al. (2001) studied the loss of heat residual removal transients with nitrogen gas injection to the upper plenum and SG collectors.

NC gases can be released into the primary circuit after a depressurization transient which triggers the injection of the nitrogen gas, which pressurizes the accumulators, following a LOCA or from hydrogen and/or fission product gases produced in the core in case of a severe accident. NC gases can also originate from the nitrogen gas dissolved in the water of the accumulators of the emergency core cooling system (ECCS). Typically, in all cases, where reactor coolant pumps (RCP) have stopped and heat transfer is ensured via natural circulation, the possibility of the presence of NC gases in the system has to be taken into account.

It is anticipated that NC gases will have the greatest effect during two-phase natural circulation and boiler-condenser modes. NC gases have a strong effect on heat transfer in VVER steam generators, where they eventually accumulate. The presence of NC gases in vapor can significantly degrade the condensation process and reduce the efficiency of heat transfer. NC gases present in hot and cold legs could also cause the stagnation of the natural circulation flow due to the loop seals. This effect would be emphasized by a rise in temperature or a pressure decrease.

The system response to the presence of NC gases depends partly on the nature of the gas. If the gas is heavier than vapor (nitrogen, for example), it may accumulate to the lowest tube rows in the SGs while the vapor continues to flow through the uppermost tubes. If the gas is lighter than vapor (hydrogen, for example) the system behavior can be different. The gas may lie in the top part of the SG tube bundle whereas the vapor flows through the lowest tubes and condenses there. The internal circulation flow pattern of the SG tube bundle is, therefore, also different in these two cases.

A secondary objective of this series of tests was to determine if the instrumentation of PACTEL was adequate for these types of test and if it functioned properly. Hence, this first series of tests, which was performed on a NC gas with PACTEL, must be considered as a preparatory series for future tests.

In this series of tests, only one loop of the primary circuit of PACTEL was used. Different natural circulation modes (for various mass inventories of the primary circuit) at low pressure were studied with compressed air or helium as the NC gas. The injection of gas took place in the vertical part of the hot leg below the HSG.

This chapter presents the analysis of the NCg-1 test, performed in a two-phase regime and with the injection of compressed air to simulate nitrogen gas, performed with the CATHARE code.

The standard version CATHARE2 V1.5a mod2.1 Revision 6, delivered by the CATHARE team, was used here. This version includes the modeling of the mass diffusion effect on condensation in the presence of NC gases (Coste and Bestion 1995). Outlines of this model are presented in Chapter 2 ‘Film Condensation Models in Thermal-Hydraulic Codes and the Related Experimental Assessment’. This model has been satisfactorily assessed (Serre 1998) against the data for vertical tubes with air and helium (Siddique et al. 1992) and with nitrogen (Nagasaka et al. 1991). Noël and Dumont reported an improvement of the prediction of the BETHSY test 10.2 calculated with Revision 6 (December 1997). The present study is an application of the CATHARE code to condensation in horizontal tubes in the presence of an NC gas for IET carried out on PACTEL.

3.2 Test Facility Description

3.2.1 PACTEL Facility

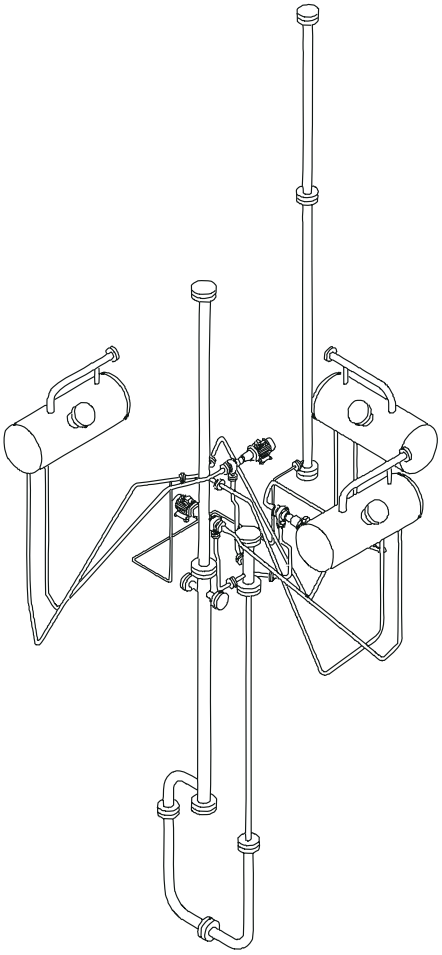

The PACTEL facility is a 1/305 volumetrically scaled, out-of-pile, full-height model of a 6-loop Soviet design VVER-440 PWR (Tuunanen et al. 1998). It has three almost symmetric equal-volume primary loops, each representing two loops in the reference PWR. The inner diameter of both the hot and cold leg is 52.5 mm. Each loop has an HSG consisting of 118 heat exchange U-tubes (di=13.0 mm), a reactor coolant pump and loop seals both in the hot and cold legs. The pressurizer as well as the main emergency core cooling systems, such as the accumulators and high and low pressure injection systems (HPIS, LPIS), have been modeled as well.

The PACTEL core comprises 144 electrical heater rods arranged in three parallel channels in a triangular grid with the same diameter (9.1 mm), a lattice pitch (12.2 mm) and heating length (2.42 m) as the VVER-440 hexagonal bundle fuel rods. The axial power profile is represented by a 9-step chopped cosine with a peaking factor of 1.4. The number and design of the rod spacer grids are identical to those of the reference reactor. The core is powered by a 1 MW (max value) electric power supply. This is about 20% of the scaled thermal power (1500 MW) of the reference reactor.

Figure 3.1. PACTEL facility.

A U-tube construction simulates the downcomer, lower plenum, core, and upper plenum of the reactor vessel. There is no bypass from the upper plenum to the downcomer in PACTEL.

Each SG primary side volume and heat transfer area of the tube bundle are scaled down so that one SG in PACTEL corresponds to two SGs in the reference plant. The average length of the heat exchange tubes is 2.819 m instead of 9.02 m in the plant. The diameter of the tubes (16 x 1.5 mm) is the same as that in the reference plant, but the space between the tube rows is doubled in order to bring the height of PACTEL SG closer to that of the reference SG. To reproduce the inclination of the SGs in the reference reactor, the PACTEL SGs are inclined from the horizontal by 0.4 degrees. A general view of PACTEL is shown in Figure 3.1.

3.2.2 Measurement Instrumentation and Data Acquisition

For this series of tests, rod cladding temperatures and primary and secondary fluid temperatures were measured. In the primary side, the pressure was measured in the upper plenum. The secondary side pressure was measured in the SG steam collector. The liquid levels in the primary circuit and in the secondary sides of the SGs were determined using differential pressure (DP) transducers.

Primary loop flow was measured in the vertical part of the cold leg below the SG. The flow meter was capable of measuring one-phase liquid flow only.

The injected mass flow rate of the NC gas was measured with a rotameter installed between PACTEL and the compressed air network (air as NC gas) or the gas container (helium as NC gas). The pressure and temperature of the injected gas were also measured from the injection line. The gas injection on/off function was performed manually.

Since the range of measurement was near atmospheric pressure conditions, the measurement accuracy was worse than for the usual operating conditions of PACTEL (Purhonen et al. 1994). In particular, a disturbing noise affected certain fluid temperature measurements. However, the values of the errors are shown below:

pressure: ±0.05 MPa in primary side
pressure: ±0.025 MPa in secondary side
temperatures: ±3^{o} C

3.3 Test Configuration and Boundary Conditions

The measured and calculated results of the NCg-1 test will be reported next.

As in all the tests of this series, only one primary loop of the PACTEL facility was in operation in NCg-1 and the flow mode was natural circulation. For the test discussed here, NCg-1, the pressurizer was isolated. Compressed air (max pressure 0.75 MPa, temperature 25-30 ºC) was used to simulate nitrogen gas. The gas was injected into the primary circuit at the entrance of the hot collector, that is, the vertical section of the hot leg, 0.85 m below the horizontal central axis of the SG (see Appendix A). This arrangement ensured that the majority of the gas flowed into the SG. Injection was performed in several steps, and before the next injection, the operators waited for the system parameters to reach a new steady state.

The initial conditions of the test were characterized by equilibrium between the primary and secondary sides. With the control valve completely open, the secondary side of the SG was slightly above atmospheric pressure (P_{sec} = 0.14 MPa). The discrepancy with atmospheric pressure can be explained by the additional pressure drop induced by the steam flow rate. The secondary side of the SG was filled with water a few centimeters above the topmost tube row. A small feed water injection (at 70^{o} C) held the secondary-side water level nearly constant throughout the test. The primary-side pressure settled at a few bars above the secondary pressure.

Because at the beginning of the actual test, the primary-side inventory was only about 50% (200 kg), the system was assumed to be in the boiler-condenser mode (Purhonen et al. 1994). According to the measurement performed between the top of the core, located at 6.05 m[1], and a point situated at 8.89 m[1] in the upper plenum (DP17 measurement), the collapsed level was about 0.2 m above the top of the core. The hot leg and tube bundle were filled mostly with vapor. Due to the sparse information on the DP measurements in the SG and loop seals, it was impossible to definitely verify the actual hot leg flow mode. It could be deduced from the measured cold leg flow that the flow mode was not, however, pure boiler-condenser and that there must have been, at least, droplets in the flow leaving the core.

The core power was about 170 ± 17 kW, which is 3.5% of the nominal power (1500 MW) of the reference reactor. The motor of the RCP was switched off. During the test, the bearing housing of the pump was cooled with a constant external water flow. Hence, there were extensive heat losses from the pump. For this test, the heat losses of the pump were estimated to be 8 ±1 kW. The test was terminated when the maximum cladding temperature exceeded 300 ºC.

The total amount of air in the first injection was 0.043 kg. The injection lasted 35 seconds. The volume of the injected air before mixing with steam was calculated by using the equation of ideal gases:

$$V_{air}=(m_{air}/M_{air})RT/P_{prim} = (43/29)*8.32*(273+110)/0.21.10^6= 0.023\ m^3 \qquad (3.1)$$

This volume is about the half of the volume of the SG tube bundle (0.044 m^3 for the tubes and 0.070 m^3 for the collectors and primary tubes together).

The second injection lasted 180 seconds, and the total amount of air after the second injection was about 0.150 kg.

$$V_{air}=(150/29)*8.32*(273+110)/0.32.10^6= 0.052\ m^3 \qquad (3.2)$$

After the second injection, a gas volume of the same order of magnitude as the total volume of the SG primary side was injected into the facility. Figure 3.2 shows the measured and calculated time histories of the cumulated injected mass of air in the NCg-1 test.

In similar tests performed with the BETHSY facility (Noël et al. 1994, May 1997), after each injection of NC gas, the steam pushes the gas in the downstream part of the SG tubes and in the cold collector. After pressure stabilization, there is an active section, near the entrance of the SG tubes, where pure steam exchanges heat with the secondary circuit and condenses. In the downstream section of the SG tubes, there is a passive zone where there is a mixture of steam and NC gas at the secondary-side saturation temperature (Hein 1982). In this non-active section, where no condensation takes place, it may be assumed that the partial pressure of the steam is $P_{sat}(T_{sec})= P_{sec}$. Then, the partial pressure of the NC gas is $(P_{prim}–P_{sec})$.

The volume of this passive steam-air mixture at T_{sec} is shown below.

[1] Zero level being situated at the bottom of the lower plenum.

After the first injection,

$$V_{passive} = nRT/(P_{prim} - P_{sec}) = (43/29)*8.32*(273+110)/(0.21.10^6 - 0.14.10^6) = 0.07\ m^3 \quad (3.3)$$

After the second injection,

$$V_{passive} = nRT/(P_{prim} - P_{sec}) = (150/29)*8.32*(273+110)/(0.32.10^6 - 0.14.10^6) = 0.092\ m^3 \quad (3.4)$$

The passive volume would then be larger than the SG volume, and air may be present in the vertical part of the cold leg.

In some BETHSY tests, reverse flow was observed in some tubes. In the tubes in which the flow direction was normal, the condensation of steam was incomplete. The steam, which arrived in the cold collector, flowed back in the reverse tubes and pushed some NC gas into the hot collector. Both the hot and cold collector contained a mixture of steam and NC gas, although there was more NC gas in the cold collector. Such behavior could also occur in an HSG, since air, as a NC gas, is heavier than steam, and the pressure at the bottom of the cold collector may be higher than at the bottom of the hot collector.

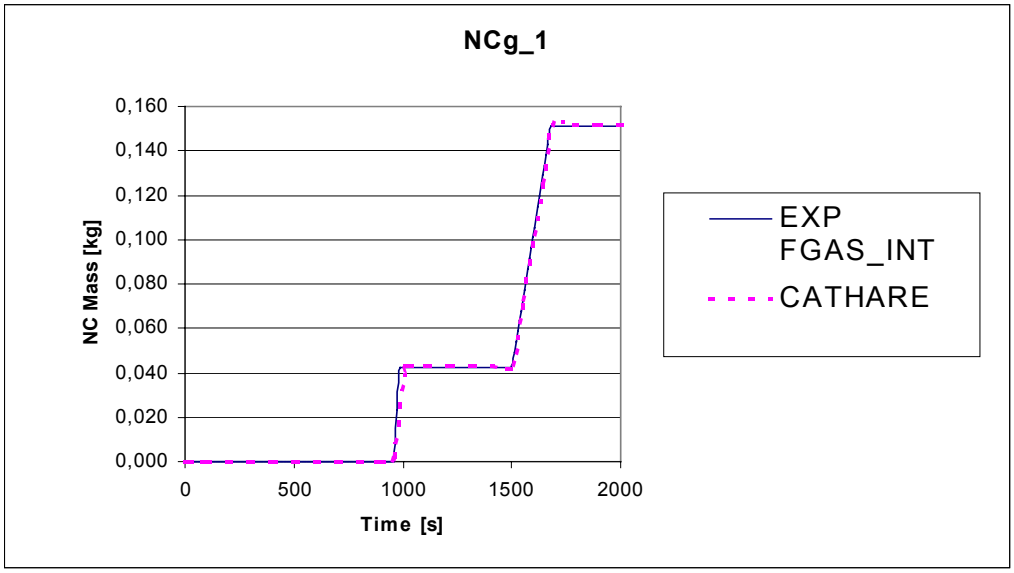

Figure 3.2. The cumulated injected mass of air in the NCg-1 test.

From the previous figures, the air mass fraction at the entrance of the SG can be estimated during each air injection.

Before both air injections, the measured primary fluid flow rate was 0.6 kg/s (Figure 3.11).

An averaged value of air mass flow rate during first air injection can be determined from the total mass of air injected (0.043 kg) and the duration of the first injection (35 s):

$$Q_{air} = 43.10^{-3}/35 = 1.23\ 10^{-3}\ kg/s \quad (3.5)$$

This gives an estimation for the air mass fraction at SG inlet during the first air injection:

$$X_{air} = 1.23\ 10^{-3} / 0.6 \cong 2.\ 10^{-3} \quad (3.5a)$$

For the second air injection, 0.110 kg injected within 180s:

$$Q_{air} = 11.10^{-2}/180 = 0.61\ 10^{-3}\ kg/s \quad (3.6)$$

The air mass fraction at SG inlet during the second air injection:

$$X_{air} = 0.61\ 10^{-3} / 0.6 \cong 1.1\ 10^{-3} \quad (3.6a)$$

3.4 Experimental Results

The NCg-1 test investigated the response of the system in an assumed boiler-condenser mode (a more detailed analysis follows later on in this section) with air as the NC gas. Table 3.1 contains the event log for NCg-1.

Table 3.1: Event log for test NCg-1

Time [s]	Event
-16500	facility heating started, core power 75-200 kW
-10200	inventory reduction started, pumps stopped, pressurizer isolated, loops 2 and 3 closed
0	data recording started, core power ~170 kW
960	first injection of gas started, max ~2 g/s
995	first injection of gas stopped
1500	second injection of gas started, max ~0.6 g/s
1680	second injection of gas stopped, cumulative injected gas mass 150 g
1950	experiment terminated, cladding temperature over 300 ºC

An examination of the pressure measurements shows that the primary pressure slightly increases shortly after both injections of air (Figure 3.10). After each injection, a new steady pressure level is quickly found and equilibrium seems to prevail between heat production in the core and heat transfer to the secondary side and heat losses. Secondary pressure is constant and close to atmospheric pressure, since the pressure control valve was totally open throughout the test. Figure 3.11 confirms that the injection of the gas causes only a short stagnation of the primary flow during the first injection and not even a total interruption of the flow during the second injection. This curve indicates that the regime may not be a pure boiler-condenser mode, but a two-phase mode. The recorded flow rate is 0.6 kg/s which is

about 10 times larger than the steam flow rate generated by the core with the used power level. The latent heat is at 0.17MPa# (2699.10^3-483.10^3)=2216 kJ/kg.

The steam flow rate generated in the core is 170 kW/2216 kJ/kg #0.08 kg/s. This would then mean that the liquid fraction of the flow in the hot leg is about 0.5 kg/s.

Two different factors could affect the flow measurement. First, the recorded value is very close to the lower limit of the measuring range of the flowmeter in the cold leg. Secondly, without void fraction measurements, which is the case, it is impossible to know if the flow coming from the SG outlet is pure liquid or not, i.e. if all the steam condenses in the steam generators or not. If the flow is two-phase, the measured value will not be correct.

The effect of the presence of the NC gas can be seen from the SG inlet and outlet temperatures shown in Figure 3.12. The temperature difference between the SG inlet and outlet spreads from a couple of degrees before the first injection of gas to about 15 degrees after injection and widens further after the second injection. The temperature at the SG outlet follows the secondary saturation temperature, indicating the presence of a mixture of air and steam or possibly condensed liquid. The temperature at the SG outlet is equal to the primary saturation temperature following the primary pressure evolution.

The system reaches a quasi-stable state after a while, when the coolant inventory is redistributed inside the facility, see the test section level (DP19 measured from the bottom of the downcomer to the top of the upper plenum) in Figure 3.3. The water level drops below the top of the core and the rod cladding temperatures start to rise soon after. The DP measurement shows that a part of the water refills the cold leg. This DP measurement in the cold leg, as well as several other DP measurements, were rather unreliable (due to technical problems) in NCg-1, and the redistribution of the coolant in the last minutes of the test cannot be reliably confirmed.

There is also an apparent contradiction concerning the initial level value obtained from the DP19 measurement. At the beginning of the experiment, the test section level obtained from DP19 equals 4.9 m, i.e. 1.15 m lower than the top of the core, see Figure 3.3. Whereas, the DP17 measurement gives a level situated at 6.25 m, i.e. 0.2 m above the top of the core. At the considered primary water inventory, strong boiling activity occurs in the core. In this situation, this could explain the inadequate conversion of the DP19 measurement into collapsed level values.

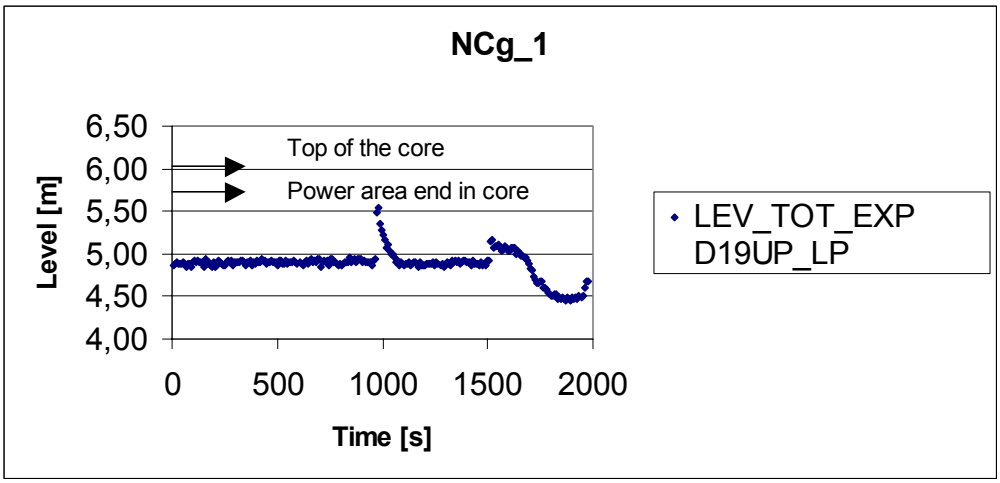

Figure 3.3. The experimental test section level in the NCg-1 test.

3.4.1 Heat Transfer at SG

Figures 3.4 and 3.5 show the primary-side temperatures of the SG tube bundle primary side temperatures at five different vertical elevations. The cross-section of the SG with the elevations of the instrumented tubes is given in Appendix A. Subscript a refers to the first measurement point along the tube at 0.2 m from the hot collector, whilst subscript e refers to the measurement point along the tube at 0.5 m from the cold collector. For more details, see the reference (Tuunanen et al. 1998). The tube temperatures in a passive zone with air would be close to the temperature on the secondary side. The already mentioned Hein's study applies on vertical tubes (Hein 1982). In the case of horizontal tubes, situation is complicated by possible presence of condensed liquid that eventually could be cooled until reach secondary temperature. The conditions of the flow stagnation occurring in one row are determined by collector density difference and friction tube respective evolutions (Hyvärinen 1996).

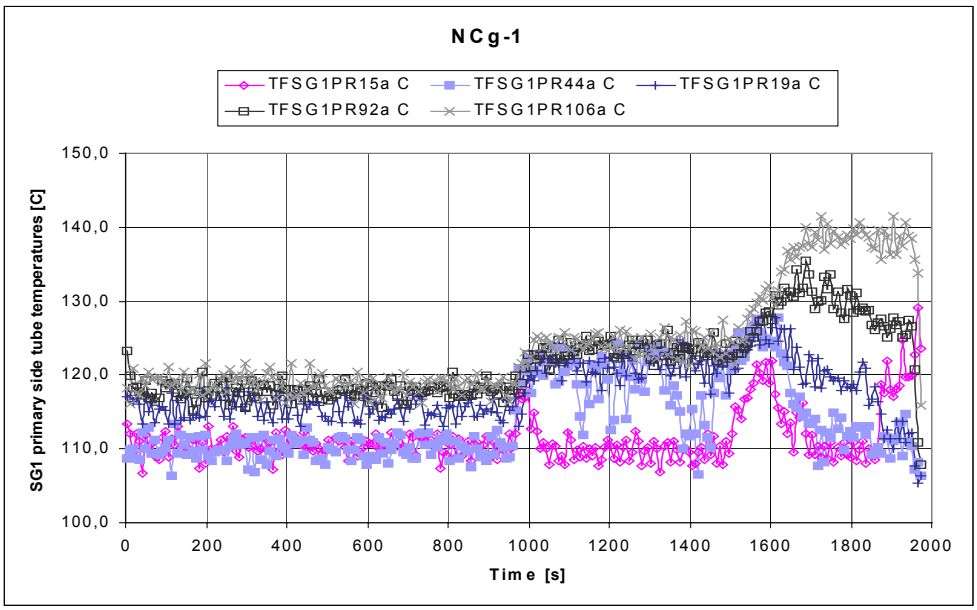

Figure 3.4. Exp. SG primary side temperatures from the beginning of the tubes in NCg-1.

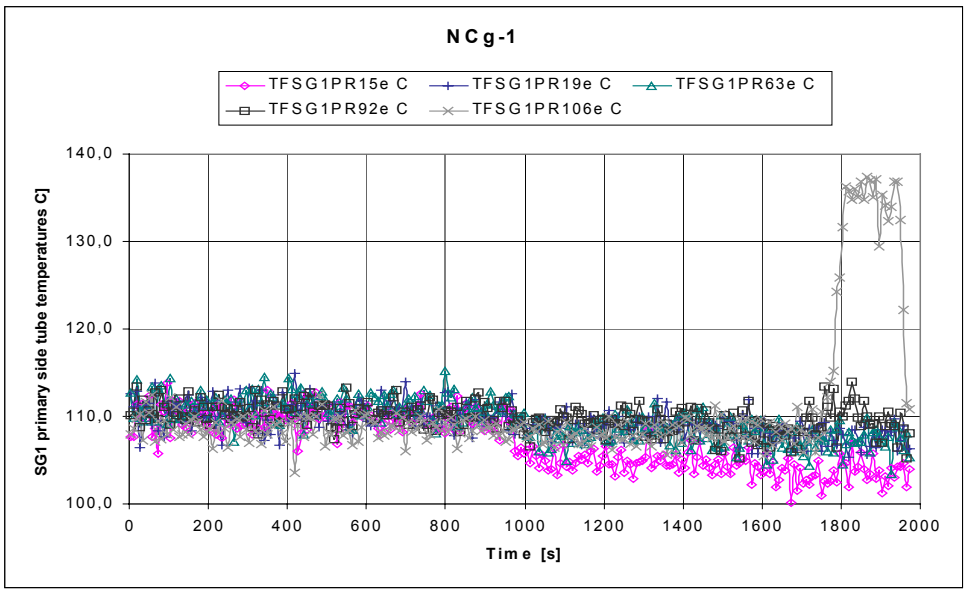

Figure 3.5. Exp. SG primary side temperatures from the end of the tubes in NCg-1.

For all the rows, the effect of the air was more visible in the region situated near the tube entrances, the temperatures at the tube outlets being very near the secondary-side temperatures already before the injections of air. After the first injection of air, only the lowest tube row (from the instrumented ones) was close to the temperature on the secondary side and did not take part in the heat transfer. The second injection effectively mixed the vapor/water mixture with the air in the tube bundle. After the second injection, the lowest and the topmost tube rows diverged from the others. The lowest tubes were again passive, whereas the topmost tubes registered clearly higher temperatures (close to the primary saturation temperature) than did the tubes in the middle region. The redistribution of the coolant inventory just before the end of the test changed the situation somewhat. The lowest tube row was partly cleared from air, whilst the tube in the fifth row from the bottom started to exhibit temperatures close to the secondary-side temperature.

3.5 Computational Results

All the calculated results presented below were obtained with the standard version CATHARE2 1.5a mod2.1 Revision 6 which incorporates the mass diffusion effect of NC gases (see Chapter 2 'Film Condensation Models in Thermal-Hydraulic Codes and the Related Experimental Assessment').

3.5.1 Nodalization

The nodalization scheme used for the calculations is based on the CATHARE standard input data deck used at LUT for the simulations of the PACTEL facility (Vihavainen et al. 1997). The mesh convergence was achieved. In the experimental settings for NCg-1, only one primary loop without the pressurizer was modeled.

The core was modeled with two parallel channels, one fuel element channel and a bypass. There is no bypass in the facility. Here, the bypass simulated the recirculation flow in the core outside and between the three fuel channel shrouds. The upper plenum was modeled using an axial module with a T-branch representing the connection with the hot leg. Hot and cold legs as well as the downcomer were represented using axial modules. The top of the downcomer and the lower plenum were each represented using a volume module.

The heat losses in the pump were represented by a constant heat transfer coefficient (5000 W/m2 ^{o}C) and a constant outside temperature of 20^{o} C. The corresponding calculated heat flux is about 12 kW. This value is larger than the value estimated from measurements (8 ± 1 kW). In addition to the heat losses in the pump, the global heat losses to the environment were modeled using a constant heat transfer coefficient (7 W/m2 ^{o}C) and a constant outside temperature of 25^{o} C. The corresponding calculated heat flux corresponds to the rough value estimated from the measurements (18 kW) by making an energy balance on the primary fluid.

In order to study the heat exchange phenomena between the primary and secondary circuits, particular attention was paid to the modeling of the steam generator. A very similar nodalization was used to analyze the experiment on the loss of feedwater in PACTEL (Korteniemi et al. 1994). On the primary side of the steam generator, the 118 heat exchange tubes were modeled using nine axial parallel modules at nine different elevations. The lowest channel (named SGTUB11) represented 46 tubes, each of the remaining eight channels (resp. named SGTUB12 for the lowest, until SGTUB19 for the highest) represented 9 tubes. Each axial module, which represented a channel, was divided horizontally into three nodes. The inclination by 0.4 degrees of the SGs of PACTEL was not modeled here. Hot and cold collectors were each represented with one volume module. The secondary side was modeled with a U-shaped axial module connected to the volume representing the steam cavity of the steam generator. The riser part represented the tube bundle, and the downcomer part the rest of the secondary pool. Feed water was injected between the second and third lowest channels.

The whole primary circuit was represented by 197 hydraulic nodes and the secondary side by 51 nodes. The 14000-second simulation of the stabilization transient, used for initialization, consumed around 13 hours of CPU time on an SGI Origin 2000 computer. The 2000-second simulation, which corresponded to the experimental transient, consumed 2400 seconds of CPU time.

3.5.2 General Analysis Conditions

Throughout the calculations reported below, the feed water injection was modeled to keep the secondary level constant in the steam generator at the experimental value, and the secondary pressure was maintained constant at 0.14 MPa via a boundary condition.

3.5.2.1 The First Part of the Calculation: Stabilization Transient

Before running the transient calculation corresponding to NCg-1, 14000 seconds of the stabilization transient were run to obtain the values corresponding to the initial experimental

conditions. The ambient conditions (0.1 MPa and 25^{o} C) were imposed on the primary circuit full of liquid water with no heat production in the core, and the reactor coolant pump was stopped. Then, the core power was increased to 170 kW within the first 500 seconds. At the same time, a boundary condition, situated at the bottom of the downcomer, imposed an out-going liquid flow rate (module 'sink') to reduce the primary liquid inventory by steps until it reached 200 kg within 9000 seconds.

For this value of the primary coolant inventory, the stabilization transient predicts a single-phase vapor mode. The primary pressure stabilizes at 0.23 MPa (Figure 3.6). The core inlet and outlet temperatures stabilize at about 10^{o} C higher than do the measured temperatures. One might note that the measured temperatures exhibit strong oscillations due to the measurement noise (Figure 3.7). The calculated core outlet temperature following the saturation curve is 126^{o} C. Not surprisingly, the primary flow rate in the cold leg is noticeably lower than the measured one (Figure 3.8). The code predicts a steam flow rate corresponding to the steam flow generated by the core: the latent heat is at 0.23 MPa# (2713.103-524.103) = 2189 kJ/kg and steam flow rate is 170 kW/2189 kJ/kg #0.08 kg/s.

The calculated collapsed level from the bottom of the downcomer to the top of the upper plenum, as well as the collapsed level in the upper plenum, is rather similar to the experimental values (Figure 3.9). However, the repartition of the water inventory in the test section exhibits a difference in the core. This difference could be attributed to the rather large error margin of the DP measurement in the core, affected there by the occurrence of strong boiling.

The sensitivity calculations performed with the imposed secondary pressure at 0.12 MPa or the increased heat losses to the environment (multiplied by a factor of two) did not change qualitatively these results.

Clearly, the initial conditions in the calculation were quite different from those in the experiment. The experimental results showed that the injection of air, the system is probably in a two-phase mode. At the measured inventory, the calculation predicts a single-phase vapor mode. The uncertainty of the measured pressure and temperatures should be examined in detail before any conclusions be drawn as to the possible code prediction defaults. Nevertheless, it was decided to run the actual transient with CATHARE in order to qualitatively compare the calculated and experimental trends.

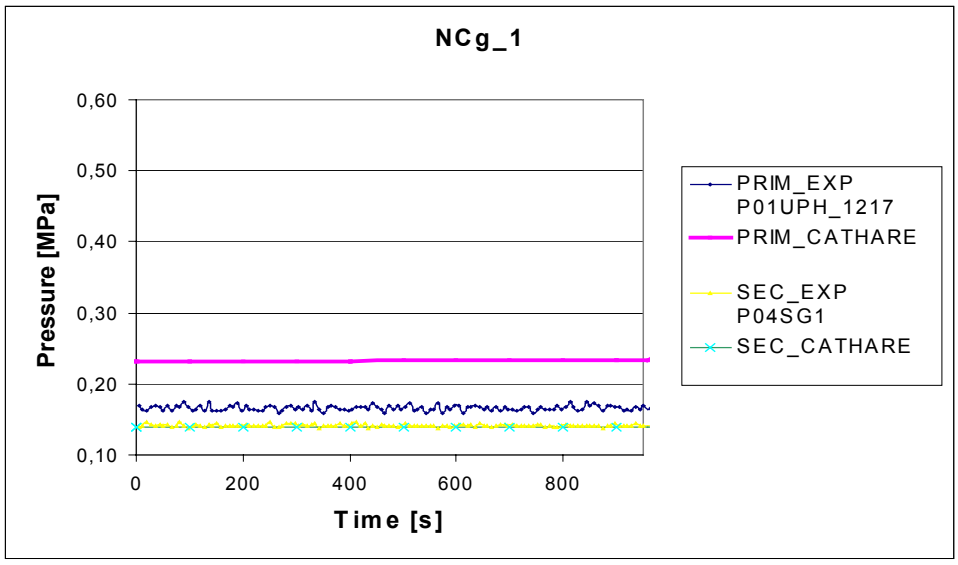

Figure 3.6. Primary side and secondary side pressures before the first air injection.

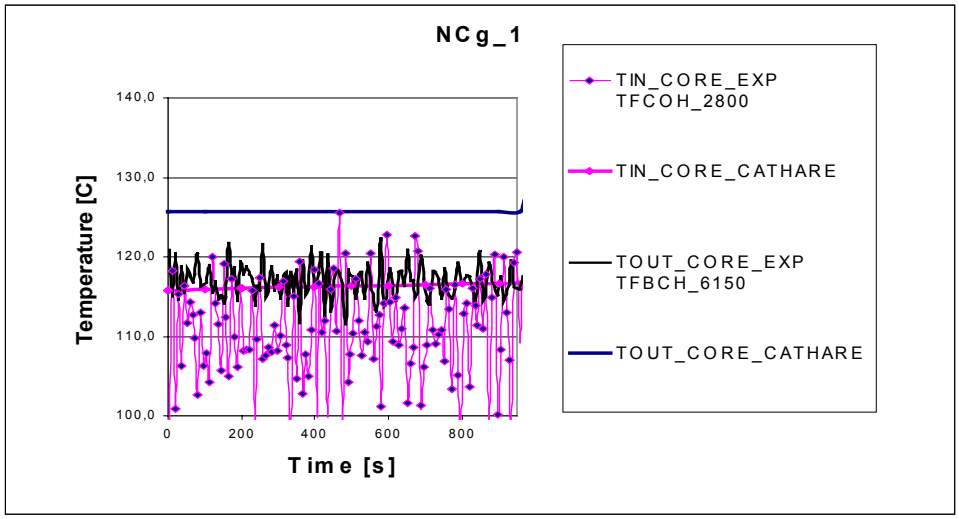

Figure 3.7. Inlet and outlet core temperatures before the first air injection.

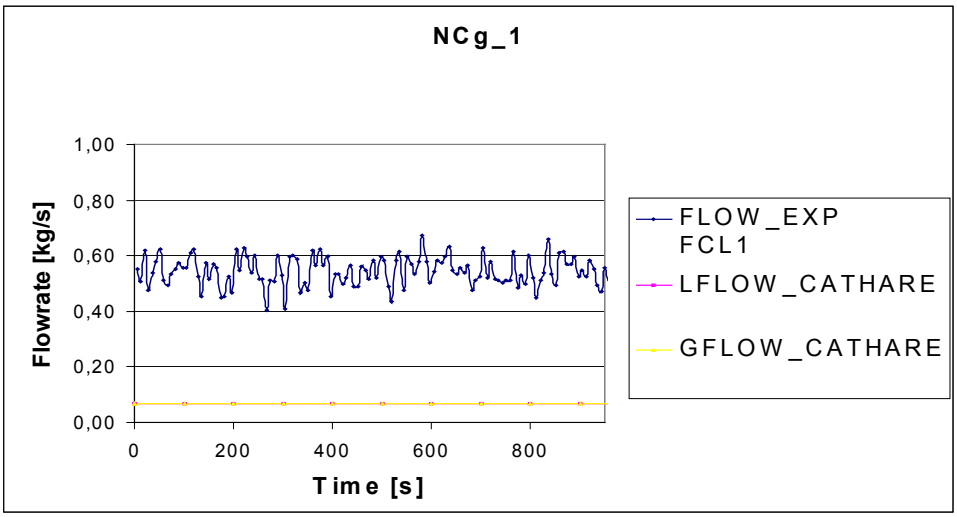

Figure 3.8. Primary side flow rate in test NCg-1 before the first air injection.

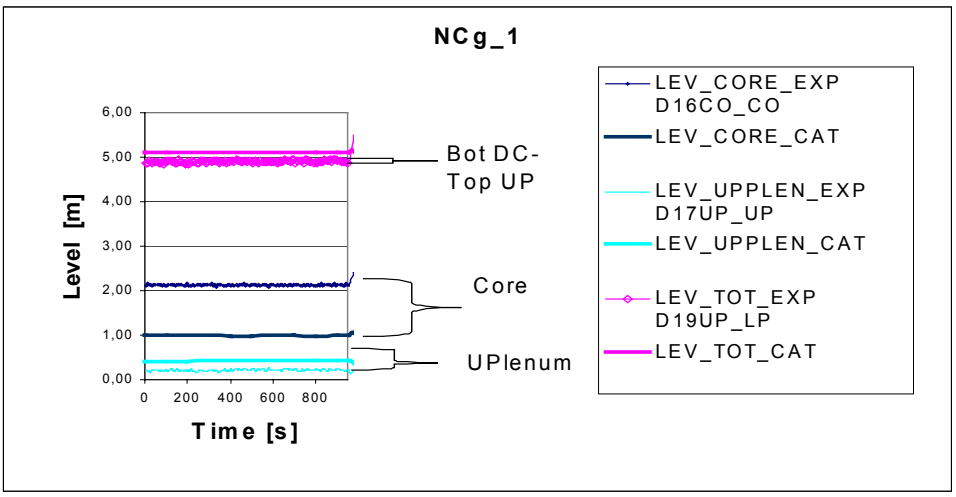

Figure 3.9. Levels in test section in test NCg-1 before the first air injection.

3.5.2.2 Second Part of the Calculation: Transient

Using the results obtained in the first phase as the initial conditions, the actual transient corresponding to the test was performed. Table 3.2 gives the main initial conditions used for this transient calculation.

Table 3.2 The initial values for the transient and a comparison with the measured values for NCg-1

	PACTEL initial value	CATHARE initial value for transient
Primary inventory (liquid) [kg]	200±5	202
Core power [kW]	170±17	170
Primary pressure [MPa]	0.17 ±0.05	0.23
Core inlet temperature [^{o}C]	105-118 ± 3 [2]	116
Core outlet temperature [^{o}C]	114-121 ± 3 [2]	126
Cold leg mass flow rate [kg/s]	0.52	0.07
Secondary pressure [MPa]	0.14 ± 0.025	0.14
Steam line mass flow rate [kg/s]	N/A	0.065

Air injection was modeled via a boundary condition (a 'source' module) imposing experimental gas flow rate at 27^{o} C. This boundary condition is situated at the last mesh (preceding the hot collector) of the axial element modeling the hot leg. The primary pressure was stabilized at 2000 s when the calculated transient was stopped.

3.5.3 Analysis Results

After each injection of air, the difference between the calculated and measured primary pressure increased from 0.1 MPa after the first to 0.2 MPa after the second injection (Figure 3.10). The calculated primary flow rate has the same value as the value obtained at the end of the stabilization transient, except for the brief drops that occurred during the air injections (Figure 3.11). Another significant difference from the experimental situation was observed after the second air injection. While the code predicts the stabilization of the parameters of the circuit, a temperature increase in the core leads to the end of the test.

As a consequence of the overestimated primary pressure, a discrepancy of 10^{o} C between the measured and calculated temperatures at the inlet and outlet of the SG was observed before the first injection of air and during the transient. However, the behavior of the calculated temperature at the inlet and outlet of the SG were qualitatively the same as in the test. The inlet temperature was close to saturation and the outlet temperature fell after each injection to finally reach the saturation temperature of the secondary side (110^{o} C) (Figure 3.12).

[2] Recorded values exhibit large oscillations.

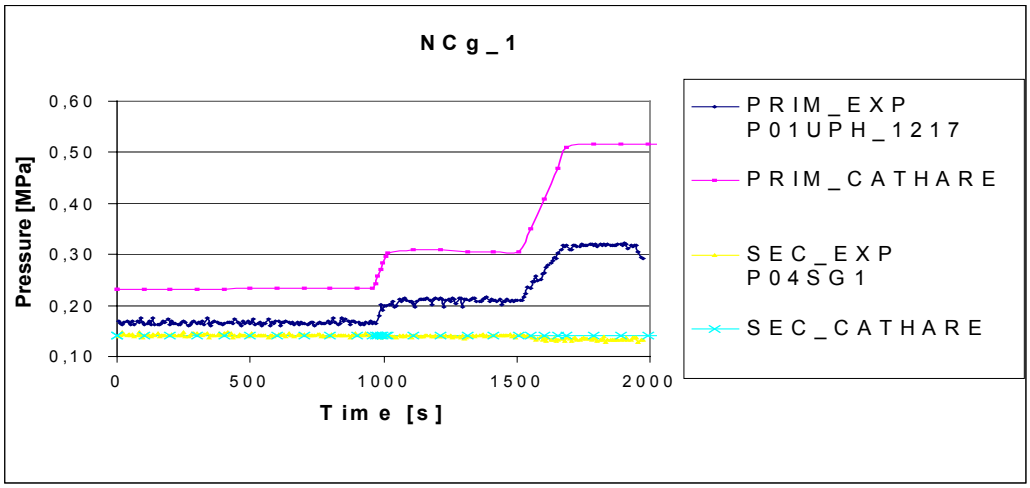

Figure 3.10. The primary- and secondary-side pressures in test NCg-1.

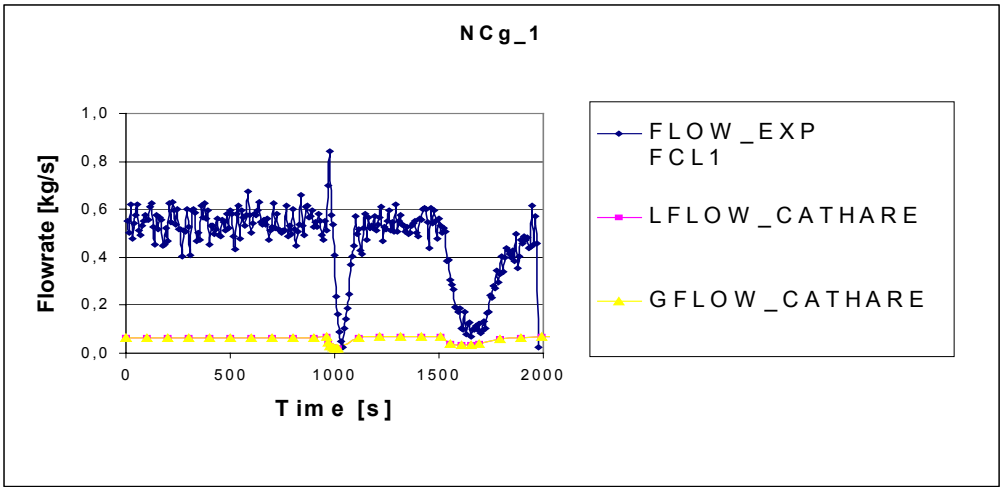

Figure 3.11. The primary-side flow rate in NCg-1.

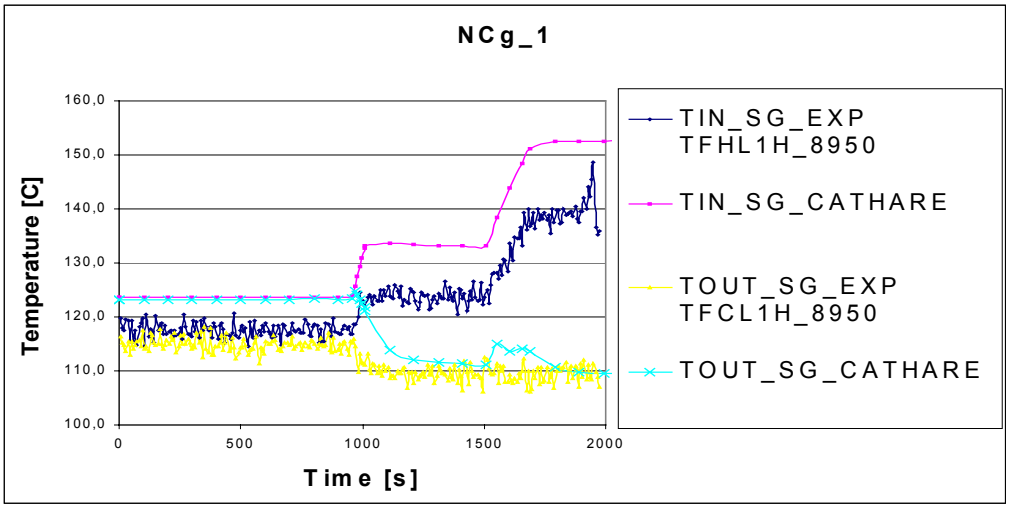

Figure 3.12. The SG inlet and outlet temperatures in NCg-1.

Figure 3.13 shows the calculated heat flux exchanged between the primary and secondary circuits. At every air injection, the temporary reduction of the flow rate in the primary circuit decreases the heat transfer from the primary to the secondary circuit. The obtained values are coherent with the experimental core power level (170 kW).

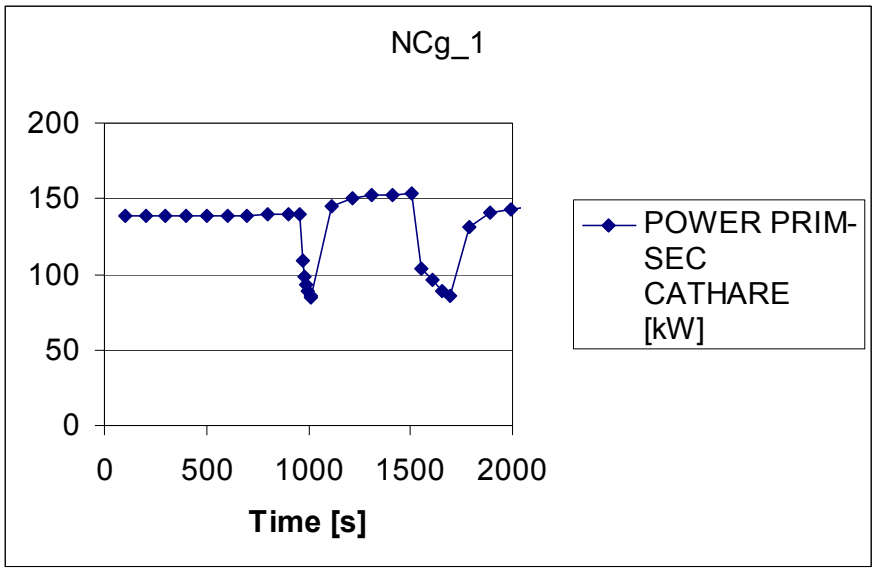

Figure 3.13. The calculated heat flux between the primary and secondary circuits.

3.5.4 Location of the Injected Air

Air was injected in the hot leg below the SG. It flowed over the hot collector, causing a temporary fall in the level of the hot collector situated at the mid-line of the layer SGTUB14. Then, the air accumulated in the neighboring parts of the circuit, which were full of steam before the first injection: the primary tubes of the SG, the cold collector and the vertical part of the cold leg situated below the SG.
After the first injection, half of the amount of the air present in the primary tubes accumulated in the lowest layer (modeling 46 tubes), the other half remaining in the rest of the layers (72 = 8 x 9 tubes) (for SG nodalization, see 'Computational results' of this chapter). After the second injection, more air entered the upper layers and the proportion changed to 2/3. Table 3.3 shows the calculated mass percentages of air in the different parts of the primary circuit.

Table 3.3 The calculated mass percentages of air in the different parts of the primary circuit

Mass percentage on the total amount of air injected	After first air injection (1300 s)	After second air injection (1800 s)
SGTUB11	20%	20%
ΣSGTUB1X X=2,3,..,9	20%	30%
COLDCOL1	40%	30%
COLDLEG1	20%	20%

3.5.5 The Situation in the Steam Generator

Due to the limited number of nodes (3) used in the axial modules modeling the primary tubes, only qualitative conclusions could be drawn concerning the quantities of air in the horizontal direction of the SG tubes. The calculated gas temperatures at the beginning and end of the primary tubes at different elevations are shown in Figures 3.14 and 3.15. The predicted gas temperature at the inlets of the tubes inlet was equal or close to the saturation temperature during the whole transient, which indicates that the tubes are fed with pure or nearly pure steam. Only the lowest tube entrance may contain some air or condensed water after the second injection. After the first injection, the calculated gas temperature at exits of the tubes was close to the secondary temperature in the two bottom-most layers (SGTUB11 and SGTUB12), which indicated a passive zone in these tubes. The tube outlets at the other elevations were more or less active, depending on the amount of air. After the second injection, all the tube outlets were close to the secondary temperature indicating a passive zone at all the tube outlets.

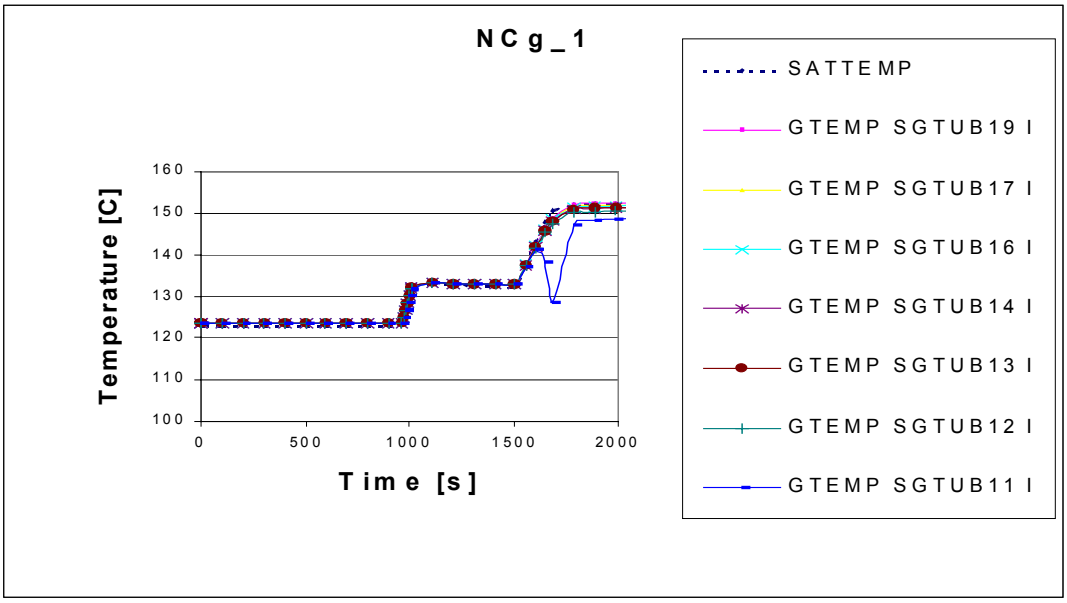

Figure 3.14. The calculated SG primary-side temperatures at the inlets of the tubes in NCg-1.

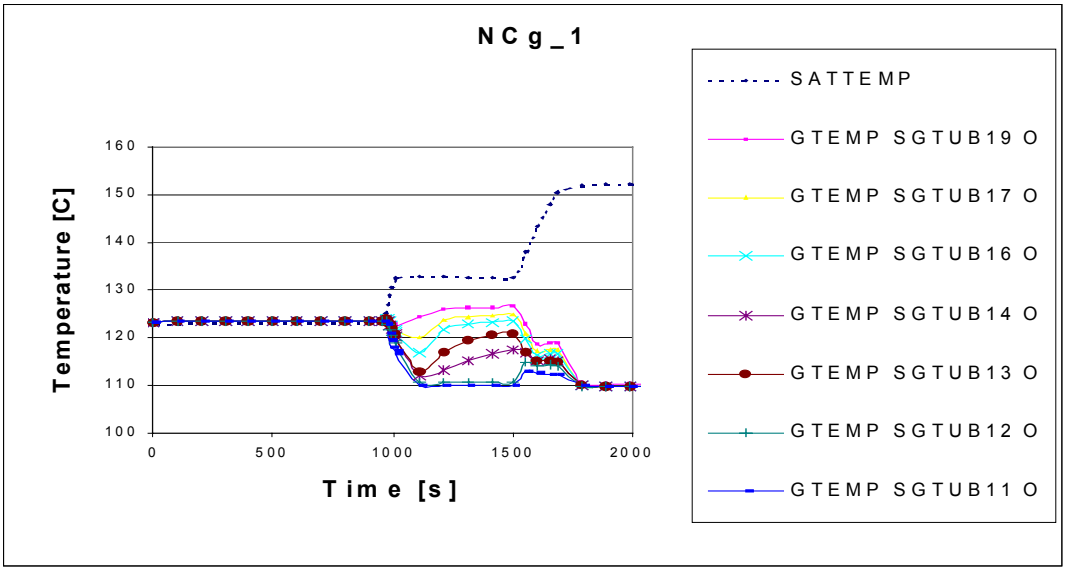

Figure 3.15. The calculated SG primary-side temperatures at the outlets of the tubes in NCg-1.

After stabilization following the first injection, air was present only in the second half-length (from the mid-length of the tubes to the cold collector) of the two bottom-most layers: the gas mass fraction there was between 0.1 and 0.3. After the second injection, air started to accumulate in the second half-length of the tubes in every layer of the SG. In this part of the tubes, the gas mass fraction of the air was 0.8.

Thus, after the first injection, the amount of air present in the primary tubes was not sufficient to create a large passive zone without any heat transfer by steam condensation. The difference between the outlet of the SG and the secondary side temperature was that of a few degrees. After the second injection, a large passive zone developed in the second half-length of every tube. Then, the temperature at the outlet of the SG stabilized at 110^{o} C, which is the secondary side saturation temperature.

Figure 3.16 presents the liquid and gaseous flow rates at the tube inlets profiles versus elevation calculated at three different instants. These profiles suggest a different behavior in the bottom-most layer and in the other layers. First, there is significant liquid flow rate at the entrance of the lowest tube only. Second, and this is confirmed by Figure 3.17, evolution of the fluid flow rates at the entrance of the lowest layer indicate changes for liquid and gaseous flow during both air injections. In the lowest layer, the first air injection stops temporarily the inlet liquid flow rate, and decreases durably the inlet gaseous flow rate. The second air injection produces strong oscillations of the inlet liquid flow which stabilizes in the nominal direction at slightly higher value than previously. This second air injection causes to decrease totally the inlet gaseous flow rate before it resumes at lower value than before the injection. In the eight upper layers (SGTUB12-SGTUB19) inlet fluid flows stay nearly constant in value and direction throughout the transient.

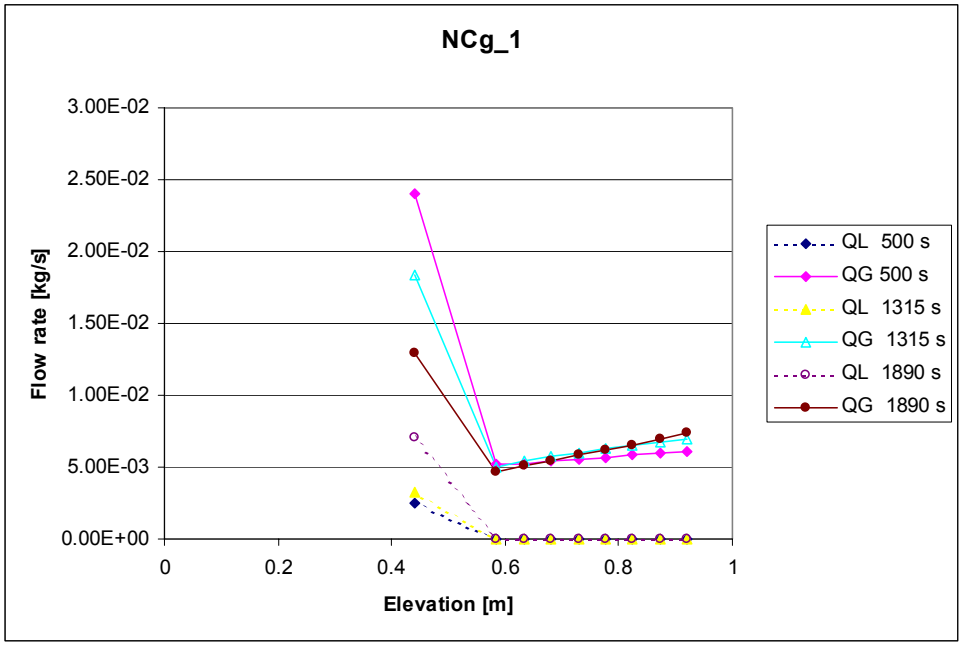

Figure 3.16. The calculated SG flowrates at the inlets of the tubes in NCg-1.

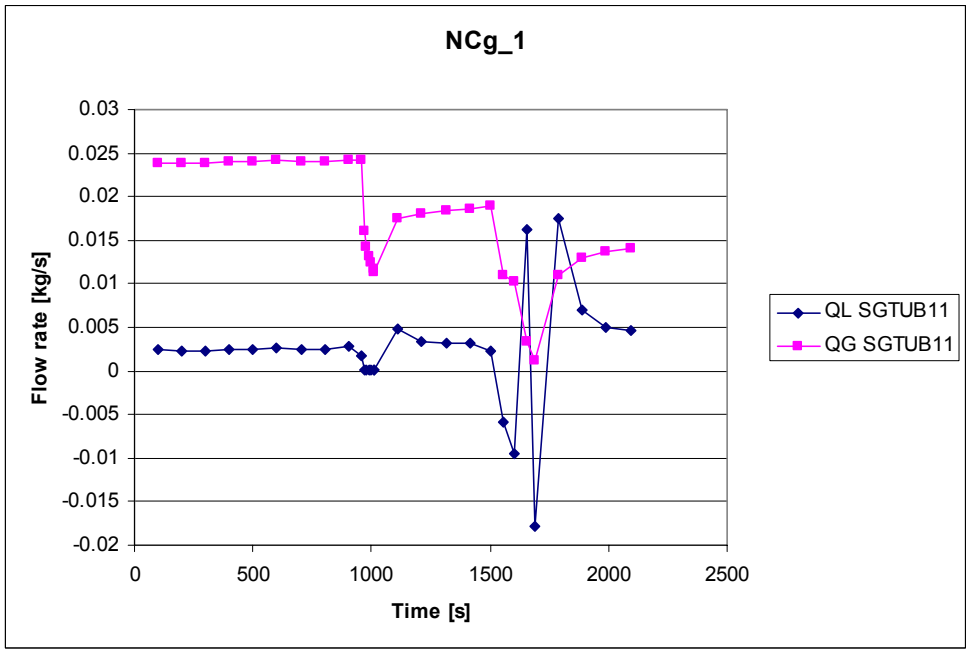

Figure 3.17. The calculated SG flowrates at the inlet of SGTUB11 in NCg-1.

The temperature profiles for the layer named SGTUB14, which modeled the ninth row from the bottom in the facility, are given in Figures 3.18, 3.19, and 3.20.

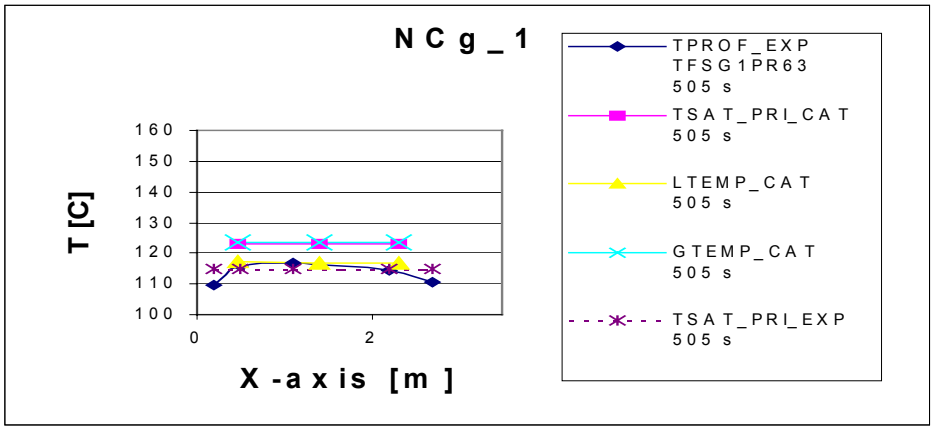

Figure 3.18. The temperature profiles in SGTUB14 before the first injection of air in NCg-1.

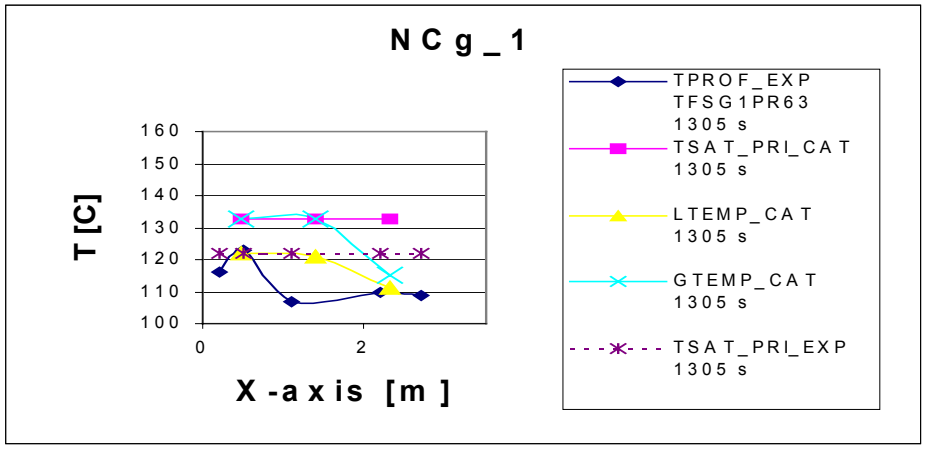

Figure 3.19. The temperature profiles in SGTUB14 after the first injection of air in NCg-1.

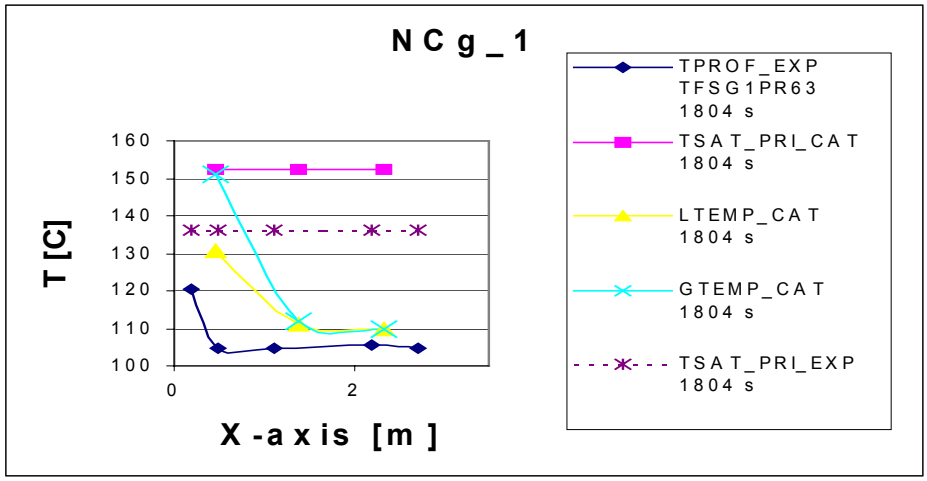

Figure 3.20. The temperature profiles in SGTUB14 after the second injection of air in NCg-1.

Before air injections, the experimental temperature profile indicates cooler fluid at both ends of the tube, suggesting variations of the fluid flow in direction (Figure 3.18). After both air injections, fluid flow seems to increase and stabilize in nominal direction (Figures 3.19 and 3.20). In this layer (SGTUB14), the corresponding computed results indicate a flow circulation towards cold collector that stabilizes in value and direction, before and after each air injection. After both air injections, the calculated temperature profiles are qualitatively in accordance with measurements.

When looking at Figures 3.14 and 3.15, it seems that

- CATHARE predicts pure steam (or nearly pure steam) in the hot collector and at the entrance of all the tubes. There may be some air recirculation in the test, which provides a better general mixing of air with steam and results in a large active zone.
- CATHARE predicts a passive zone in the lowest tubes after the first injection and a passive zone in all the tubes after the second injection.

3.6 Conclusion

The analysis of the effect of air on the heat transfer in the SG was performed using the CATHARE code. The initial and boundary conditions were derived from the preliminary experiment, NCg-1, performed on the PACTEL facility.

The code predicts a primary pressure increase after each injection of air and the formation of passive zones in the SG tubes. These passive zones start to develop from the bottom of the SG tube bundle and from the cold collector side and, after the second air injection, fill the second half-length (from the mid-length of the tubes to the cold collector) in all tubes. The hot collector remained full of steam during the transient.

The calculated results agree with the general trends of the preliminary experiment. Further experiments with more accurate measurements of pressures, coolant repartition, flow rates in the primary circuit would provide more reliable values for conducting a code analysis of the phenomena in the SG in the presence of a NC gas. Sensitivity studies on the SG nodalization must be performed: would a more accurate nodalization, including one layer for each tube row, change significantly the predictions? The possible occurrence of reverse flow in some tubes must be examined. Only then, relevant conclusions on the validity of the CATHARE models could be drawn.

4 Analysis of NC Gas Release Experiment

4.1 Introduction

This study investigates the effects of the release of nitrogen from the accumulators of the emergency core cooling system (ECCS) in the primary circuit of a pressurized water reactor (PWR). Some nitrogen is dissolved in the water of the accumulators of a PWR due to the protracted contact of the water of the accumulator with the nitrogen cover. In the case of a hypothetical loss of coolant accident (LOCA) in the primary circuit of a PWR, the pressure in the primary circuit decreases and after the accumulators discharge, the dissolved nitrogen may degas from the liquid into the primary circuit in the form of small bubbles. This situation may affect the circulation within the primary circuit, significantly decrease the heat transfer to the secondary circuit and, hence, prevent the proper cooling of the core.

Dissolved gases in liquids could be released during transients, when the local pressure falls below the saturation pressure of the dissolved gas. The mass diffusion of the dissolved gas from the liquid bulk to the interfaces, which is a rather slow process, controls the rate mass transfer. This mass transfer is proportional to the interfacial area and to the difference between the NC gas concentration and its equilibrium value and inversely proportional to a time constant. Degassing produces many small bubbles like vaporization in a flashing process, the interfacial area then rapidly increases and this accelerates the mass transfer. On the contrary, when the NC gas concentration is below its equilibrium value, dissolution occurs on the existing interfaces. Due to this asymmetric behavior, two different time constants are associated with the dissolution and release. A rather large time constant is expected for dissolution, whereas a smaller one is expected for degassing. Similarly to flashing conditions, NC bubble inception is believed to occur according two mechanisms: homogeneous nucleation via molecular processes within the bulk of the fluid, or heterogeneous nucleation due to interactions with walls.

The CATHARE code for nuclear safety was used to investigate these situations. A model of the transport of NC gases in both the liquid and gas phases has been implemented in the CATHARE code (see the section ‘The Dissolution-release model in CATHARE 2 V1.3L’ in the present chapter). The physical properties have been implemented for the N_2 gas. This model requires a knowledge of the relaxation time constants associated with the dissolution and release of nitrogen gas.

In order to evaluate the time constant associated with the release of nitrogen gas under rapid depressurization conditions, an experimental program was performed using some components of the PACTEL facility, see description in Chapter 3 ‘Horizontal Steam Generator Calculations with CATHARE2 V1.5a: NC Gas Effect on SG Heat Transfer’.

A series of analytical tests (series RUN-1,2,3) was performed in a vertical cylindrical geometry (referred to hereinafter as a *pipe* geometry). The test section was partially filled with subcooled water saturated with dissolved nitrogen. The upper part of the cylinder was filled with nitrogen. The test section was depressurized using a top break and some nitrogen was degassed from the water (see the section ‘Analytical Experiments (RUN-1,2,3)’).

The reduction of the data from the RUN-1 test gave a rough evaluation of the rise velocity of the nitrogen gas bubbles and of the time constant associated with the release of nitrogen gas. This rise velocity of gas bubbles was compared to existing bubble drag models, and the diameter of the gas bubbles was also evaluated. Then, an interfacial friction model, consistent with this flow configuration, was proposed (see the section 'Determination of the Parameters of the Dissolution-Release Model').

The gas-release time constant and proposed interfacial friction correlation were implemented in the CATHARE code. The RUN-1 test was calculated using this modified version of CATHARE to validate the obtained results, (see the section 'RUN-1 Calculations with CATHARE2 V1.3L').

Then, the code was used to investigate the effects of nitrogen degassing in some PWR LOCA transients. The applicability of the modified interfacial friction to LOCA calculations at full reactor scale is first discussed. Finally, the CATHARE code with the dissolution-release model and standard laws for interfacial friction was used to simulate the LOCA transients in the VVER-440 geometry taking into account the release of nitrogen gas dissolved in the water of the accumulators. The corresponding results were reported to complete this study (see Chapter 5 'LOCA Calculations with CATHARE2 V1.3L').

4.2 The Dissolution-Release Model in CATHARE 2 V1.3L

As already mentioned in Chapter 2, CATHARE is based on the two-fluid, six-equation model and includes two mass-balance equations, two momentum-balance equations, two energy-balance equations and transport equations for one or two NC gases (Bestion 1994). In the present study, the term "gas" used alone refers to a gas mixture (steam + NC gas).

A model for the transport of a NC gas in both the liquid and gas phases was implemented in the CATHARE code in the framework of collaboration between LUT and CEA-Grenoble. In the standard version of the code, the NC gas is assumed to be present only in the gas phase. Therefore, an additive transport equation for the NC gas dissolved in the liquid was developed by CEA-Grenoble and implemented by the author in the CATHARE version CATHARE2 V1.3L. The physical properties were implemented for the N_2 gas. This model requires a knowledge of the relaxation time constants associated with the dissolution and release of nitrogen gas.

The following modules are available in CATHARE: a one-dimensional module (*1-D axial* module) for pipes with two connections, a two-node volume module (*volume* module) for large capacities with one or several connections, and a T module to connect a branch pipe to a main pipe. The new modeling for a NC gas was implemented in *the 1-D axial* module and in the *volume* module.

4.2.1 Modeling Principle

This model includes one additional transport equation for the NC gas in the liquid, and modifications were made to the equations for the NC gas transport in the gas mixture and for the gas mixture energy. Similar modifications were made to the *1-D axial* and *volume* modules. A mass transfer term was added to the transport equations for modeling dissolution and release. This mass transfer term is a function of the NC gas mass fraction dissolved in the liquid at equilibrium, calculated according to Henry's law. An energy transfer term was added for the gas phase. This energy transfer term depends on the enthalpy of the donor phase. Only the changes to the standard version of the code for the *1-D axial* module will be discussed in detail hereinafter. The modifications made to the *volume* module can be found in (Sarrette 1996).

The transport equations for the NC gas in the gas phase are written as follows.

- NC gas transport equation in the gas phase:

$$\frac{A\partial\alpha\rho_g X_{ag}}{\partial t} + \frac{A\partial(\alpha\rho_g X_{ag} V_g)}{\partial z} = +AS_{aI} \qquad [\text{kg.m}^{-1}.\text{s}^{-1}] \qquad (4.1)$$

- NC gas transport equation in the liquid phase:

$$\frac{A\partial(1-\alpha)\rho_l X_{al}}{\partial t} + \frac{A\partial(1-\alpha)\rho_l X_{al} V_l}{\partial z} = -AS_{aI} \qquad [\text{kg.m}^{-1}.\text{s}^{-1}] \qquad (4.2)$$

SaI, the interfacial NC gas mass flux per unit of volume, is expressed as

$$S_{aI} = \frac{(1-\alpha)\rho_l (X_{al} - X_{aleq})}{\tau}, \qquad [\text{kg.m}^{-3}.\text{s}^{-1}] \qquad (4.3)$$

where X_{al} is the NC gas mass fraction dissolved in the liquid phase at time t, X_{aleq} is the NC gas mass fraction dissolved in the liquid phase at equilibrium, and τ [s] is the time constant of the NC gas transfer between the liquid and gas.

X_{aleq}, is function of the NC gas mole fraction in the solution at equilibrium N_{aeq}:

$$X_{aleq} = \frac{N_{aeq} M_a}{N_{aeq} M_a + (1 - N_{aeq}) M_{H_2O}} \qquad (4.4)$$

According to Henry's law, N_{aeq}. is proportional to the partial pressure of the gas.

$$N_{aeq} = \frac{P_a}{K(T_l)} \qquad (4.5)$$

A polynomial form for the constant of Henry's law, $K(T_l)$, obtained by interpolation of the experimental results of Pray et al. (1952), is used for the nitrogen gas (Figure 4.1) as follows:

$$K(T_l) = 0.57541.10^{10} + 0.13803.10^{9}\,T_l + 0.94804.10^{5}\,T_l^{2} - 0.13955.10^{5}\,T_l^{3} + 0.68700.10^{2}\,T_l^{4} - 0.95821.10^{-1}\,T_l^{5} \qquad (4.5a)$$

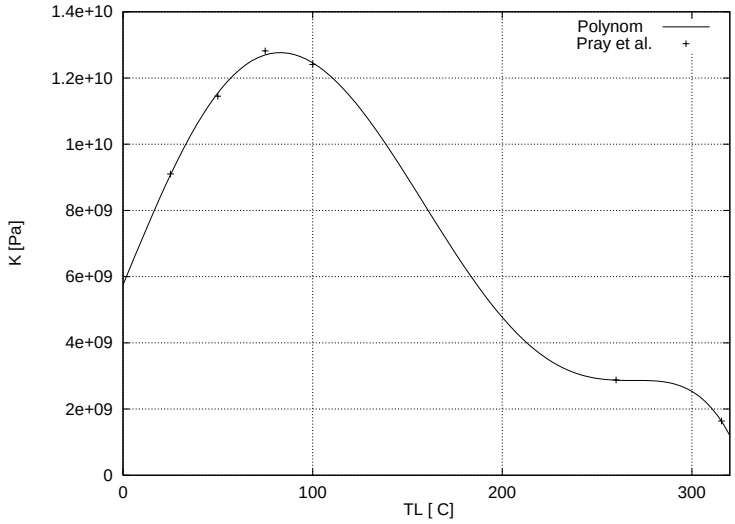

Figure 4.1. The constant of Henry's law for nitrogen gas as a function of pressure.

It should be pointed out that Pray does not provide any data between 100° C and 260° C (see Figure 4.1). For temperatures ranging in the region [177° C - 260° C], the values of $K(T_l)$ resulting from the interpolation are appreciably lower than those reported by Cohen (1980). The relative difference could reach 35%.

In the series of tests RUN-1, 2, 3, the liquid temperature was about 32° C and so the results were not affected. With respect to the LOCA calculations reported in Chapter 5 'LOCA Calculations with CATHARE2 V1.3L', the effect of the eventual underestimation of $K(T_l)$, for temperatures ranging between 177° C and 260° C will be discussed later.

Finally, N_{aeq} is expressed as follows:

$$N_{aeq} = \frac{X_{ag}\rho_g R(273+T_g)}{M_a K(T_l)} \qquad (4.5b)$$

- The gas phase energy equation:

The energy transfer term $S_{aI} H_a^*$ due to mass transfer is added in the total enthalpy of the gas balance equations. The complete documentation of the other terms on the right-hand side of the gas energy equation is presented in (Bestion 1994).

$$\frac{A\partial\alpha\rho_g(h_g + V_g^2/2)}{\partial t} + \frac{A\partial\alpha\rho_g V_g(h_g + V_g^2/2)}{\partial z} - A\alpha\frac{\partial P}{\partial t} = AQ_{IG} + \chi Q_{WG} + A\alpha\rho_g V_g + AS_{aI}H_a^* \qquad (4.6)$$

In the case of NC gas release $\quad H_a^* = Cp_a T_l + H_{a0}$ (4.6a)

In the case of NC gas dissolution $\quad H_a^* = Cp_a T_g + H_{a0}$ (4.6b)

4.2.2 Time Discretization and Resolution

The time discretization of all the mass momentum and energy equations of the standard code is fully implicit. Here, the additional equation is explicitly coupled. As will be seen later, this causes convergence difficulties and results in very large CPU time consumption.

4.2.3 Choice of the Time Constant of NC Gas Transfer between the Liquid and Gas

According to Henry's law (Pray et al. 1952), the solubility of NC gases in liquids depends mainly on the pressure and temperature (Eq. 4.5). In the case of nitrogen, the solubility of the gas increases with the pressure and liquid temperature, if this temperature is above 84^{o} C. Variations in pressure will induce either the prompt release of the dissolved NC gas from the water-NC gas mixture or the rather slow dissolution of the NC gas from the steam-NC gas mixture.

Two different time constants may be associated with the release and dissolution of the gas:

- τ_{rel} the time constant of the transfer of the NC gas from the liquid to gas in the case of the release of the NC gas in the gaseous phase
- τ_{dis} the time constant of the transfer of the NC gas from the gas to liquid in the case of the dissolution of the NC in the liquid phase

The exact knowledge of the time constant associated with dissolution is not that important because it is not likely that the pressure will increase in the studied transients (LOCA). This time constant is to be estimated rather large: it is arbitrarily set to 100 seconds. The time constant associated with the release is of particular interest. The release phenomenon comprises two steps: firstly, when the threshold pressure is reached, NC gas micro-bubbles are produced, and these bubbles may grow and coalesce. The associated time is referred to as τ_{rel}. Secondly, the stratification of the bubbles occurs in the upper volumes. The gas rising time τ_{gr} measures this stratification capability. It is rather easy to experimentally observe the overall time constant which is the sum of τ_{rel} and τ_{gr} but not as easy to determine τ_{rel} and τ_{gr} separately. In the analysis of the RUN-1 experiment described hereinafter, some assumptions will be necessary in order to obtain rough evaluations of τ_{gr}. Then, τ_{rel} will be estimated.

4.3 Analytical Experiments (RUN-1,2,3)

4.3.1 Test Facility Description

A series of three tests (RUN-1, RUN-2, RUN-3) were carried out using two components of the PACTEL facility (VTT and LUT) (Purhonen et al. 1995). They aimed at studying the phenomena associated with nitrogen gas release from water during depressurization, in particular, to provide an estimation of the time constants τ_{rel} and τ_{gr}. The test parameters (initial pressure, rate of depressurization) were chosen to be those typical of a PWR SBLOCA.

The pressurizer of the PACTEL test facility was used as the test section and an accumulator was used as the release tank. These components have the adequate geometry and design parameters (range of operating pressure). The test section was an 8.8-m long vertical pipe and the inner diameter was 139.7 mm. Figure 4.2 shows the test section.

A complete description of the test facility and tests results can be found in (Sarrette and Kouhia 1998). From here onwards, only the RUN-1 test will be discussed.

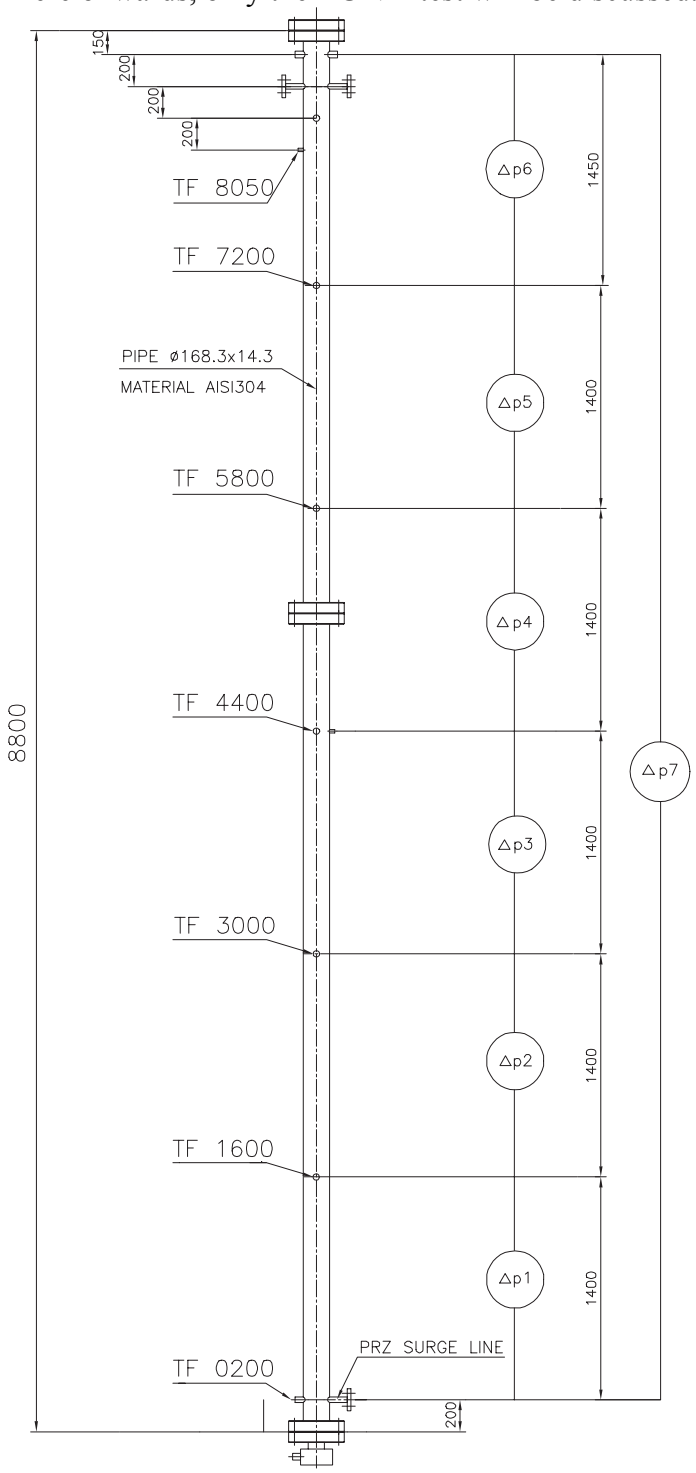

Figure 4.2. The test section geometry and instrumentation.

4.3.2 Measurement Instrumentation

K-type thermocouples were used for temperature measurements (accuracy ±3° C), in the test section and in the release tank. Figure 4.2 shows the thermocouple locations in the test section.

A chain of differential pressure transducers measured the collapsed level profile in the test section. There were altogether seven differential pressure measurements. Five measurements were spaced 1.40 m each, and the topmost transducer had elevation difference of 1.45 m (accuracy ±0.1 kPa). An additional transducer indicated differential pressure over the whole test section (DP7). Differential pressure transducers were numbered from the bottom to the top: from 1 to 6. Corresponding sections are also numbered from 1 to 6. Pressure was measured at the top of the test section and in the release tank (accuracy ± 0.03 MPa).

It has not been possible to measure how much nitrogen gas was dissolved in water. Nevertheless, considering how the test section was filled, it was reasonable to assume that water was saturated or nearly saturated with dissolved nitrogen at the beginning of test RUN-1. The mass balance of nitrogen made for test RUN-1 gave a sound basis for this assumption (Sarrette and Kouhia 1998).

4.3.3 Test Procedure

In this series of experiments, the test section was connected to the release tank with a release valve at the top of the test section. First, the test section was filled with water. Then, the operators injected nitrogen gas through a nozzle at the bottom of the test section. This procedure speeded up the dissolution of the nitrogen in water: the better the nitrogen is mixed with the water, the better the saturation of the dissolved nitrogen in the water. Simultaneously to the nitrogen injection, water was drained from the test section. The initial water level in the test section was set at two thirds of its height, at 2 cm below the TF5800 thermocouple in section 4 (Figure 4.2).

For all the tests, the initial temperature of the water in the test section was set to 33º C, and the initial temperature of the gas volume to 27º C.

The release valve at the top of the test section was used to depressurize the vessel. An orifice plate was located before the release valve (in the direction of the flow). The diameter of the orifice (2 mm) was chosen so that the flow rate through it was, at most times, critical under the considered pressure conditions. The nitrogen gas dissolved in the water forms bubbles in the liquid when the release valve is open. These nitrogen bubbles rise towards the free surface and reach the upper gas volume. The formation of the bubbles in the water swells the level of the water. The water level falls when the bubbles have reached the surface (Figure 4.3).

For RUN-1, the initial pressure in the test section was set to the nominal pressure existing in the accumulators that inject in the upper plenum of the Loviisa Nuclear Power Plant, that is

5.5 MPa [3]. A steady state was measured for 700 seconds. The transient started at 700 s when the operators opened the release valve. They closed the valve when the pressure in the test section reached 2.0 MPa (at 787 s). The test section was allowed to stabilize before the operators reopened the release valve at 1300 s. The pressure in the test section decreased gradually and stabilized at around 0.48 MPa when it was equal to the release tank pressure. The release tank was initially at ambient conditions for pressure and temperature (0.1 MPa and 21º C, respectively). The recording of data was stopped at 1800 s. The events in RUN-1 are summarized in Table 4.1.

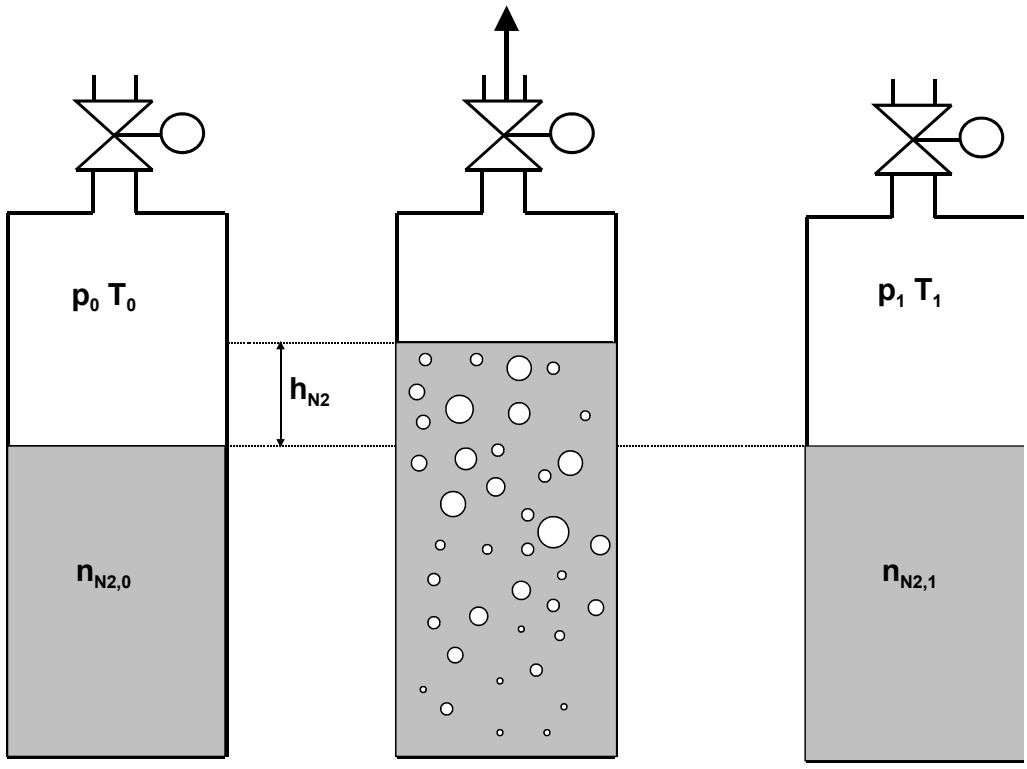

Figure 4.3. Level behavior during the tests.

Table 4.1: The events in RUN-1.

Initial test section pressure p_{pres}	First opening of release valve	Closure time of release valve	Second opening of release valve	End of data Recording
5.5 MPa	700 s	787 s $p_{test\ section}$=2.0 MPa	1300 s	1800 s $p_{test\ section}=p_{release\ tank}$ = 0.48 MPa

[3] The hypotheses used here for the plant protection system, are those that were in use before the modernization and other more recent modifications of the plant.

4.3.4 Test Results

Figure 4.4 shows the pressure history in RUN-1. Immediately after the closure of the release valve, the pressure in the test section rose by about 0.12 MPa. The pressure during the steady state decreased slowly, which is due to a small leakage at the top of the test section at an elevation of 8450 mm.

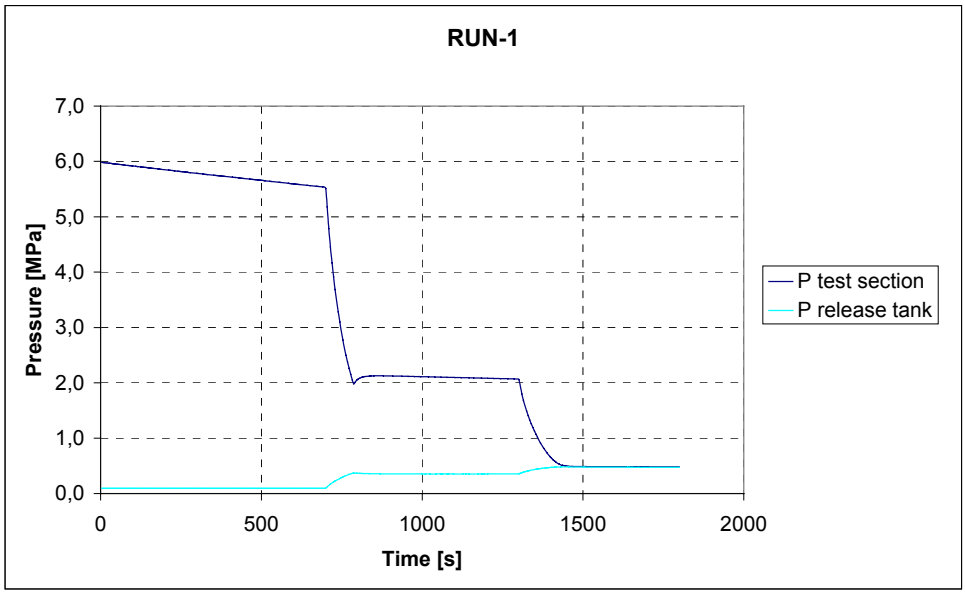

Figure 4.4. The pressure in the test section and release tank as a function of time in RUN-1.

The liquid temperature was almost constant in the test section in all the tests (about 32º C). According to Henry's law, the amount of dissolved nitrogen gas in the water was only a function of the pressure in the test section. The gas temperature fell dramatically when the release valve was opened. The temperature increased back to near the original value after the operators closed the release valve. Figure 4.5 shows the gas temperature evolution versus time at two different elevations in the test section in RUN-1. The increase in the gas temperature is due to the release of heat from the walls and is responsible for the rise in pressure.

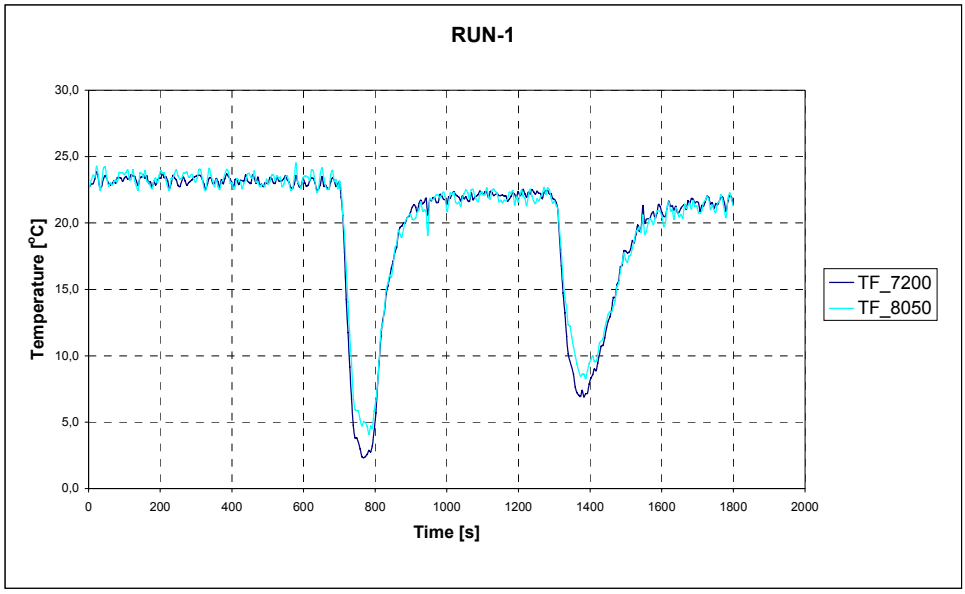

Figure 4.5. The temperature history of the gas volume in RUN-1.

The differential pressure measurements clearly showed a displacement of the free surface of the liquid during the blowdown periods. The values were used to calculate the averaged void fractions in the different parts of the test section. Given the void fraction range, $3.10^{-3} < \alpha < 2.10^{-2}$, the relative uncertainty is about 40%.

Figure 4.6 shows the behavior of the void fractions versus time in four axial positions in RUN-1. Bubbling starts in all the sections after the initiation of depressurization. Before the second depressurization, bubbling has stopped in sections 1 and 2 (the non-zero value of the stabilized void fraction is certainly due to the non-zero bias in the measurements), while bubbles are still present in sections 3 and 4. At the second opening of the valve, there is a degassing delay in the lowest sections, 1 and 2, and not in sections 3 and 4. In sections 1 and 2, bubbling stops when the pressure stabilizes. In the upper sections, 3 and 4, the refilling of pure water occurs later, with the lowest section refilling faster than the highest one.

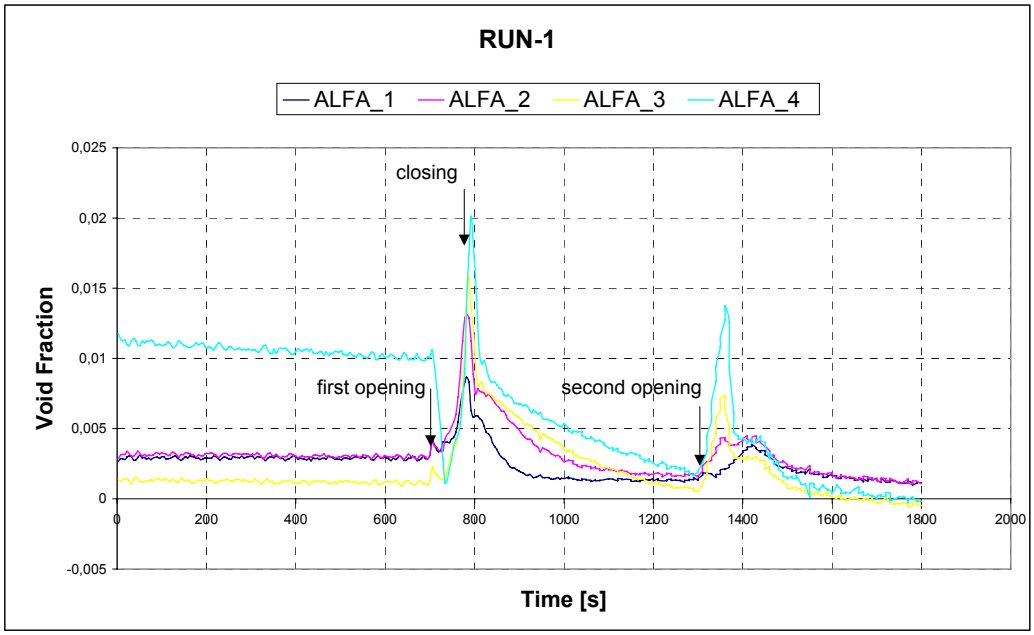

Figure 4.6. Experimental void fractions as a function of time in sections 1 to 4 in RUN-1.

4.4 Determination of the Parameters of the Dissolution-Release Model

The rise velocity V_g, and release time constant τ_{rel} of the gas bubbles during the first depressurization were determined using the data reduction of RUN-1.

The first depressurization of RUN-1 consisted of three phases:

- Phase 1: the first depressurization itself (release-valve open)
  $700s \prec t \prec 787s$

- Phase 2: the short re-pressurization (after the closure of the valve before the new thermal equilibrium was reached)
  $787s \prec t \prec 821s$

- Phase 3: the stabilization phase after the short re-pressurization
  $821s \prec t \prec 1300s$

The rising velocity of the gas bubbles can be obtained from the nitrogen mass balance equation during the stabilization phase (Phase 3), assuming zero interfacial mass transfer. Then, assuming that the rise velocity of the bubbles is constant and uniform, Eq. 4.1 and 4.2 and the measured values of the pressure and temperature are used to determine the following parameters during Phase 1 (depressurization):

- the interfacial mass flux of nitrogen gas per unit of volume released from water (S_{aI})
- the nitrogen gas mass fraction dissolved in the liquid (X_{al})
- the nitrogen gas mass fraction dissolved in the liquid at equilibrium (X_{aleq})

Then, the release time constant, τ_{rel}, is obtained from Eq. 4.3.

4.4.1 The Rise Velocity of N_2 Gas Bubbles

The NC transport equations in the gas and liquid are used in sections 1, 2 and 3 of equal volume.

- the NC transport equation in the gas (from Eq. 4.1 and assuming that $X_{ag} = 1$):

$$\frac{\partial \alpha \rho_g}{\partial t} + \frac{\partial (\alpha \rho_g V_g)}{\partial z} = S_{aI} \qquad [\text{kg.m}^{-1}.\text{s}^{-1}] \qquad (4.1a)$$

- the dissolved NC transport equation in liquid (from Eq. 4.2):

$$\frac{\partial (1-\alpha)\rho_l X_{al}}{\partial t} + \frac{\partial (1-\alpha)\rho_l X_{al} V_l}{\partial z} = -S_{aI} \qquad [\text{kg.m}^{-1}.\text{s}^{-1}] \qquad (4.2a)$$

$$S_{aI} \neq 0 \qquad 700s \prec t \prec 821s$$
$$S_{aI} = 0 \qquad 821s \prec t \prec 1300s$$

Then, the time constant associated to a non-zero S_{aI} :is obtained from Eq. 4.3.

$$\tau = \frac{(1-\alpha)\rho_l (X_{al} - X_{aleq})}{S_{aI}} \qquad [\text{s}] \qquad (4.7)$$

In order to determine the time constant, every term of Eq. 4.7 will be evaluated using the measured values during RUN-1. They correspond to the values of S_{aI} global to the set of sections 1, 2, and 3 and the mean values of $X_{al,mean}$ and $X_{aleq,mean}$ in the set of sections 1, 2, and 3.

For each section x, densities $\rho_{g_x}(t)$, $\rho_{l_x}(t)$, and void fraction $\alpha_x(t)$ are calculated using the measured values. The gas velocity from section x to section x+1 is obtained for phase 3 from

$$V_{g_{x\to x+1}} = -\frac{L}{(\alpha\rho_g)_{x\to x+1}} \sum_{i=1}^{x} \frac{\partial (\alpha\rho_g)_i}{\partial t} = -\frac{2L}{(\alpha\rho_g)_x + (\alpha\rho_g)_{x+1}} \sum_{i=1}^{x} \frac{\partial (\alpha\rho_g)_i}{\partial t} \qquad (4.8)$$

where $L=L_1= L_2=L_3= 1.4$ m and $(\alpha\rho_g)_x(t)$ are determined for section 1 to 4.

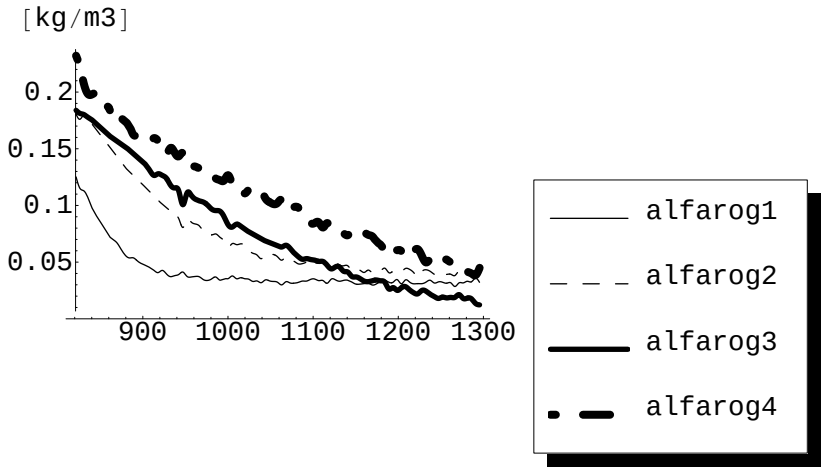

Figure 4.7. (αρg) versus time in sections 1 to 4 during Phase 3.

From Figure 4.7, it can be seen that at 1300s $(\alpha\rho_g)_3(t)$ and $(\alpha\rho_g)_4(t)$ have still not yet reached a zero (or constant) value, and so bubbles are still rising in sections 3 and 4 when the release-valve is opened a second time.

It seems there is a non-zero bias for $(\alpha\rho_g)_1(t)$ and $(\alpha\rho_g)_2(t)$ shifting the curves upward by 0.05 kg/m^3. It is assumed that there are no more bubbles at 950 s in section 1, and at 1150 s in section 2. From these values, an approximate value for the rising velocity of the bubbles could be calculated:

$$V_{g_1} = 1.4/(950-820) \approx 0.01 m.s^{-1} \qquad (4.9a)$$

$$V_{g_2} = 2.8/(1150-820) \approx 0.009 m.s^{-1} \qquad (4.9b)$$

Figure 4.8 shows values of $V_{g_{x\to x+1}}(t)$ obtained from Eq. 4.8.

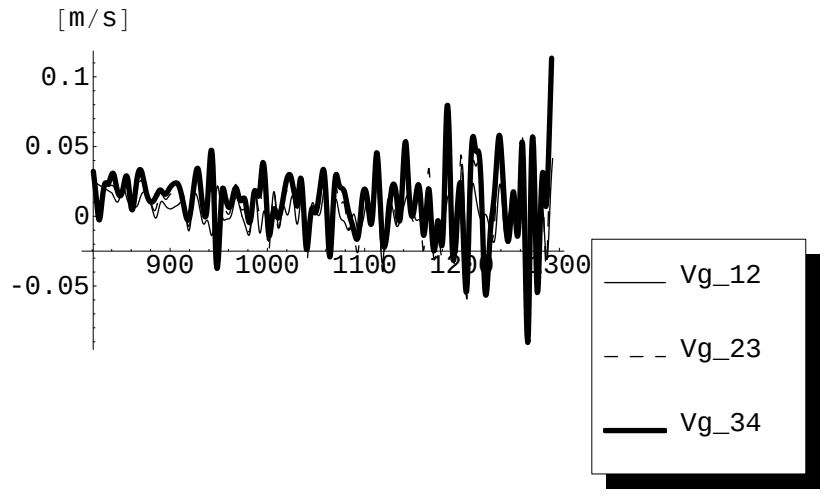

Figure 4.8. The gas velocities Vg ,x->x+1 versus time in sections 1 to 3 during Phase 3

Due to a noisy signal, only a constant and uniform gas velocity can be estimated from the averaged value in the three sections:

$$V_{g_{x\to x+1}}(t) = C^{te} = V_g \approx \frac{1}{3}\sum_{x=1}^{3} V_{g_{x\to x+1}} \approx 10^{-2}\, m.s^{-1} \qquad (4.9c)$$

4.4.2 Degassing Delay

Figure 4.9 shows $(\alpha\rho_g)_x(t)$ calculated for each section during first depressurization (Phase 1):

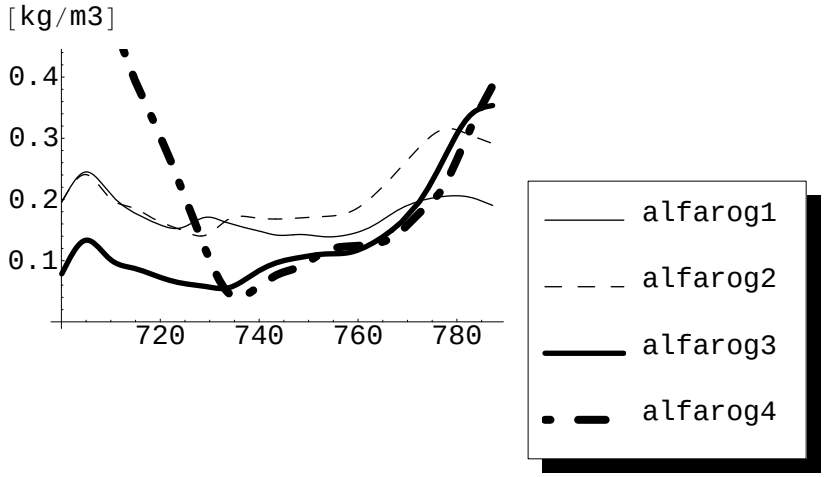

Figure 4.9. (αρg) versus time in sections 1 to 4 during Phase 1.

From 700 s until 760 s the obtained curves exhibit a 'strange' behavior, which is attributed to a measurement noise. Actual degassing is assumed to start at 760 s. This 'degassing delay' of 60 s could be compared to a flashing delay. This degassing delay disappears when there already are bubbles in the section, as was observed during the second depressurization in sections 3 and 4 (after 1300 s) (Figure 4.6). A proposal to model this degassing delay is made at the end of this chapter. It uses a criterion based on the relative values of the dissolved gas mass fraction X_{al} with the equilibrium value $X_{al,aleq}$.

4.4.3 N_2 Interfacial Mass Flux per Unit of Volume

The gas mass transfer in sections 1 to 3 during the first depressurization (Phase 1) is calculated as follows (Figure 4.10):

$$S_{aI} = S_{aI_1}(t) + S_{aI_2}(t) + S_{aI_3}(t) = \sum_{x=1}^{3} \frac{\partial(\alpha\rho_g)_x}{\partial t} + \frac{V_g(\alpha\rho_g)_3}{L_1 + L_2 + L_3} \qquad (4.10)$$

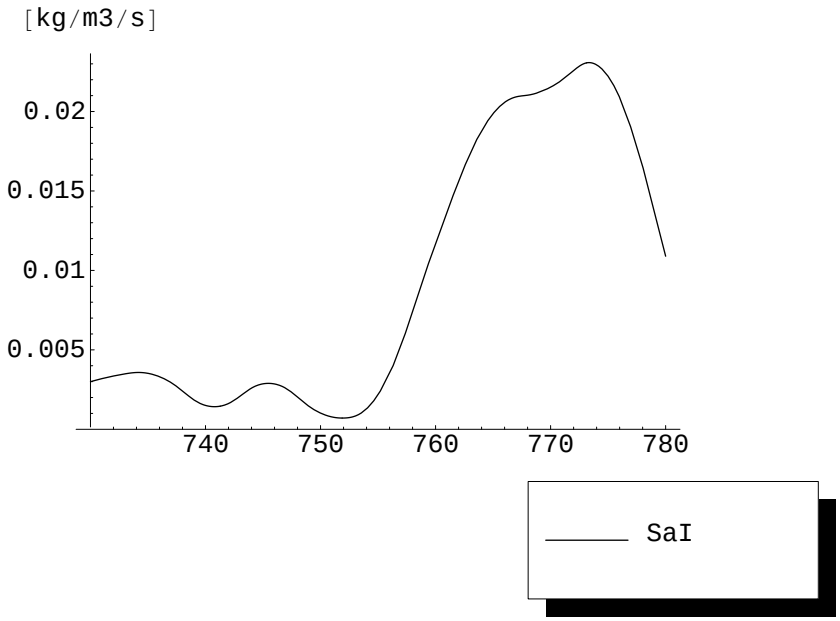

Figure 4.10. N2 mass flux released per unit of volume versus time during Phase 1.

4.4.4 The N_2 Mass Fraction Dissolved in the Liquid

From Eq. 4.2 and assuming $V_{l_{x\to x+1}} \approx 0$,

$$\frac{\partial\left((1-\alpha)\rho_l\right)_x X_{al_x}}{\partial t} = -S_{aI_x} \tag{4.2b}$$

$\left((1-\alpha)\rho_l\right)_x(t)$ is calculated for each section during depressurization when $700s \prec t \prec 787s$ (Figure 4.11).

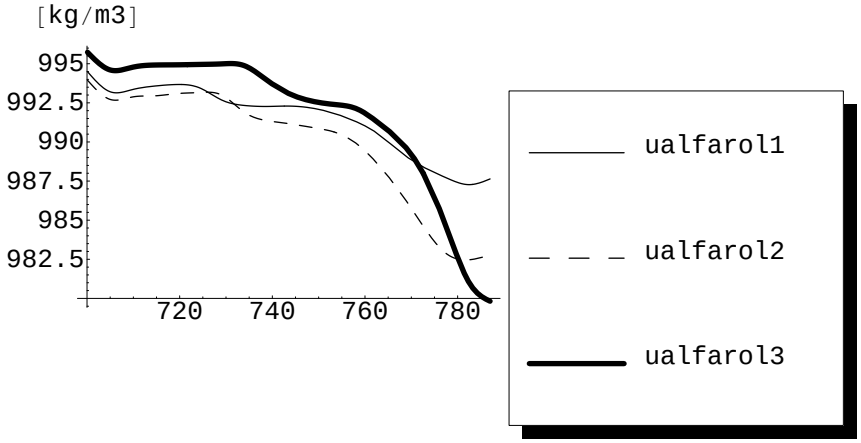

Figure 4.11. [(1-α)ρl]x(t) versus time in sections 1 to 4 during Phase 1.

The mean value for sections 1 to 3, $X_{al,mean}$ (t) is calculated:

$$\sum_{x=1}^{3} \frac{\partial\left((1-\alpha)\rho_l\right)_x X_{al,mean}}{\partial t} = -\left(S_{aI_1}(t) + S_{aI_2}(t) + S_{aI_3}(t)\right) = -S_{aI} \tag{4.11}$$

The average equilibrium dissolved nitrogen mass fraction in liquid $X_{aleq,mean}$ in sections 1 to 3 is calculated from Eq. 4.4 and 4.5 (Figure 4.12).

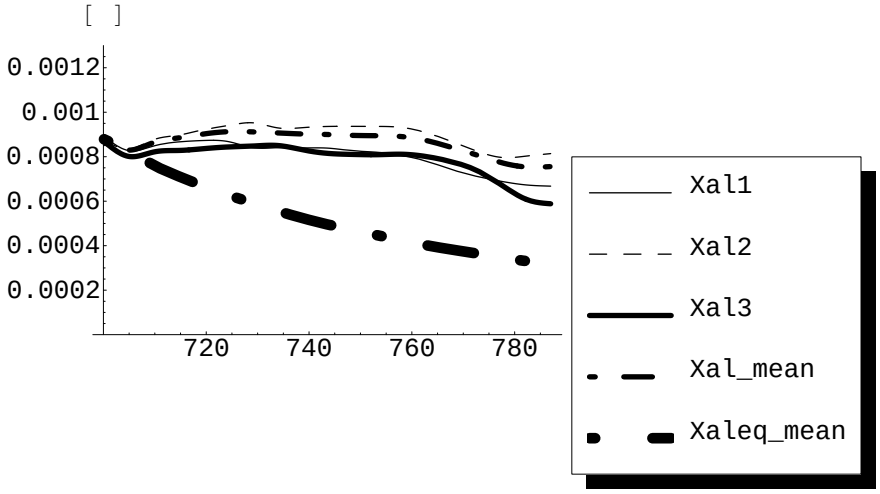

Figure 4.12. The N_2 mass fraction dissolved in liquid versus time in sections 1 to 3 during Phase 1.

4.4.5 Release Time Constant τ

Finally, an average value of τ_{rel} is obtained:

$$\tau_{rel}(t) = \frac{\sum_{x=1}^{3}\left((1-\alpha)\rho_l\right)_x \left(X_{al,mean} - X_{aleq,mean}\right)}{S_{al}} \qquad (4.12)$$

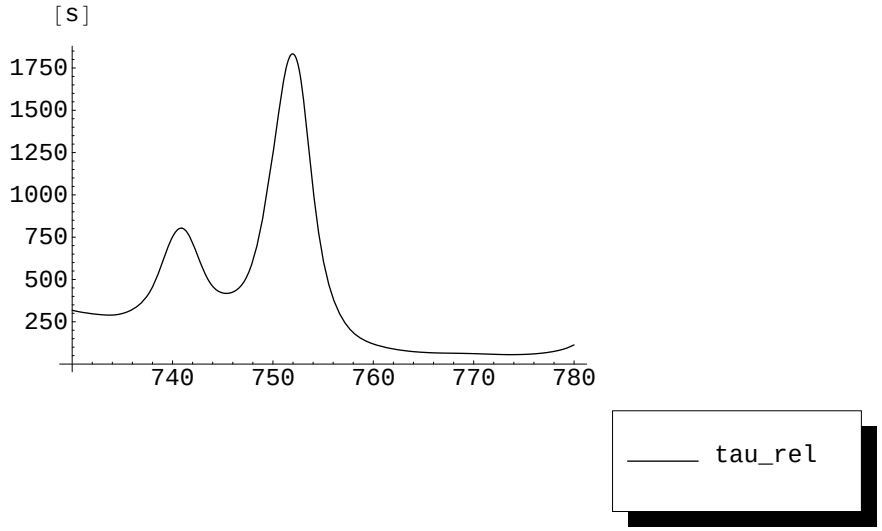

Figure 4.13. The release time constant versus time during Phase 1.

As mentioned above, the rather high values obtained up to time 760 s are attributed to a zero or very low mass transfer corresponding to a degassing delay. After time 760 s, clear degassing takes place, and an average value of τ_{rel} of about 50 s is then proposed (Figure 4.13).

4.4.6 Bubble Diameter

Ishii and Zuber (1979) proposed a bubble drag coefficient and relative velocity for various bubble regimes.

- The case of a regime of undistorted particles

$$C_D = \frac{24}{\mathrm{Re}}(1 + 0.1.\mathrm{Re}^{0.75}) \quad \text{with } \mathrm{Re} = \frac{\rho_l.(|V_g - V_l|).d}{\mu_l} \tag{4.13}$$

Here, the relative velocity (V_g -V_l) is the rise velocity of the gas bubbles.
When $Re << 1$, the model is consistent with the Stokes regime.

- The case of a regime of distorted particles

For such a regime, it has been experimentally observed that the rise velocity of gas bubbles is independent of the bubble size. Equating the drag and buoyancy forces implies a proportionality of drag coefficient with bubble size:

$$C_D = \frac{2}{3} d \sqrt{\frac{g\Delta\rho}{\sigma}} function(\alpha) \tag{4.14}$$

- Churn turbulent flow

The drag coefficient no longer depends on the bubble size:

$$C_D = \frac{8}{3} function(\alpha) \tag{4.15}$$

Based on the previous equations, the rise velocity of gas bubbles is plotted (Figure 4.14) versus the bubble diameter for experimental conditions of the first depressurization of test RUN-1: (pressures ranging between 2.0 MPa and 5.5 MPa, and void fractions between $\alpha = 0.005$ and 0.02). The value of the diameter, at which the transition between the distorted and undistorted bubble regime occurs, is 2.10^{-3}m, and the associated rise velocity of gas bubbles is 0.23 $m.s^{-1}$.

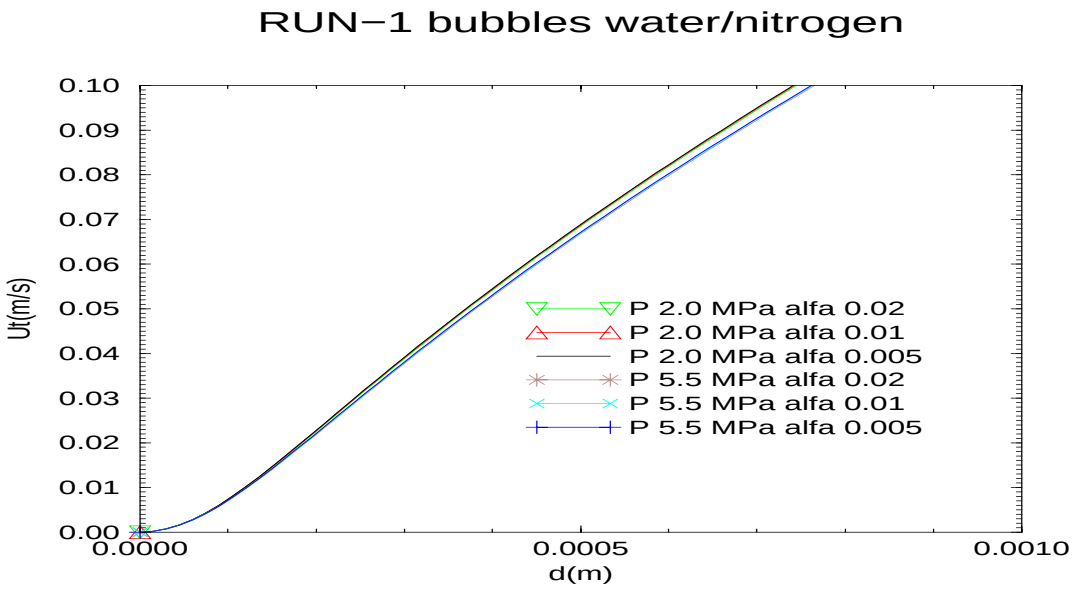

Figure 4.14. The velocity of N2 gas bubbles as a function of the bubble diameter.

Considering a rise velocity of gas bubbles equal to 10^{-2} m.s^{-1}, the regime is an 'undistorted particle regime'. The corresponding bubble diameter, read from the plot, is $d \approx 10^{-4}$m, the Reynolds number 1.66 and the drag coefficient

$$C_D = \frac{24}{\mathrm{Re}}(1 + 0.1.\mathrm{Re}^{0.75}) \approx 17 \qquad (4.13a)$$

4.4.7 Modeling the Degassing Delay and Release Time Constant

From the analysis of RUN 1, the following model is proposed:

- if $\alpha \cong 0$ and $X_{aleq} < X_{al} < X_{aleq} + 10^{-4}$,

  then $S_{aI} = 0$

- if $(\alpha \cong 0$ and $X_{aleq} + 10^{-4} < X_{al})$ or if $(\alpha > 0$ and $X_{aleq} < X_{al})$,

  then $S_{aI} = \dfrac{(1-\alpha)\rho_l (X_{al} - X_{aleq})}{\tau}$ with $\tau_{rel} = 50s$ (4.16)

In practice, the limit $\alpha = 0$ is replaced in the code by a minimum void fraction.

4.5 RUN-1 Calculations with CATHARE2 V1.3L

4.5.1 Standard Interfacial Friction in CATHARE

In the standard version of CATHARE, interfacial friction τ_I correlation for bubbly flow in pipe geometry (and also for annuli and rod bundles geometries) is derived from the original drift models for the mixture of water and steam (Serre and Bestion 1999).

$$\tau_I = \frac{1}{2} \cdot a_I \cdot f_I \cdot \rho_l \cdot \left| V_g - V_l \right| \cdot \left(V_g - V_l \right), \tag{4.17}$$

where

a_I volumetric interfacial area
f_I friction coefficient

For bubbly flow, the standard correlations used for the a_I and f_I terms are validated on steam bubbles. These correlations are not appropriate in the case of very small nitrogen bubbles in water. The standard model is consistent with steam bubbles the size of which is larger than a few millimeters, whereas the diameter determined for nitrogen bubbles is 10^{-4}m.

Therefore, from test RUN-1, a specific version of the interfacial friction for nitrogen gas bubbles in water was developed. This specific model was used to recalculate RUN-1.

4.5.2 Interfacial Friction for N_2 Gas Bubbles in Water

An interfacial friction τ_I model consistent with the flow regime observed during RUN-1 was developed.

Replacing the volumetric interfacial area, a_I, and friction coefficient, f_I, in the general form of interfacial friction τ_I (Eq. 4.17) with their expressions gives the following:

$$\tau_I = \frac{1}{2} \cdot N_b . \frac{\pi . d^2}{4} \cdot C_D \cdot \rho_l \cdot \left| V_g - V_l \right| \cdot \left(V_g - V_l \right) \tag{4.18}$$

N_b the volumetric number of bubbles

Two cases are considered:

- during depressurization, N_b is assumed constant

$$\tau_i = \frac{1}{8} \cdot \left(N_b . \pi\right)^{1/3} \left(6 \cdot \alpha\right)^{2/3} \cdot C_D \cdot \rho_l \cdot \left|V_g - V_l\right| \cdot \left(V_g - V_l\right), \qquad (4.18a)$$

where $N_b = 10^{10}$ and $C_D = \frac{24}{\mathrm{Re}}(1 + 0.1.\mathrm{Re}^{0.75})$

The value taken for N_b is an average value calculated from the values obtained in the case of RUN-1, as follows:

$$N_b = \frac{6 \cdot \alpha}{\pi . d^3} = \frac{6 \cdot \left(8.10^{-3}..2.10^{-2}\right)}{\pi . \left(10^{-4}\right)^3} = \left(1.5 \times 10^{10} ... 3.8 \times 10^{10}\right)$$

- between depressurizations, the diameter of the nitrogen bubbles is assumed constant

$$\tau_i = \frac{3\alpha}{4d} \cdot C_D \cdot \rho_l \cdot \left|V_g - V_l\right| \cdot \left(V_g - V_l\right), \qquad (4.18b)$$

where $d = 10^{-4}$ and $C_D = \frac{24}{\mathrm{Re}}(1 + 0.1.\mathrm{Re}^{0.75})$

4.5.3 General Trends of the Various Calculations

Different sensitivity calculations were performed (a detailed content of the versions in Appendix B) and the obtained void fraction profiles were compared to the experimental values.

In the different calculations presented below (Figures 4.15 and 4.16), the void peak amplitudes are generally overestimated compared to experimental results. Yet, the error remains within the limits of a rather high experimental uncertainty.

The slope of the rising section of the peaks is well predicted, while that of the decreasing section is not. As a result, the shape of the calculated peaks is sensibly larger than that of the measured peaks. Particularly, during the second depressurization, the calculations predict a significantly longer period of bubbling than that observed in the experiment.

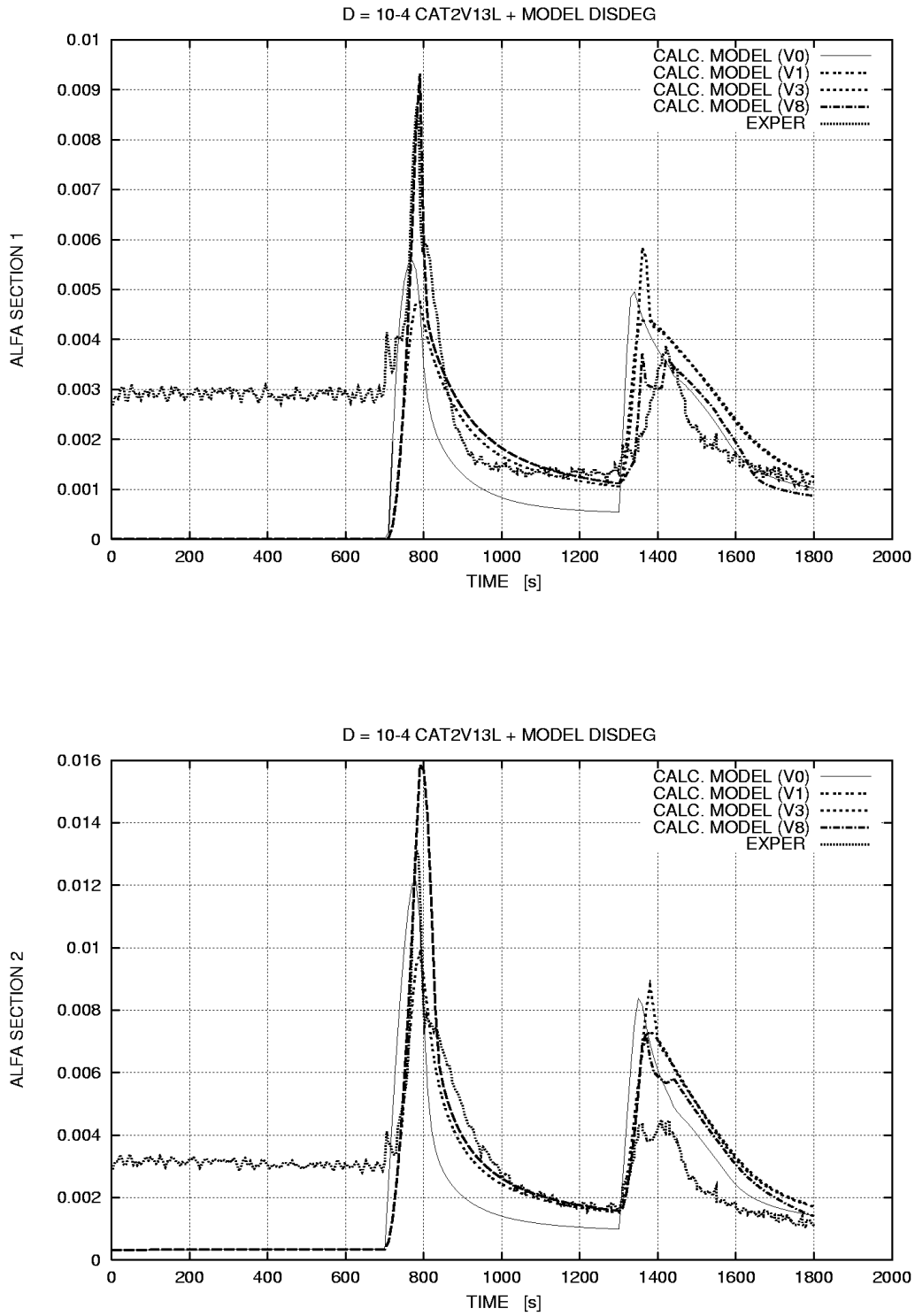

Figure 4.15: The experimental and calculated void fractions as functions of time in sections 1 and 2 in RUN-1.

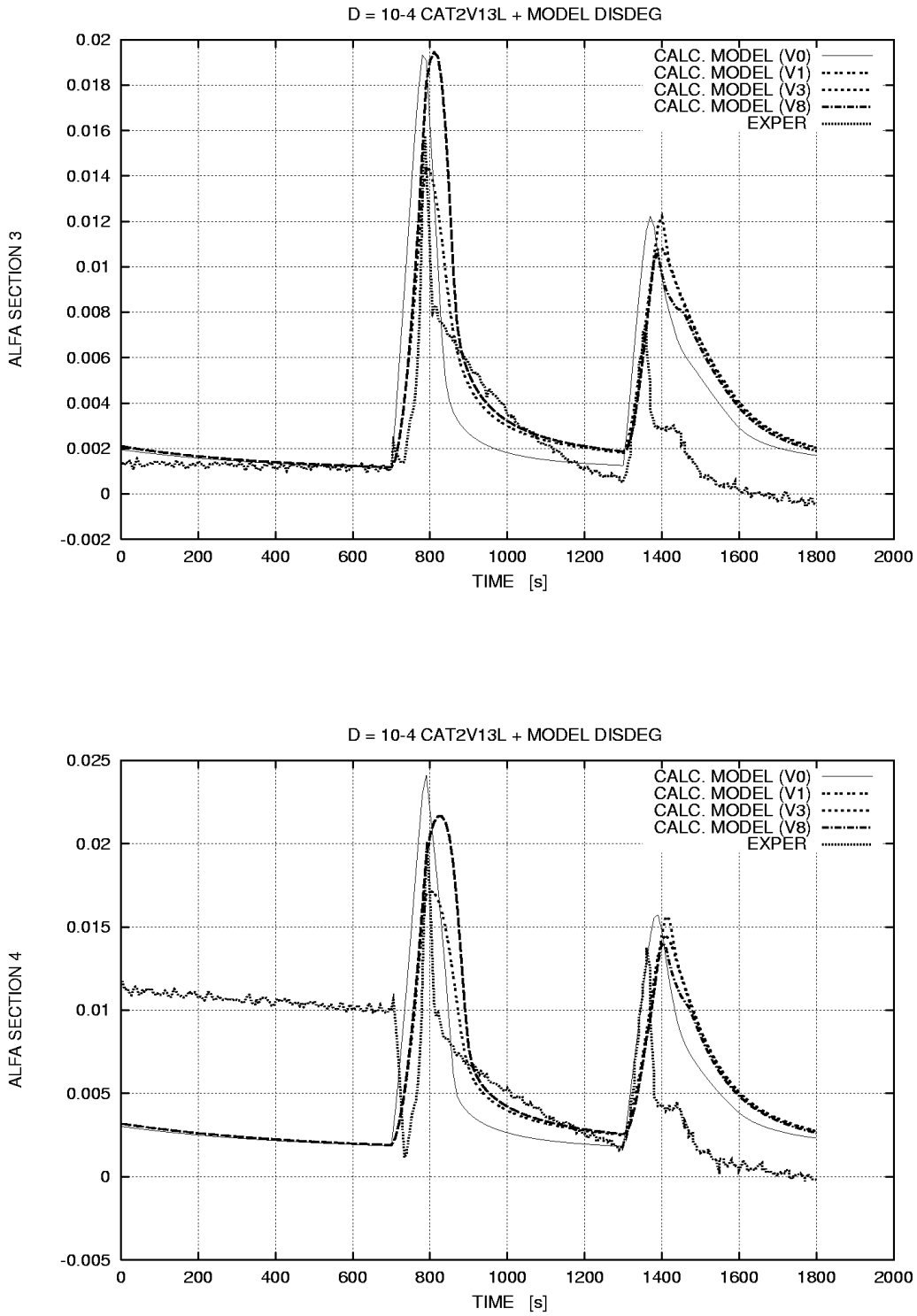

Figure 4.16: The experimental and calculated void fractions as functions of time in sections 3 and 4 in RUN-1.

4.5.4 Effect of the Release Time Constant (versions 1/0)

As expected, using a larger release time constant (50 s instead of 1 s) improves the rising slope of the α profiles, at least during the first depressurization, reduces the maximum height of the peaks and increases their width.

Compared to experimental results, the size of the peaks is under-estimated during the first depressurization, overestimated during the second depressurization, and the width of the peaks is over-estimated.

4.5.5 Effect of the Interfacial Friction Correlations during the Depressurizations (versions 3/1)

Using the correlation at constant, N_b, for interfacial friction τ_I (Eq. 4.18a) during the depressurizations increases the peaks sizes. Then, the calculated and experimental results better fit the peak that corresponds to the first depressurization.

4.5.6 Effect of the Interfacial Friction Correlations after the Depressurizations (versions 3bis/3, versions 4/3)

The use of the correlation at constant d for τ_I (Eq. 4.18b) between the two depressurizations (787 s < t < 1300 s) (V3bis) firmly maintains α at the value reached at the top of the peak corresponding to the first depressurization.

An attempt was made to impose the correlation at constant d, only during 30-40 s after each of the two depressurizations (V4). The result of this was the overestimation of the height and width of the peaks for the first depressurization. For the second depressurization, the height of the peaks increased as well. However, their widths narrowed, indicating a shorter period of bubbling, which was in better agreement with the measurements.

4.5.7 Effect of the Degassing Delay (versions 8/3)

The criterion given in 'Determination of Dissolution-Release Model Parameters', was used at low void fraction values:

- if ($\alpha < 1.6.10^{-3}$).and $X_{aleq} < X_{al} < X_{aleq}+10^{-4}$,

  then $S_{aI} = 0$

- if ($\alpha < 1.6.10^{-3}$ and $X_{aleq}+10^{-4} < X_{al}$) or if ($\alpha > 1.6.10^{-3}$ and $X_{aleq} < X_{al}$),

  then $S_{aI} = \dfrac{(1-\alpha)\rho_l (X_{al} - X_{aleq})}{\tau}$ with $\tau_{rel} = 50s$ (4.16)

This criterion was used for the second depressurization only, allowing a better prediction of the peaks, particularly in the two lowest sections (V8).

Using it for the first depressurization totally or partly prevented degassing in the two lowest sections. This unsatisfactory result indicates that other parameters, not included in this criterion, might drive the degassing process. The depressurization rate, faster during the first valve opening, might explain this situation.

4.6 Conclusion

The results gained from the present study of the release, during depressurization, of nitrogen gas dissolved in water are listed below.

- An analytical depressurization experiment was performed under typical pressure conditions in a hypothetical LOCA in the primary circuit of a PWR, in a subcooled regime. An average value of the release time constant was obtained from the reduction of the pressure drop and temperature measurement data: $\tau = 50$ s.
  One should keep in mind that the experimental values were obtained with a rather large relative uncertainty. This was due to a much lower void fraction range than normally measured with the used apparatus. The average diameter of the nitrogen gas bubbles was estimated at 0.1 mm.

- A model for the dissolution and release of a NC gas (nitrogen) has been included in the thermal-hydraulic code CATHARE2 V1.3L using relaxation time constants for release and degassing.

- The calculations of the analytical experiment were performed with CATHARE2 V1.3L which includes the dissolution-release model and a modified interfacial friction for nitrogen gas bubbles in water. The results reveal better agreement between the experimental and calculated results with the obtained value of the release time constant ($\tau = 50$ s), than for faster degassing. The modification of the interfacial friction coefficient improved the prediction of the gaseous temperatures measured at the top of the test section. Still, the large uncertainties of the experimental values validate the trends only.

5 LOCA Calculations with CATHARE2 V1.3L

The purpose of the calculations of loss of coolant accidents (LOCA) is to study how the release of dissolved nitrogen in the water of the accumulator of the ECCS would affect the cooling of the core during such scenarios on the VVER-440 geometry. What amount of nitrogen gas will be released? What amount of nitrogen gas will be evacuated to the break? And where will the nitrogen gas eventually accumulate in the primary circuit? Will the nitrogen gas bubbles present in the primary circuit interrupt natural circulation and how will the heat exchanges between the primary and secondary circuits be affected?

This chapter presents the results of LOCA calculations performed on the Loviisa nuclear power plant (NPP) geometry using the CATHARE code. The results include:

- a reference case for a 1-% break calculated with a release time constant equal to 50 s (value determined in Chapter 4 'Analysis of NC Gas Release Experiment')
- sensitivity calculations on the value of release time constant (τ = 1, 10, 100 s) for a 1% break
- sensitivity calculations on the value of the break size (1%, 1.5%, and 2%) for τ = 1s

5.1 Introduction

The set points used for this study are close to the set points implemented at the Loviisa NPP prior to modernization (1994-1998). The objective is to define a clear accident that does not depend too closely on procedures; therefore, the procedures used here are simplified. The accumulators are pressurized at 5.5 MPa, the water temperature is 40° C for the two accumulators injecting in the upper plenum and 105° C for the two accumulators injecting in the downcomer. The total mass of the nitrogen gas dissolved in the four accumulators is calculated [4]: at 128 kg using Henry's law (Eq. 4.5).

As mentioned in Chapter 4 'Analysis of NC Gas Release Experiment', the employed values of $K(T_l)$, which were obtained from the interpolation of the values published by Pray et al. (1952), are appreciably lower than those reported by Cohen (1980) in the temperature range of between 177° C and 260° C.

In reality, this does not affect the initial amount of nitrogen gas dissolved in the accumulators, because their liquid temperature is set to T_l = 40° C.

During the considered LOCA transients, the average liquid temperature in the primary circuit ranged between 140° C and 280° C. For this reason, the amount of nitrogen gas dissolved in the water for this temperature range was overestimated, which is not a conservative hypothesis. Nevertheless, at the end of the calculated transients, there is almost no nitrogen gas dissolved in water, and this eventual underestimation remains moderate.

[4] The value for the four accumulators is calculated from the initial pressure and liquid temperature of the two accumulators injecting in the upper plenum: 5.5 MPa and 40° C. At the given pressure, Henry's constant being lower at 40° C than at 105° C, this simplification maximizes the amount of nitrogen dissolved in the accumulators.

Table 5.1 shows the calculated values of the volume occupied by this mass of nitrogen for different pressures and two temperatures in case of its complete release in gaseous phase. Nitrogen is considered an ideal gas. At the given pressure and saturation margin[5], these values are the maximum expected if the gaseous phase only contains nitrogen gas. In a mixture of nitrogen gas and steam, under the same pressure and temperature conditions, the partial pressure of the nitrogen gas would decrease and its occupied volume increase.

Table 5.1 The maximum gaseous volumes occupied by the nitrogen gas dissolved in the accumulators (complete release case)

Pressure [MPa]	Volume of N_2 in gaseous phase [m^3] M_{N2}= 128 kg, $\Delta T_{out\text{-}core,sat}$ = 10° C	Volume of N_2 in gaseous phase [m^3] M_{N2}= 128 kg, $\Delta T_{out\text{-}core,sat}$ = 20° C	Volume of N_2 in gaseous phase [m^3] M_{N2}= 128 kg, $\Delta T_{out\text{-}core,sat}$ = 40° C
4.0	4.9	4.8	4.6
2.1	8.7	8.5	8.1
1.0	16.8	16.5	15.7
0.75	21.9	21.3	20.3
0.27	55.4	54.0	51.1
0.1	138.1	134.3	126.7

Table 5.2 shows the volumes of the different possible locations where nitrogen could be trapped in the primary circuit. If the volume of the nitrogen trapped in these different dead-ends is larger, natural circulation is likely to stop, because the level of the liquid is lower than the bottom of the junctions connected to the corresponding vessel. Schematics of these dead-ends is shown in the Figure 5.1. Owing to its geometry and location, the RCPs upper part is expected to fill easily and durably with nitrogen gas. The other dead-ends do not seem so crucial in this respect. For example, venting of the upper plenum (resp the top of the downcomer) would be ensured by a break situated in the hot leg (resp. in the cold leg).

Table 5.2 The volume of the different dead-ends in the primary circuit

Component	Volume [m^3]
Top of downcomer	1.4
Upper plenum	21.9
Pressurizer	38.0
Hot collectors	1.5 *6
Rod bundle in SGs	6.8 *6
Cold collectors	1.5 *6
Upper part of RCPs	0.1 *6

[5] In this chapter, saturation margin or sub-cooling at core outlet will refer to:
$\Delta T_{out\text{-}core,sat} = T_{sat}(P) - T_{out\text{-}core}$ with P, the total pressure of gaseous mixture (nitrogen gas + steam).

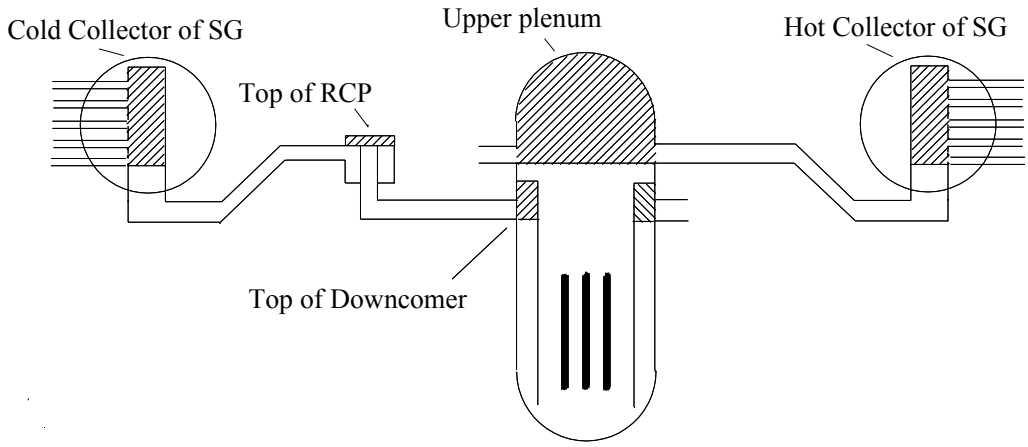

Figure 5.1. The different dead-ends in the primary circuit.

While a large break LOCA is able to remove the decay heat, depressurize the primary circuit and evacuate part of total NC gas to the break, the term, which describes the energy sink to the break, may not be able to remove the decay heat in the case of a small break LOCA (SBLOCA); heat transfer to the secondary circuit is needed. The active volume of one SG is equal to 10 m^3 for the collectors + the primary tubes. The total volume of the nitrogen gas potentially released at pressures equal to or lower than 0.27 MPa exceeds the total active volume of the SG. Therefore, the SBLOCA case must be examined in more detail. The present study is dedicated to small and intermediate breaks (IBLOCA) situated in the loop seal of the cold leg.

The particular case of a steam generator tube rupture (SGTR) is regarded, however, as being potentially even more problematic. In the case of SGTR, operator measures tend to promptly reduce the primary pressure below the set point of the secondary-side safety valve to avoid the release of the primary coolant to the environment. This has two potential effects: the low-pressure nitrogen gas will not be expelled to the break. Then, the volume of the nitrogen gas trapped in the primary circuit will expand along this rapid primary pressure decrease.

SGTR transients are strongly dependent on operating procedures. Such procedures are commercially protected and not usually provided by plant operators. Moreover, these procedures can vary substantially from one plant to another. Therefore, as mentioned above, the choice was made to study SBLOCA and IBLOCA, whose scenario does not depend too strongly on operating procedures.

5.2 Input Description

5.2.1 Nodalization

The nodalization scheme used for the calculations is based on the CATHARE2 V1.3U standard input data deck used at LUT for the simulation of the Loviisa NPP (Haapalehto 1995), (see also section 'Choice of the Code Version' in this Chapter). This input deck has been verified against data measured in the Loviisa plant during startup tests and during a reactor coolant pump trip transient that occurred in the Loviisa NPP in 1991 (Tuunanen et al. 1993). All six loops are represented: the broken loop leg (denoted by loop 1), two loops are connected to the pressurizer with surge lines (denoted by loops 2 and 5), and three loops, which have loop seal connections between the hot leg and cold leg (denoted loops 3, 4, and 6). Figure 5.2 shows the main components that model the loops (in this figure, the secondary side of the steam generator is depicted for the broken loop only).

The core was modeled with two parallel channels, one fuel element channel and the bypass. The model of the downcomer includes a *1-D axial* module, and a *volume* module, the voldown, that allows several connections to the cold legs. The upper plenum, lower plenum, and pressurizer are represented using a *volume* module for each.

The pressurizer was modeled with a *volume* and includes seven groups of heaters. These heaters are used during the stationary transient step to obtain the nominal primary pressure. They do not operate during the transient.

On the primary side of the steam generator, the heat exchange tubes were modeled using five *1-D axial* modules at five different elevations. These channels, from the lowest to the highest, represent 1320, 1306, 1150, 1080 and 680 tubes, respectively. Each *1-D axial* module, which represents a channel, is divided horizontally into 5 nodes. The hot and cold collectors are each represented with one *volume* module. The secondary side was modeled with a U-shaped *1-D axial* module connected to the *volume* representing the steam cavity of the steam generator. The riser part represents the tube bundle and the downcomer part the rest of the secondary pool. Feed water is injected at 0.37 m below the upper part of the tube bundle.

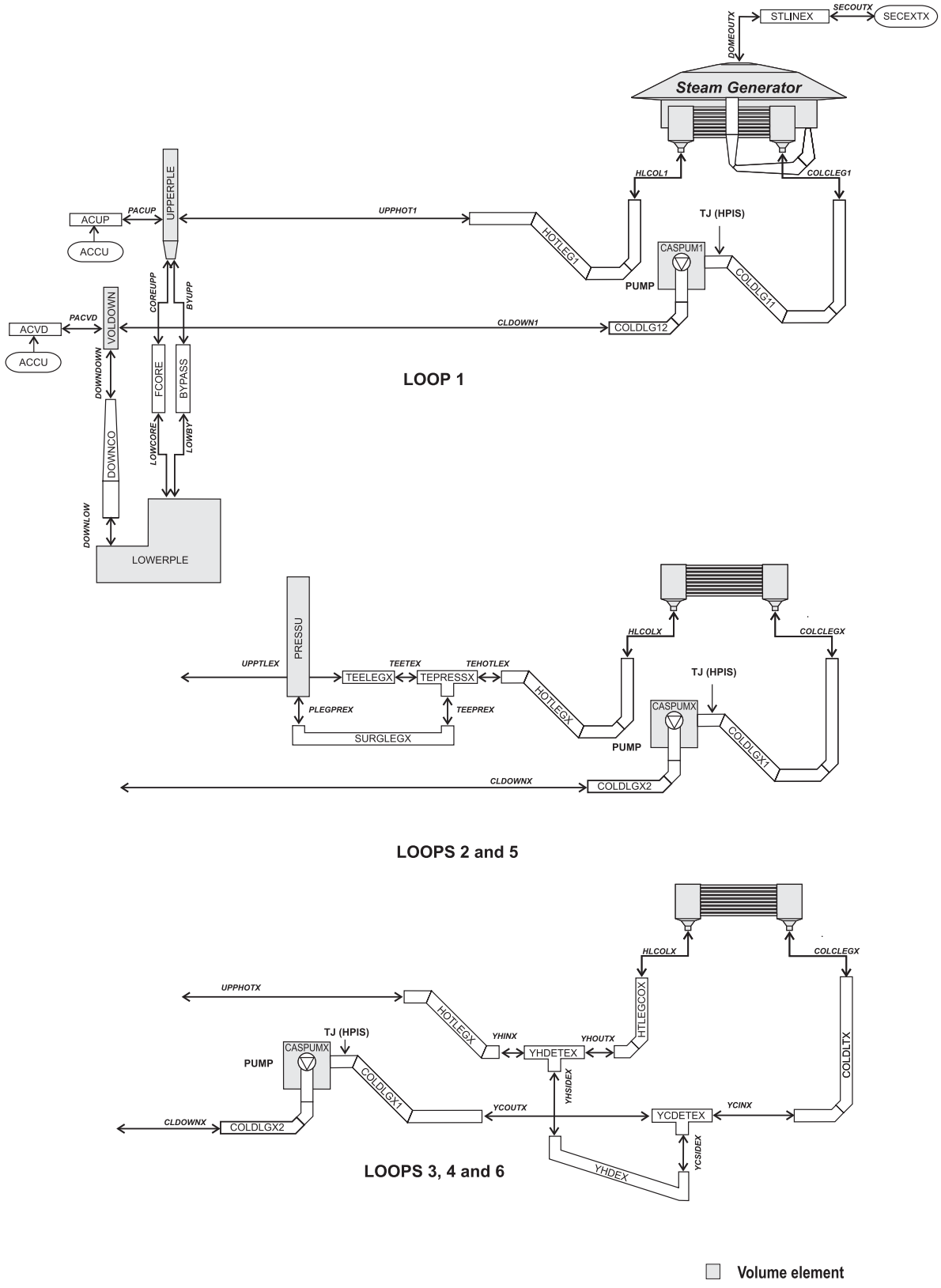

Figure 5.2: The CATHARE2 V1.3L nodalization for Loviisa.

The reactor coolant pumps (RCPs), one in each loop, were modeled in detail. To investigate possible bubble formation at the top of the pump, the pump inlet was modeled using a *volume* module and the impeller, casing and diffuser were modeled as one unit using a vertical *1-D axial* module consisting of 4 meshes. The connection between the *volume* element and the pipe element is a junction that has a penetration length inside the capacity (Farvacque et al. 1991, 1992). The top of the pipe is, as is the top of the impeller in the RCP, 24 cm higher than the mid-line of the cold leg (see Figure 5.3). The characteristics of the RCP were modeled with the one-node pump sub-module located on the elevation of the impeller. This sub-module writes the momentum and energy source terms due to the pump calculated from the head and torque characteristics, which are the input.

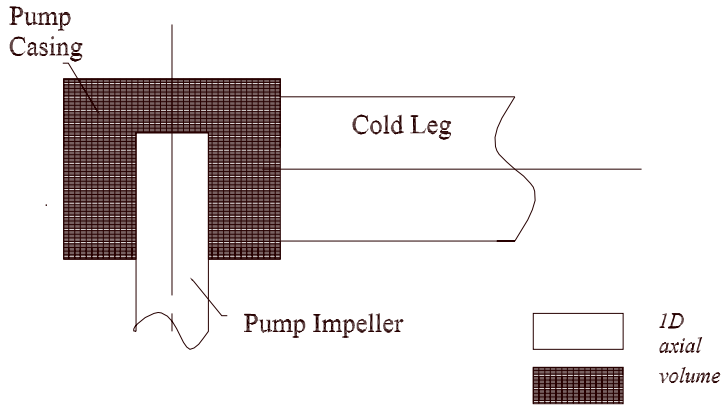

Figure 5.3: The CATHARE2 V1.3L nodalization for the reactor coolant pump.

The break was modeled with a break sub-module, which is a sink term using a critical mass flow rate correlation (Bestion 1989).

The emergency core coolant system (ECCS) is represented by two accumulators that inject in the upper plenum, two accumulators that inject at the top of the downcomer, the high pressure injection system (HPIS), and the low pressure injection system (LPIS).

Because it was not possible to connect an accumulator sub-module directly to a *volume* module in CATHARE2 V1.3L, the accumulators were connected to auxiliary pipes that were themselves connected to the upper plenum and the top of the downcomer. The mass fraction of the dissolved nitrogen gas in the water for all the accumulators was set to the value corresponding to the water saturated with nitrogen. This value ($7.9 \cdot 10^{-4}$) was calculated according to Henry's law (Eq. 4.5) from the initial pressure and liquid temperature of the accumulators, which injected in the upper plenum [6], which are 5.5 MPa and 40° C.

[6] The value for the four accumulators is calculated from the initial pressure and liquid temperature of the two accumulators injecting in the upper plenum: 5.5 MPa and 40° C. At the given pressure, Henry's constant being lower at 40° C than at 105° C, this simplification maximizes the amount of nitrogen dissolved in the accumulators.

The HPIS includes two high pressure injection pumps (one per redundancy) for all the loops. The two pumps are represented with one source sub-module per loop. The injection point of this source is situated on each cold leg at 0.93 m from the inlet of the RCPs. The HPIS injection rate was modeled according to the number of loops, and it was assumed that the flow was equally distributed between the loops.

The LPIS includes two low pressure injection pumps (one per redundancy) for all the loops. The two pumps are represented with one source sub-module situated in the upper plenum at the level of the hot legs and another source situated at the top of the downcomer at the level of the cold legs. The LPIS starts when the primary pressure drops below 0.75 MPa, and the injection rate is equally divided between the upper plenum and downcomer. Both HPIS and LPIS inject water at 60^{o} C. The assumption is made that there is no gas injected via the HPIS and LPIS. The accumulators close at the end of the water discharge in the primary circuit (i.e. no cover nitrogen gas present above the water of the accumulators is injected in the primary circuit).

The whole primary circuit is represented by 661 hydraulic nodes and the secondary side by 132 nodes.

5.2.2 General Analysis Conditions

The transient calculations are based on the initial conditions previously described for three break diameters: 50 mm, 62 mm, and 71 mm (1%, 1.5%, and 2% of the loop cross-section, respectively). A break size of 1% of the loop cross-section corresponds to the typical value of a hypothetical SBLOCA in the Loviisa NPP. This break is situated at the bottom of the cold leg loop seal.

Before running the transient calculations, 1000 seconds of stationary transient were run to obtain nominal values for the balanced steady state conditions. Table 5.3 shows the main initial conditions for the different calculations.

Table 5.3: Comparison of the steady-state calculation results with plant data

	Plant nominal value	Calculated steady-state value
Core power [MW]	1375.0	1375.0
Primary pressure [MPa]	12.25	12.25
Cold leg temperature at junction with Pressure Vessel [^{o}C]	264.0	265.4
Downcomer mass flow rate [kg/s]	8500.0	8508.0
Core mass flow rate [kg/s]	7480.0	7454.0
Bypass mass flow rate [kg/s]	1020.0	1059.0
Secondary pressure [MPa]	4.48	4.40
Steam lines mass flow rate [kg/s]	750.0	650.4[7]

After this step, the following scenario was assumed. The break is opened at the very beginning of the transient. The scram, reactor coolant pumps trip and HPIS actuation takes place according to the plant protection system. The scram of the reactor occurs when the pressure in the hot legs is below 9.3 MPa or if the hot leg pressure is below 10.8 MPa and the level in pressurizer has decreased more than 2.7 m. The decay heat curve follows the ANS-79 curve. When the level of the pressurizer has decreased more than 3.2 m, the high-pressure injection system starts operating, the valves of the loop seals connections are opened and the reactor coolant pumps tripped. The accumulators starts to inject when the primary pressure drops below 5.5 MPa. The low pressure injection system starts operating when the primary pressure falls below 0.75 MPa.

On the secondary side, after the turbine trip following the reactor scram, feed water injection is modeled to keep the secondary level constant. The secondary pressure is regulated by the turbine by-pass valves that start to open at 4.7 MPa and are fully open at 5.1 MPa. The total turbine by-pass capacity is 70% of nominal steam generation. As formerly stated, the objective of these calculations was to use really simplified operating procedures. So, the secondary circuit was not depressurized. This likely extended the transient duration.

The transient is stopped when the primary pressure stabilizes. In the case of the smallest break size (without nitrogen gas and with nitrogen gas $\tau = 1$ s), this stabilization occurs above the set point of LPIS (at about 0.80 MPa)[8]. In the other cases, the primary pressure falls below this set point.

[7] The difference between nominal and calculated values for steam line mass flow rate is due to the following simplification made to the input deck. The feed water temperature is forced to have the same value before and after the turbine trip, or 164^{o}C.

[8] 0.82 MPa without nitrogen gas; 0.79 MPa with nitrogen gas

5.3 Content of the CATHARE Version

5.3.1 Choice of the Code Version

In a first attempt, version V1.3U of the CATHARE2 code was used to calculate the 1% break size case without a NC gas.

In this and the earlier versions of the code, the accumulator sub-module was explicitly coupled to the *1-D axial* module. The discharge flow rate at time t^{n+1} is calculated from the accumulator pressure at time t^{n+1} and the pipe pressure at time t^{n}. The pressure in the mesh of the pipe, into which the accumulator injects, oscillates from one iteration to another. Thus, it is difficult to obtain convergence in this module. This situation causes a decrease of the time step at the opening of the accumulators, and the calculation finally stops.

This problem is overcome in a new version of the CATHARE2 code, version V1.3L, which incorporates the implicit coupling of the accumulator sub-module. Therefore, version V1.3L was used as the basis for all the calculations performed for the present study.

5.3.2 Modification of the Correlation for the Condensation in the *Volumes*

Version V1.3L of CATHARE2 includes a set of physical laws named Revision 5 (see Chapter 2 'Film Condensation Models in Thermal-Hydraulic Codes and the Related Experimental Assessment').

The analysis of the calculations performed with the standard version of the code without the presence of a NC gas showed a clear underestimation of condensation in the upper plenum at the injection of the accumulators. Then, the correlation for condensation in the *volumes* was modified. A comparison for the 1-% break size between the calculations performed with the standard version of the code and a version, which included modifications of the correlation for condensation in *volumes*, is presented in the section 'Sensitivity to Condensation Correlation in *volumes*'. The reinforced condensation in the *volumes* modification is retained for all LOCA calculations (without[9] and with NC gas) reported from here onwards.

5.3.3 Numerics and Numero-Physical Modifications

During the transient calculations performed with the dissolution-release model, convergence problems were encountered. Firstly, there was the problem of evaluating inter-phase heat transfer when the fluid is a one-phase liquid with only the NC gas in the residual gaseous phase. Secondly, there was a discretisation problem in the mass and energy transport equations in the pipes. This appeared when the code attempted to transport the NC gas from a cell that had no gas. These different problems were investigated by the developers of the code and the anomalies were corrected in the further versions of the code (Bryce 1999), (Kadri 1999). Some of these corrections were introduced in the version of CATHARE used for the calculations with nitrogen gas.

[9] When not labeled as a standard case.

5.3.4 Interfacial Friction modifications

This section discussed the applicability of the modified interfacial friction (see section 'Interfacial Friction for Nitrogen Gas Bubbles in Water' in Chapter 4) to the reactor LOCA transients.

In the standard two-fluid model of the CATHARE code, bubbly flows are modeled for cases where rather large steam bubbles are generated either by flashing or boiling due to the heat released from the walls and fuel rods. If small nitrogen bubbles are released from the dissolved NC gas, the standard model cannot be consistent with both large steam bubbles and small nitrogen bubbles. Many models are sensitive to the bubble size.

- Interfacial friction is larger when the bubble size is smaller.
- Stratification in horizontal pipes is easier and more rapid with large bubble than with small bubbles.
- Interfacial heat and mass transfer also depend on the bubble size.

In the present status of the CATHARE code, it would be extremely difficult to properly model the effects of having two types of bubbles with a different gas content and different sizes. Only the transport of nitrogen and the dissolution and degassing phenomena have been taken into account. The standard interfacial friction, stratification criterion, and interfacial heat and mass transfer models are used for reactor calculations.

The expected trends of the LOCA calculations performed with the CATHARE code, including the transport and dissolution-release model for nitrogen gas, are listed below.

- In vertical pipes, the interfacial friction, τ_I, is underestimated for nitrogen gas bubbles, and nitrogen gas bubbles will, therefore, tend to accumulate faster on top of vertical pipes.
- On the other hand, the excessively low value of standard τ_I will minimize the entrainment of nitrogen gas by the liquid to components from which nitrogen could separate from water.
- In horizontal pipes, the separation of nitrogen gas by stratification will be made easier with the use of a standard stratification criterion validated for steam-water.

Hence, with standard τ_I, the separation of N_2 gas from the liquid may be overestimated in vertical or horizontal *1-D axial* modules, and the transport of N_2 bubbles to large *volumes* may be underestimated.

A complete approach to the degassing problem of an NC gas, would include, besides the existing standard set of physical laws validated for steam bubbles, an additional set of physical laws specific to the characteristics of the NC gas bubbles.

Regarding this, the approach developed by Narumo and Rajamäki (1996), known as the Separation of the Flow According to Velocity, has potentialities. In the SFAV model, the NC gas-steam mixture could be divided into two sub-flows with distinct velocities. This method

then allows distinct physical laws to be used for each sub-fluid. This modeling, however, would require a very important work to model the corresponding closure laws. Furthermore, serious difficulties have been experienced to introduce SFAV in the present state-of-art computer codes.

5.3.5 Dissolution-Release Model

The dissolution-release model described in the section 'The Dissolution-Release Model in CATHARE 2 V1.3L' of Chapter 4, was used for the calculations for nitrogen gas with the following settings.

In the reference case, the value of the release time constant was set to 50 seconds (to 1, 10, and 100 s in the sensitivity calculations). The exact knowledge of the time constant associated with dissolution is not that important because the pressure will not likely increase in the studied transients. It is arbitrarily set to 100 seconds. There is no degassing delay.

Table 5.4 summarizes the different versions of the CATHARE code used in the present chapter.

Table 5.4: The versions of CATHARE used for the LOCA Calculations

Name	standard	reinforced condensation	NC dissolution release model
without N_2	CATHARE2 V1.3L	CATHARE2 V1.3L+ reinforced condensation in *volumes*	NA
with N_2	NA	CATHARE2 V1.3L+ reinforced condensation in *volumes* + NC dissolution release model	

5.4 Calculations Performed without N_2 Gas

5.4.1 Main Results

As mentioned in Table 5.4, all the calculations presented in the continuation of this study were performed with 'reinforced condensation' in the *volumes*.

The early stage of the transients is characterized by a fast depressurization of the primary circuit. The primary pressure drops below the secondary pressure a few minutes after the opening of the break.

The chronology of the main events for the 1%, 1.5%, and 2% break sizes is given in Table 5.5. Figures 5.6b and 5.6c shows the global power balances for the coolant of the primary circuit for the different cases (with and without nitrogen gas).

Table 5.5: The chronology of the main events for 1-, 1.5-, and 2-% breaks without nitrogen gas

	1%	1.5%	2%
Accumulators opening	195 s	98 s	77 s
Primary pressure ≤ secondary pressure	400 s - 2 900 s	200 s -	160 s -
Accumulators closure	4922 s SG5 empty	2038 s SG2,3,4,5 empty	1587 s SG2,3,4,5,6 empty
LPIS start $\Delta T_{out\text{-}core,sat}$ [^{o} C] (at LPIS start)	no 20^o C (no LPIS, 10 000 s)	6013 s – 6700 s 22^o C	3520 s – 4040 s 15^o C
Stabilized liquid flow rate through core [kg/s]	225. (at 10 000 s)	150. (at 10 000 s)	105. (at 8 000 s)

Break size 1%

In the case of the smallest break size (1%), the primary inventory of water remains above 85%: limited boiling occurs at the top of the core at the opening of the break. The level in the upper plenum does not reach the level of the entrances to the hot legs.

Heat removal from the core to the steam generators is ensured by single-phase natural circulation. When the primary pressure drops below the secondary pressure (at 400 s), the heat transfer in the steam generators reverses from the secondary to the primary side. The temperatures in the cold legs increase, but the heat exchange tubes are not uncovered. The reduction of the temperature difference between the hot and cold legs causes the loop mass flow rate to fall to a stable value until the closure of the accumulators.

The heat transfer from the secondary to the primary side causes the depressurization of the secondary side. However, when the secondary steam cavities of the SGs further depressurize below the primary pressure (at 2900 s), the sub-cooling of the fluid in the primary circuit prevents any heat transfer from the primary to the secondary until the end of the transient.

When the accumulators close, the primary pressure shows a sharp drop of 0.7 MPa. This is due to the enhanced condensation that occurs in the upper plenum full of sub-cooled water. This condensation in the upper plenum strongly reduces the primary pressure.

The pressurizer fills temporarily, while one of the loops connected to the pressurizer empties. In the corresponding loop (loop 5), the primary side of the SG boils. The downcomer, the

upper plenum and the upper parts of the reactor coolant pumps stay full of water (see Figure 5.7). The water coming from the HPIS maintains a sufficient level at the inlet of the RCPs, even in the loop connected to the pressurizer, which is nearly empty.

The primary pressure stabilizes above the LPIS set point, at 0.82 MPa. This is due to a large water inventory in the primary circuit coupled with a steam inventory that remains constant. This steam is mainly located in the pressurizer where no more condensation occurs. Steam is not evacuated to the break and neither is it condensed.

At stabilization, the levels in the steam generator are above the top-most tubes, except in loop 5.

Break size 1.5%

For the larger break sizes (1.5-2%), the early boiling at the top of the core lasted for between 10 and 15 min and produced steam flows into the collectors of the SGs.

All the steam generators in the unbroken loops, except the one which has a loop seal connection (loop 6), empty on the primary side. The formation of steam plugs in the vertical parts of the loop seals in the corresponding hot and cold legs prevents almost any circulation. Therefore, most of the liquid flows into the broken loop and loop 6. The primary pressure decreases enough to allow the LPIS pumps to be started 1 hour and 40 minutes after the beginning of the transient.

Break size 2%

The situation is quite similar to that for a break size of 1.5%: all the steam generators, except in the broken loop, empty on the primary side. The set point of the LPIS pumps is reached after one hour of the transient.

5.4.1.1 Situation at Break

For every break size, the flow to the break is purely a one-phase liquid throughout the transient, except during a short period in the early stage of the transient. After peaking at the beginning of the transient, the flow rate lessens and reaches a quasi-stable value after the closing of the accumulators and before the LPIS are started (see Figures 5.6b and 5.6c). According to the correlation for the critical mass flow rate (Bestion 1994), the break mass flow rate varies proportionally in relation to the pressure and inversely in relation to the liquid temperature. As long as the effect of the pressure is predominant, the break flow rate falls and then stabilizes along with the primary pressure. In the two larger break size cases, the primary pressure reaches the LPIS set point, the liquid temperature decreases and the break mass flow rate re-increases.

For the smallest break size (1%), there is no flow direction change in the broken cold leg, between the downcomer and the break, until the closure of the accumulators. Then, the flow rate in the broken loop decreases enough to allow a durable flow reversal at the break location: water of the HPIS goes to the break and not in direction of the reactor pressure

vessel (RPV). The temperature at the core outlet stays sub-cooled, the saturation margin reaches 20^{o} C 2 hours and 45 minutes after the opening of the break.

When the break size is large enough (1.5-2%), this flow reversal occurs at the beginning of the transient. Nevertheless, when the collectors of the SGs in intact loops empty, the mass flow rate in the broken loop increases because the blockage of the other loops by steam pockets in the primary side of the steam generators, and liquid may flow from the break towards the RPV.

In the case of a size of 1.5%, the increase of the flow in the broken loop is not large enough to divert the flow from the break towards the RPV before the accumulators close. For the 2% break, the flow reversal lasts for about 10 min before the liquid flows from break towards the RPV.

In both cases, the saturation margin at the core outlet, equal to zero at the beginning of transient, increases after between 10 and 15 min and reaches 15-22^{o} C at the start of the LPIS.

Table 5.6 presents the main events for the different calculations performed.

Table 5.6 The main events for the LOCA calculations

	2%	1.5%	1%
without N_2	opening accus: 76-77 s closure accus: 1586-1589 s LPIS 3520 s UP – 4040 s VD	opening accus: 97-98 s closure accus: 2036-2040 s LPIS 6013 s UP – 6700 s VD	opening accus: 194-195 s closure accus: 4917-4927 s at 11 000 s prim pressure stabilized 0.07 MPa above LPIS set point
with N_2 τ = 1s	opening accus: 75-76 s closure accus: 1443-1445 s LPIS 7010 s UP – 7090 s VD	opening accus: 97-98 s closure accus: 2096-2102 s LPIS 11 701s UP – 11 864 s VD	opening accus: 205-206 s closure accus: 4769-4772 s at 10 000 s prim pressure stabilized 0.04 MPa above LPIS set point
with N_2 τ = 10s	not calculated	not calculated	opening accus: 194-196 s closure accus: 5000 – 5012 s LPIS 9643 s UP – 9932 s VD
with N_2 τ = 50s	not calculated	not calculated	opening accus: 194 – 196 s closure accus: 5094 – 5106 s LPIS 8901 s UP – 9247 s VD
with N_2 τ = 100s	not calculated	not calculated	opening accus: 194 – 196 s closure accus: 5089 – 5102 s LPIS 9035 s UP – 9230 s VD

5.4.2 Sensitivity to Condensation Correlation in *volumes*

This section deals with the injection of sub-cooled water into a *volume*. The standard correlation for condensation in *volumes* was modified to enhance condensation in the upper plenum at the injection of accumulators, which was underestimated. The comparison of the results obtained with the standard version of the code with those obtained with a modification to the condensation in the *volume* module is given here for the 1-% break.

5.4.2.1 Phenomena in the Upper Plenum

At the beginning of the transient, the liquid temperature in the upper plenum reaches the saturation temperature prior to the opening of the accumulators. Then, the water sub-cooling of the upper plenum and the hot legs increases regularly and reaches between 40 and 50^{o} C when the accumulators close. This sub-cooling, substantially reduced after the closure of the accumulators, depends on the break size, a larger sub-cooling that corresponds to a smaller break size. In the case of the smaller break size, the slower fall of the saturation temperature, in accordance with the primary pressure evolution, directly controls the value of the sub-cooling in the upper plenum.

However, the abnormal behavior of the temperature of the steam in the upper plenum was observed for the case of the 1-% break calculated with the standard CATHARE2 V1.3L. Around 500 seconds after the opening of the break, the temperature of the steam shows a superheated value. This superheating could reach 60^{o} C during the transient. It seems, therefore, that the direct contact condensation of the steam by the cold water (40^{o} C), which comes from the accumulators, is underestimated.

5.4.2.2 The Correlation for Condensation in *volumes*

The situation described above is due to a weakness in the condensation correlation used to model transfers of thermal origin between a fluid in the lower sub-volume Ω^{-} and the upper sub-volume Ω^{+} in CATHARE (Dor 1994). This type of problem has not been observed before, because in French pressurized water reactors, the sub-cooled water, which comes from the accumulators, is injected into the cold legs which are modeled as *1-D axial* modules. Thereby, in the standard version of the code, additive condensation terms are used in a *1-D axial* module mesh when this mesh has a sub-cooled liquid source term. Such additive condensation terms do not exist in the case of the *volume* module. For the present study, a modification was introduced into the code in order to increase the energy transfer associated with the condensation of the upper sub-volume towards the lower sub-volume if the lower sub-volume contains a sub-cooled liquid.

This energy transfer term is written as follows:

$$Q^{-} = A_C X_1 \frac{\alpha^{+}(1-\alpha^{-})}{D_H^{0.5}} \frac{(Z_{\max} - Z_C)}{Z_{\max}} (H_l^{-} - H_{lsat}^{-}(P_V)) \qquad (5.1)$$

In the standard version of the code: $X_1 = 0.35$
A modification that was made to increase energy transfer: $X_1 = 0.35 * 1000$

This modification will be referred to in the next section as "reinforced condensation in *volumes*".

5.4.2.3 The Effect of the Modified Correlation for Condensation in *volumes*

The comparison concerns the 1-% break size. Table 5.7 shows a comparison of the histories for standard and reinforced condensation in *volumes*.

With standard condensation in *volumes*, water injected by the accumulators is vaporized in the upper plenum using the over-heated steam present above the water level (i.e. in the upper sub-volume Ω^{+}). The steam fills the upper plenum and at 1400 s the water level reaches the top of the hot leg connections where it stays until the closure of the accumulators (at 400 s). The steam penetrates the hot legs and condenses before reaching the loop seals of the hot legs. The upper plenum refills when the accumulators close at 4000 s.

The collectors of the steam generators (SGs), also modeled by *volumes*, do not exhibit the same phenomenon of steam over-heating. Nevertheless, boiling in the upper tubes layer of the SGs starts when the primary pressure drops below the secondary pressure. At the closure of the accumulators, further reduction of the mass inventory due to the break increases the uncovering of the heat exchange tube bundle. The levels in the SGs oscillate between the two top-most layers.

At the closure of the accumulators, the pressurizer does not refill. The reduction of the primary pressure is regular throughout the rest of the transient and stays above the secondary pressure. The saturation margin is not reduced as in the case of reinforced condensation. The calculation was performed until 8500 s, at which point the primary pressure was still higher than the LPIS set point.

With the reinforced condensation model in *volumes*, the steam in the upper sub-volume stays at the saturation temperature; there is no vaporization of the water coming from the accumulators in the upper plenum. The upper plenum stays full of water throughout the transient. Before the closure of the accumulators, the collectors of the SGs stay full in all the loops as well. When the primary pressure drops below the secondary pressure, the reinforced condensation in collectors maintains the water level above the upper layer. The depressurization rate on the secondary side is faster than in the standard case, and the secondary pressure falls below the primary pressure before the accumulators close.

First, the main effect of enhanced condensation is the faster fall in the primary pressure.

Then, the trend is inverted in comparison to the standard case, when water accumulates in the primary circuit.

The mean discharge flow rate of the accumulators follows this evolution of the primary pressure: a lower primary pressure corresponds to a higher flow rate. Primary pressure with reinforced condensation is higher than with standard condensation during the largest part of the discharge of the accumulators. On the whole, the discharge of the accumulators is about 15 min longer with enhanced condensation.

Table 5.7 A comparison of histories for a 1-% break for standard and reinforced condensation in *volumes*, without nitrogen gas

1%	standard condensation in *volumes*	reinforced condensation in *volumes*
Accumulators opening	195 s	195 s
Primary pressure drops below secondary pressure	600 s level in collectors reaches top-most layer of tubes in SGs	400s collectors stay full
Level in UP reaches HL connections	1400 s	no
Secondary pressure drops below primary pressure	no	2900 s
Accumulators closure	4000 s	5000 s

5.5 *Calculations Performed with N_2 gas*

A reference calculation was performed with the value of the release time constant proposed in the section 'Determination of the Parameters of the Dissolution-Release Model' of Chapter 4, τ =50 s, for a break diameter of 50 mm (1% of the loop cross-section) which corresponds to the typical value of a hypothetical SBLOCA in the Loviisa NPP.

Since the value of the proposed time constant is an average value, sensitivity calculations were performed for the 1-% break size with a release time constant ranging between 1 and 100 s.

Calculations for two other break diameters, 62 mm and 71 mm (1.5% and 2% of the loop cross-section, respectively), were carried out with the release time constant set to 1 s.

5.5.1 Reference Case

This reference case corresponds to the analysis of a 1% break with the release time constant of the dissolution-release model set to τ = 50 s.

Significant degassing occurs mainly in the collectors of the SGs. The water levels in the upper plenum, the top of the downcomer, the casings of the reactor coolant pumps (RCPs) never reach the junctions with neighboring components (see Figure 5.7). Therefore, the break flow is almost purely liquid throughout the transient, and nitrogen gas is expelled mainly by water and not by gas. The levels in the collectors of the SGs are temporarily lowered below the layers of the higher tubes. However, the flow of liquid is maintained through the lowest primary tubes. Hence, natural flow circulation ensures the proper cooling of the core.

Table 5.8 gives a transient scenario and the main thermo-hydraulic events. Three stages can be identified.

Stage 1: Accumulator Injection (195 – 5 100 s)

As in the case without nitrogen gas, the core boils briefly after the opening of the break and the accumulators open at 195 s. The proportion of nitrogen gas increases steadily in the gaseous phase in the primary circuit. The volume of nitrogen gas released in the upper plenum is negligible in comparison to the volume situated above the junctions with the hot legs. At the top of the downcomer, the amount of released nitrogen gas represents a larger percentage of the volume situated above the junctions with the cold legs, but the level remains high. The top of the downcomer does not empty from nitrogen gas. The casings of the RCPs remain full of water.

The flow from the accumulators goes preferentially to the break and stays at a sufficient level in the broken loop to prevent the accumulation of almost any nitrogen gas in the collectors of the SG which stay full of water in the broken loop.

At about 400 s after the opening of the break, the primary pressure falls below the secondary pressure. As long as the primary pressure is lower than the secondary pressure (400 –3000 s), boiling occurs in the highest tube-layer in the SGs of the intact loops. The produced steam accumulates in the collectors, nitrogen gas degasses and also accumulates in the collectors of the SGs in intact loops.

When the secondary pressure drops below the primary pressure at 3000 s, boiling stops in the SGs in intact loops. Steam is then entrained towards the cold legs. At 4000 s, due to the continuous accumulation of nitrogen gas in the cold collectors, $T_{sat}(P_v)$ drops below the liquid temperature and an important boiling event occurs. Steam accumulates in the cold collectors completely expelling the nitrogen gas in the direction of the hot collectors through the highest tube-layer. As a result, the nitrogen-steam mixture, where nitrogen gas is dominant, accumulates in the hot collectors. At the closure of the accumulators, the level in the collectors in the intact loops is at that of the highest tube-layer, the cold collectors are emptied of nitrogen gas that fills the hot collectors.

Stage 2: After the Closure of the Accumulators and Before LPIS (5100 – 9050 s)

When the accumulators close at 5100 s (4900 s without nitrogen gas), the release of nitrogen gas in the gaseous phase in the primary circuit increases shortly. This jump is due to the sudden drop in pressure already mentioned in the calculation without nitrogen gas; then the

release of nitrogen gas in the gaseous phase of primary circuit almost stops. The liquid flow rate is significantly reduced in the broken loop and increased in the intact loops.

The primary pressure drop causes a drop in the partial pressure of the steam in all the loops in the collectors of the SGs. This drop in pressure, combined with the accumulation of nitrogen gas in the hot collectors, increases the liquid temperature above $T_{sat}(P_v)$ in the collectors. The water in the hot collectors boils as well; the levels in the collectors of the SGs reach the first, second or third top-most layers. Along with an increased flow rate in the intact loops, the steam created by boiling in the collectors of the SGs pushes nitrogen gas into the cold legs. The nitrogen gas enters the casings of the RCPs but not sufficiently to significantly drop the level in the casings. Part of the nitrogen gas accumulates at the top of the downcomer. The remaining part of this nitrogen flows through the core bundle and accumulates in the upper plenum up to 5% of the volume situated above the junctions with the hot legs. The level in the upper plenum drops briefly but not until the junctions with the hot legs.

In the intact loops, boiling continues in the hot collectors until 6000 s. Boiling continues in the cold collectors until 8000 s. The nitrogen gas stays trapped in the intact collectors. When boiling stops in the intact cold collectors, condensation refills the collectors above the top-most layer. The nitrogen gas present in highest tube-layers refills the hot and cold intact collectors.

In the broken loop, the primary side of the SG is full of water when the accumulators close. Along with the sharp primary pressure drop, nitrogen gas degasses in both collectors, boiling starts, and a mixture of steam and nitrogen gas opens the highest tube-layer. When boiling stops in the hot collector at 6800 s, the nitrogen gas present in the broken cold collector refills the hot collector via the highest tube-layer.

Stage 3: LPIS Injection (after 9 050 – 9 200 s)

The low pressure safety injection conditions are reached about 2 h 30 min after the opening of the break. The flow rates in the surge lines oscillate in phase opposition: the water entering the pressurizer from one surge line leaves via the second surge line. There is no condensation in the pressurizer that stays saturated. Hence, the level in the pressurizer stays at 2.5 m and the primary circuit holds the steam. When boiling stops in the cold collector at 9500 s in the broken loop, level re-increases in the SG above the top-most layer trapping nitrogen gas in the hot collector.

About 15 min after the LPIS start, subcooling at the core outlet is equal to 18^{o} C. The liquid flow rate through core stabilizes at 350 kg/s (see Figure 5.5). The levels in all the steam generators are stabilized at about 30 cm above the layer of the top-most tubes.

There is nearly no more nitrogen gas in the liquid phase in the primary circuit. During the injection of the accumulators, about 70% of the whole amount of the initial nitrogen gas from the water of the accumulators was ejected in the liquid phase to the break. The amount of nitrogen gas in the gaseous phase of the primary circuit is stabilized. It represents about 30% of the initial amount of nitrogen gas dissolved in accumulators (Table 5.11). The evolution versus time of the distribution of the mass of nitrogen gas between the liquid and gaseous phases is shown in Figure 5.4.

Table 5.9 gives the localization of nitrogen gas in the primary circuit. The nitrogen gas is essentially located at the top of the downcomer, in the collectors of all the loops (except in the cold collector of the broken loop). In these vessels, the volume of nitrogen gas represents about one third of the dead-end volumes. Natural circulation is maintained in the different loops.

Table 5.8 The scenario and main events in the reference case (break 1%, τ = 50 s)

Action	Condition	Time [s]	Thermo-hydraulic event	Steam and N_2 gas behavior
Break in cold leg loop seal opening		0		
Reactor scram	P_{HL}< 10.8 MPa and L_{PRZ} < 2.8 m	46		
HPIS injection RCPs coast down Loop seals connections opening	L_{PRZ} < 2.3 m	52		
Accumulators injection	P_{prim} < 5.5 MPa	195		
		400	$P_{prim} < P_{sec}$ Boiling in SG2-6 starts	Steam cumulates in SG2-6
		3 000	$P_{sec} < P_{prim}$ Boiling in SG2-6 stops	N_2 degasses in SG2-6
		4 000	$T_l > T_{sat}(P_v)$ Boiling in COLDCOL2-6 starts	Steam cumulates in COLDCOL2-6,
Accumulators closure	Accus empty	5 100	Levels in SG2-6 above tube bundle SG1 full of water	N_2 pushed in HOTCOL2-6
		5 100	Drop of P_{prim} Boiling in HOTCOL1-6 and COLDCOL1 starts	Steam produced in SG2-6 pushes N_2 gas accumulated in collectors into cold legs, N_2 gas goes into UP via core
		6 000	Boiling in HOTCOL2-6 stops	
		6 800	Boiling in HOTCOL1 stops	Mass of N_2 in gaseous phase of primary circuit stabilizes
		8 000	Boiling in COLDCOL2-6 stops	
LPIS injection in UP	P_{HL}< 0.75 MPa	8 900		N_2 gas nearly disappeared from the liquid phase in primary circuit
LPIS injection at top of DC	P_{DC}< 0.75 MPa	9 300		
		9 500	Boiling in COLDCOL1 stops	
		10 000	Levels above tube bundle in SG1-6 $\Delta T_{core,out}$= 18° C	N_2 gas at top of DC N_2 gas in HOTCOL1-6 N_2 gas in COLDCOL2-6

Table 5.9 The localisation of nitrogen gas in the vessels[10] of primary circuit at 10 000 s for break 1% (τ=1, 50 s)

Component	Content of gaseous mixture above water level (10 000 s) (τ=1 s)	% of dead-end volume occupied by gaseous mixture (10 000 s) (τ=1 s)	Content of gaseous mixture above water level (10 000 s) (τ=50 s)	% of dead-end volume occupied by gaseous mixture (10 000 s) (τ=50 s)
Top of downcomer	nitrogen gas	15	nitrogen gas	30
Upper plenum	nitrogen gas	20	nitrogen gas	2
Hot collector in broken loop	nitrogen gas + steam	10	nitrogen gas	25
Cold collector in broken loop	steam + nitrogen gas	45	-	-
Pump casing in broken loop	nitrogen gas	100	-	-
Hot collectors in loops 3,4,6	nitrogen gas + steam	35	nitrogen gas	30
Cold collectors in loops 3,4,6	nitrogen gas + steam	25	nitrogen gas	30
Hot collector in loop 2	-	-	nitrogen gas	30
Cold collector in loop 2	-	-	nitrogen gas	35
Pump casing in loop 2	nitrogen gas	100	-	-
Hot collector in loop 5	nitrogen gas	60	nitrogen gas	35
Cold collector in loop 5	steam	60	nitrogen gas	30
Pump casing in loop 5	nitrogen gas	70	-	-
Pressurizer	-	-	steam	85

[10] Not mentioned in this table, for fast degassing (τ = 1s), there is also N_2 gas present in cold legs at the inlet of the RCPs in the broken loop and loop 2.

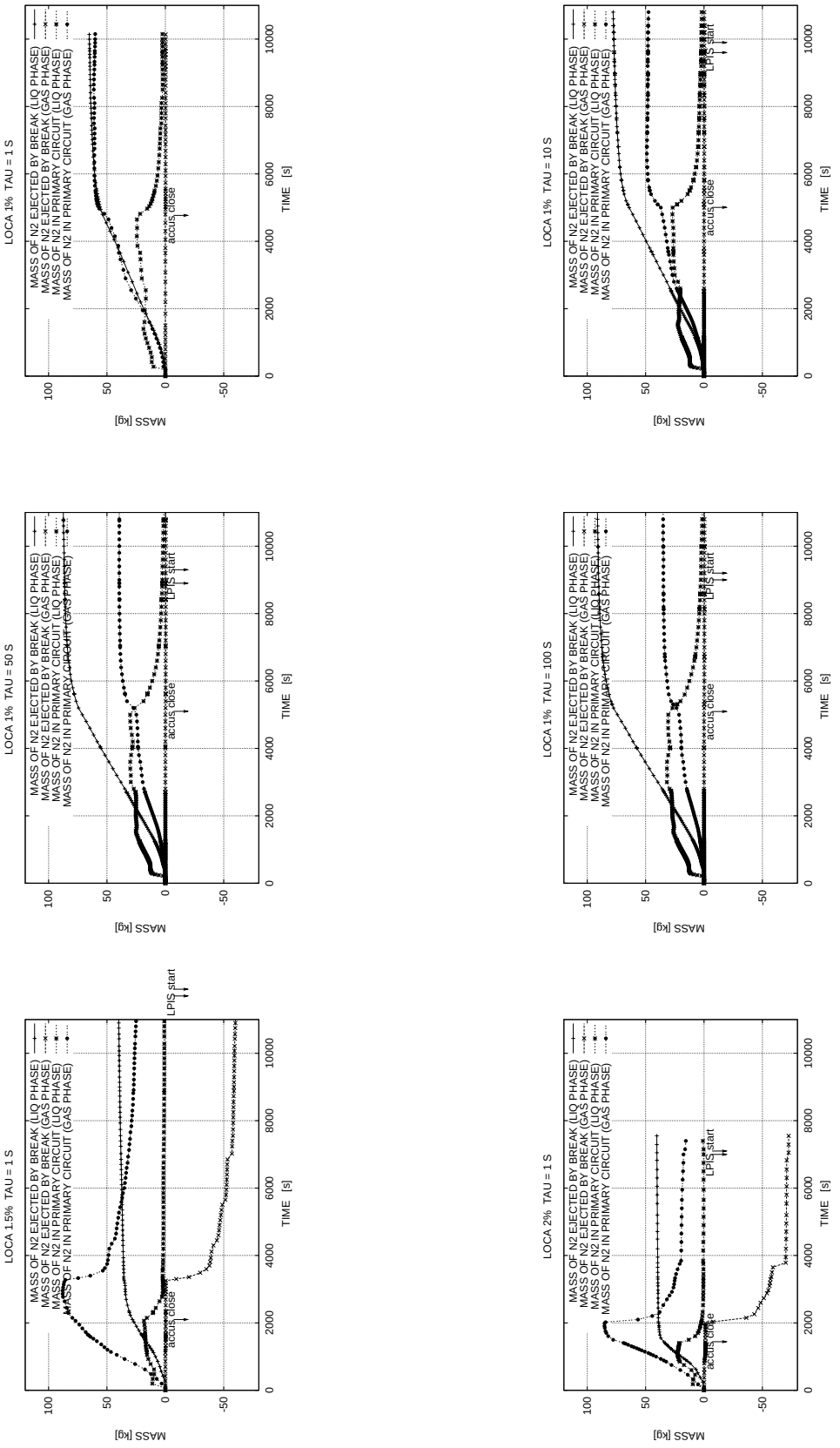

Figure 5.4. The histories of the distribution of masses of nitrogen gas between the liquid and gaseous phases for the different cases.

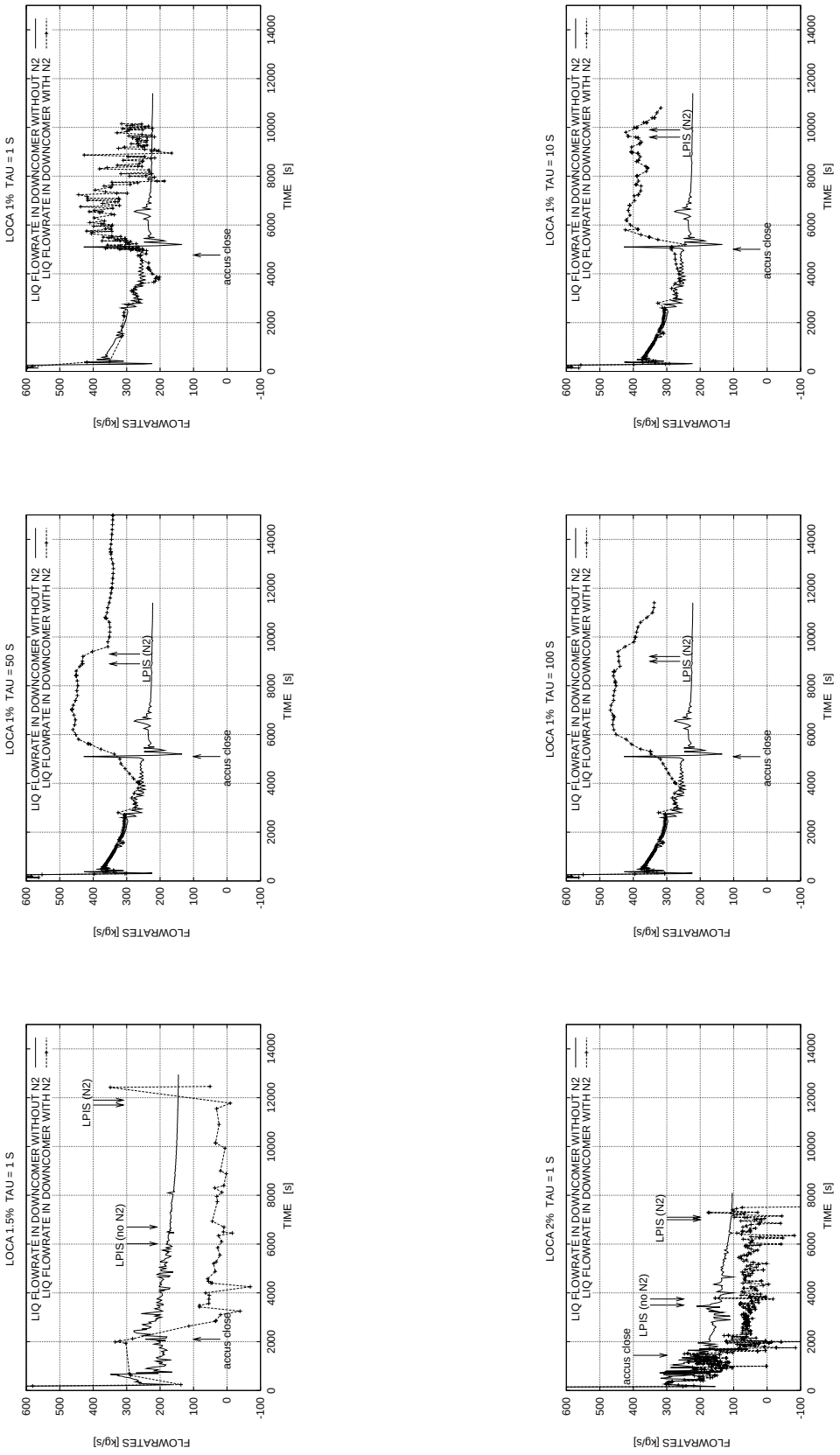

Figure 5.5. The liquid flow rate in the downcomer, with and without nitrogen gas, for the different cases.

5.5.2 Sensitivity to the Release Time Constant τ

The influence of the value of the release time constant, τ, was studied for the 1-% break for three values of the release time constant (τ =1, 10, 100 s).

In the primary loops, the typical values of liquid flow rate range from 50 to 150 kg/s. The corresponding velocities in the hot and cold legs are not larger than 1 m/s. For a release time constant of 1 s, the released nitrogen dissolved in the water of the accumulators will likely be located in the vessels where the accumulators inject: the upper plenum and top of the downcomer. An increase of one or two orders of magnitude of τ delays the release of nitrogen. Then, less nitrogen is released in the upper plenum and the top of the downcomer and more in the collectors of the steam generators which are situated at about 15 m from the upper plenum. It should be pointed out that the dissolution-release model homogenizes the NC gas-water mixture in the *volumes*. In reality, these *volumes* contain higher local concentrations of NC gases in the water near the injection points of the accumulators.

The early stage of the transient is the same than as in the case in which nitrogen was not included and in the reference case. The opening and closure of the accumulators occur at nearly the same instant with or without nitrogen. The top of the core boils temporarily at the very beginning of the transient.

As in the cases calculated without nitrogen gas, heat transfer at the steam generators reverses from the secondary to the primary side.

As for the reference case, for the studied range of release time constants, the amount of released nitrogen gas in the upper plenum is too small to lower the water level until the junctions with hot legs (see Figure 5.7). Therefore, the break flow is almost purely liquid throughout the transient, the nitrogen gas is expelled mainly by the water and not by the gas.

τ = 1 – 10 s

When the release time constant decreases, the release of nitrogen gas in the gaseous phase is faster and the amount of nitrogen gas dissolved in the liquid ejected to the break is smaller. Hence, the amount of nitrogen gas present in the gaseous phase in the primary circuit at stabilization will be larger (see Figure 5.4). In the case of the fastest degassing (τ = 1 s), the primary pressure remains about 0.4 MPa above the LPIS set point in the late phase of the transient. This is due to the large amount of nitrogen gas trapped in the primary circuit, supplemented by a large liquid mass inventory in the primary circuit - the HPIS mass flow rate is slightly larger than the break mass flow, and all the steam is condensed.

Nitrogen gas retention at the top of downcomer is more important; the quantity of degassed nitrogen gas is large enough to escape from the top of downcomer, which drains partly from nitrogen gas (see Figure 5.7). The faster degassing takes place, the earlier draining occurs and the longer it lasts. This draining occurs between 1 and 1.5 hours after the opening of the break and lasts for between 10 and 15 min.

Nitrogen gas flows into the cold legs and fills the casings of the RCPs in the broken loop (loop 1) and one loop connected at pressurizer (loop 2). The level is situated below the junction with the pump impeller. The junction of the cold leg with the *volume* representing the pump casing is 24 cm lower than the top of the *1-D axial* representing the impeller (see the section entitled "Nodalization" in the present chapter, and Figure 5.3). For the considered break size, the liquid flow circulates in the direction of the Reactor Vessel along the broken cold leg. Hence, circulation is interrupted in the casings of the RCPs of loops 1 and 2. In loop 2, the flow from the HPIS injection returns to the cold collector and maintains the water level in the steam generator far above the top-most tubes layer or at the top of the collectors. The flow rate in loop 2 being inverted, the flow from the HPIS is pushed in the pressurizer via the surge line, and the pressurizer starts to refill about 2 hours after the break opening. In loop 1, the HPIS flow goes to the break. Despite the interruptions in the circulation in the casings of the pumps of the broken loop and loop 2, the value of the liquid flow rate through the core remains at 300 kg/s, thanks to the HPIS of the intact loops 3-6 (see Figure 5.5).

For τ = 1 s, nitrogen gas is liberated from the upper part of the casing of the RCP in the broken loop, the water level drops below the junction with the cold leg. Nitrogen gas flows towards the steam generator and stays trapped in the loop seal of the cold leg. This two-phase mixture in the neighborhood of the break induces strong oscillations of the flow to the break in primary circuit and levels in the SGs. Nevertheless, the amount of nitrogen gas expelled to the break is negligible.
For τ = 10 s, the void fraction in the neighborhood of the break is lower and there are no oscillations.

For the faster degassing (τ = 1, 10 s), 2.75 h after break opening nitrogen gas is essentially located at the top of the downcomer, in the casings of the pumps and in the horizontal part of the cold leg at the inlet of the RCPs in the broken loop and loop 2. There is mixture of nitrogen gas and steam in the collectors of all the loops (except in loop 2, where the HPIS injection flows through the steam generator) representing from 10 to 60% of the dead-end volumes there.

<u>τ = 100 s</u>

The transient scenario described for the reference case (τ = 50 s) is reproduced for the larger release time constant (τ = 100 s) with the exception of the total disappearance of steam from the primary circuit at stabilization. This is due to a complete condensation of the steam in the pressurizer.

Table 5.6 presents the main events for the different calculations performed. Figures 5.6a, 5.6b and 5.6c show the global power balances for the coolant of the primary circuit for the different cases in question.

A detailed repartition of the nitrogen gas and steam in the vessels of the primary circuit is given in Table 5.9 for the two main different regimes types observed (τ =1 and 50 s).

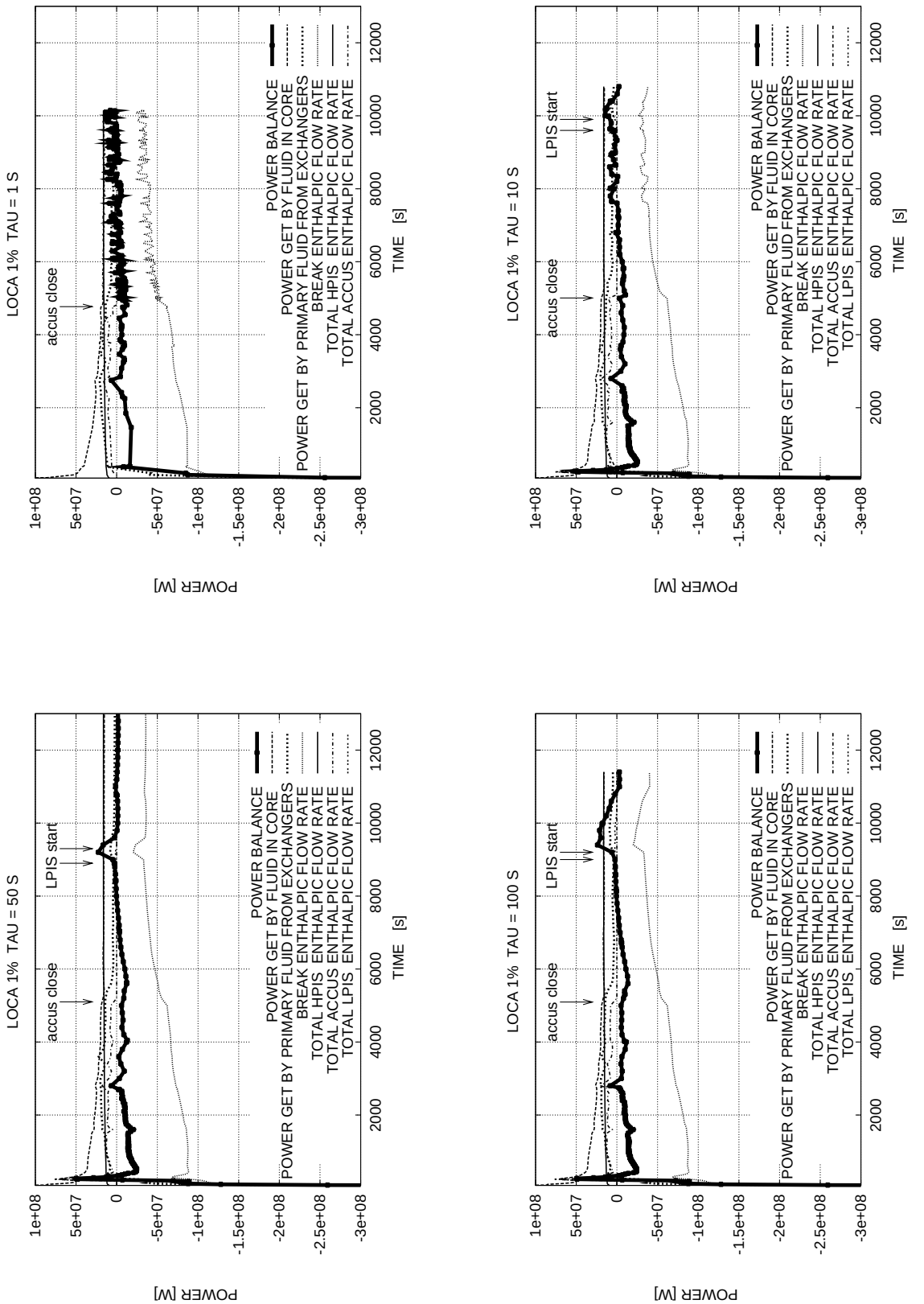

Figure 5.6a. The global power balances for the coolant of the primary circuit for the break size 1%, for the different values of the release time constant.

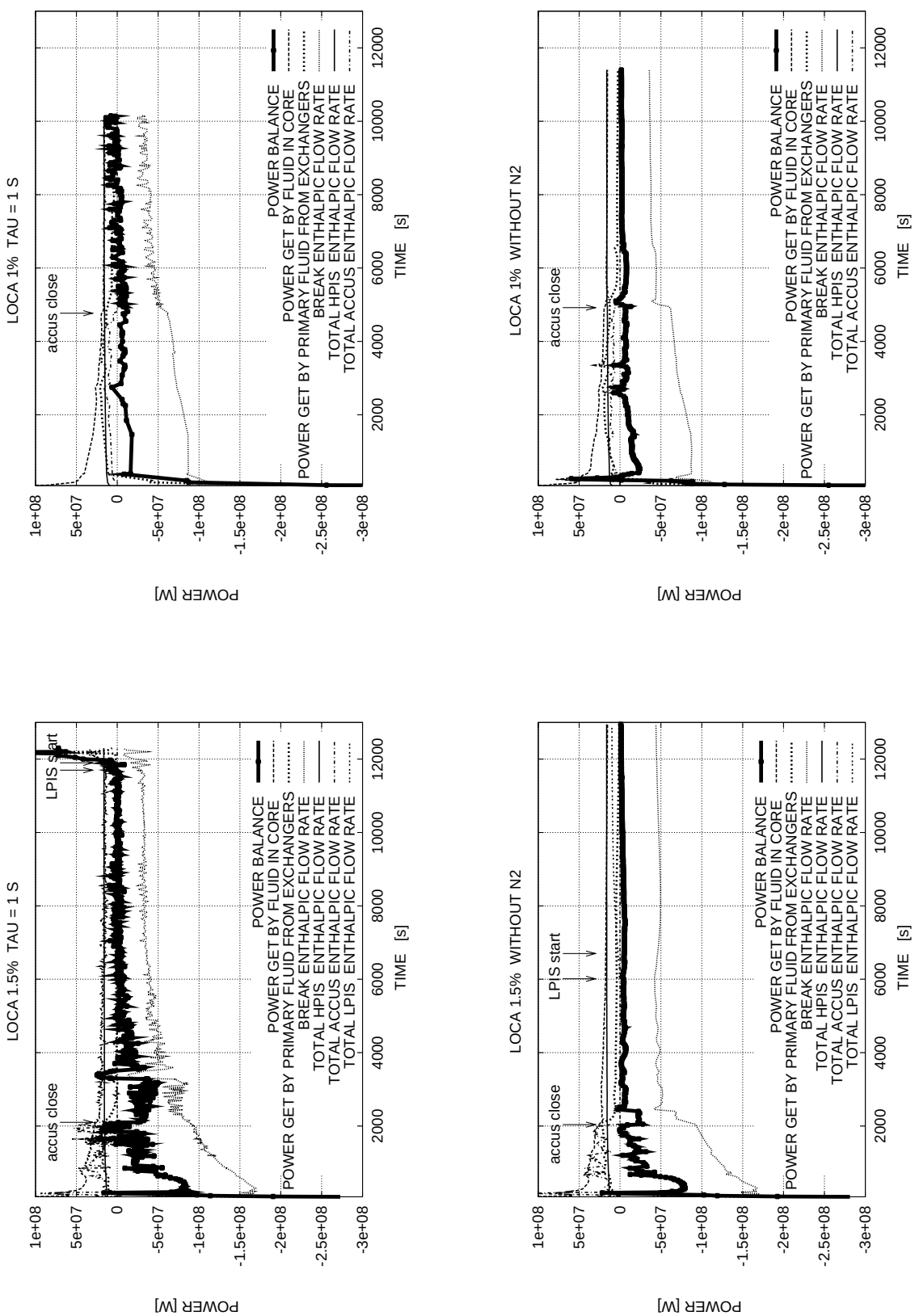

Figure 5.6b. The global power balances for the coolant of the primary circuit, with and without nitrogen gas, for the break sizes 1%, 1.5%.

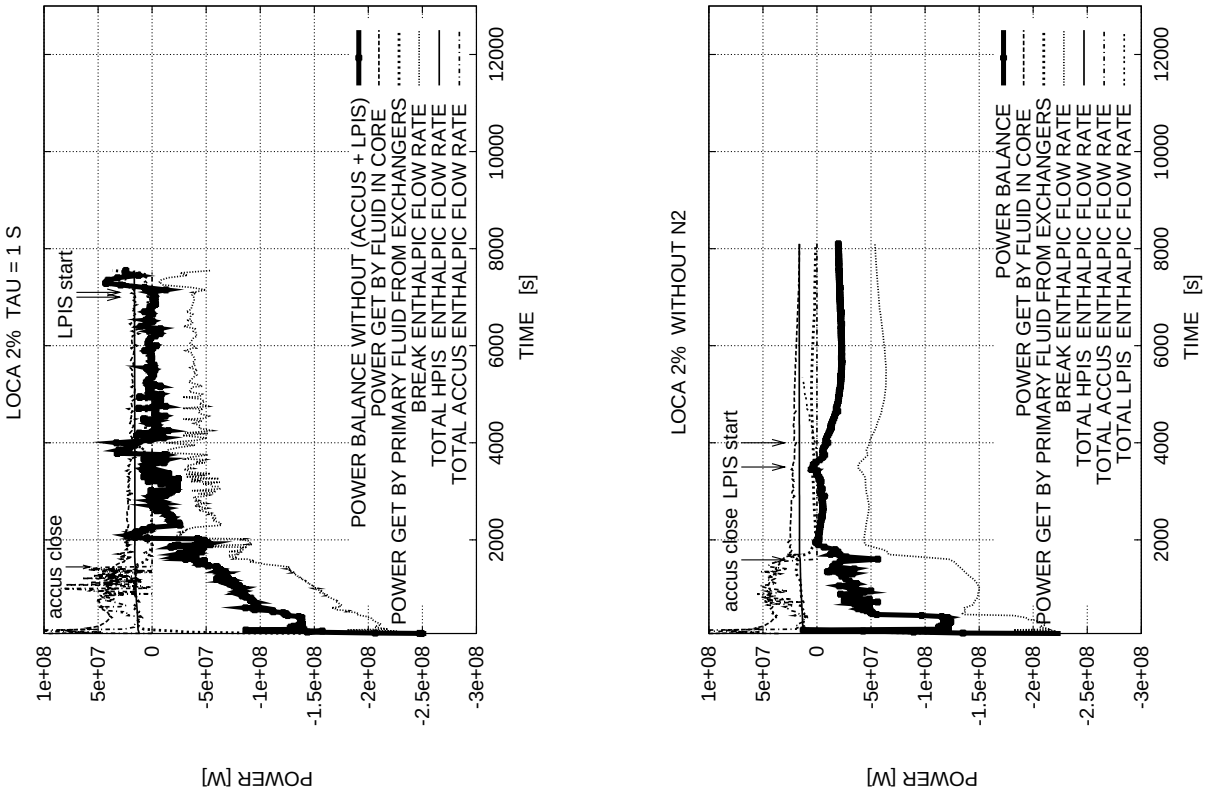

Figure 5.6c. The global power balances for the coolant of the primary circuit, with and without nitrogen gas, for the break size 2%[11].

For this value of the break size, the main effect of considering the effect of the NC gas dissolved in the primary coolant is a clear reduction of the saturation margin at the core outlet. At the start of LPIS - between 2.5 and 3 h after the break opening - (or 2.75 h after the opening of the break for τ = 1 s), the subcooling at the core outlet is about 10^{o} C, for all the values of τ (see Table 5.10). This value is half of the value obtained in similar conditions without nitrogen gas.

When LPIS starts, the amounts and locations of the nitrogen gas in the primary circuit under the different phases are nearly stabilized. The masses and volumes of nitrogen gas and the masses of steam present in the primary circuit are given in Table 5.10 for the different release time constants studied. The calculation of the volumes of nitrogen gas and steam were been performed using the formula of ideal gases at the mentioned temperature and pressure.

For all the considered values of the release time constant, the water level in the SGs stabilizes at or above the layer of the top-most tubes in every loop.

Contrary to the reference case, the primary circuit emptied steam 2.75 h after the break opening for every release time constant studied.

[11] In the figure with nitrogen gas, due to problems encountered in the post-processing of the results:
- the curve of the power balance does not include terms related to the accumulators and LPIS
- the curve of LPIS is not represented here.

Table 5.10 The masses of nitrogen gas /steam in the primary circuit when the LPIS starts (τ = 1, 10, 50, 100 s) (1% break)

τ [s] P, T at core outlet	1 10 000 s (LPIS not started) 0.80 MPa, 161° C	10 9 600 s 0.77 MPa, 161° C	50 8 900 s 0.77 MPa, 159° C	100 9 000 s 0.78 MPa, 160° C
$\Delta T_{out\text{-}core,sat}$	9° C	7° C	10° C	9° C
N2 gas mass [kg]	60	48	39	35
Steam mass [kg]	21 (0% in PRZ)	79 (86% in PRZ)	174 (66% in PRZ)	187 (62% in PRZ)
N2 gas volume [m^3]	9.7	8.0	6.5	5.8
Steam volume [m^3]	5.3	20.5	45.1	48.0
Total volume of gas [m^3]	15.0	28.5	51.6	53.8

5.5.3 Sensitivity to the Break Size

The calculations were performed for intermediate break sizes: 1.5%, 2%, for fast degassing (τ = 1 s).

For this value of the release time constant and these break sizes, the main effect of considering the NC gas dissolved in the primary coolant is:

- a clear reduction in the flow rate through the core,
- a clear reduction of the water inventory in the Steam Generators,
- a delay in the LPIS actuation (1h45 for 1.5%, 1h00 for 2% break).

Soon after the break opening and as with the cases calculated without nitrogen gas, first boiling occurs at the top of the core. The steam from the core fills the collectors in two (1.5%, loops 2 and 5) or four (2%, loops 2, 3, 4, and 6) intact loops. Natural circulation is definitively stopped in the SGs of these loops 10 to 15 min after the break opening. In the other loops, the steam flows in hot legs in direction of the SGs: the water level stabilizes in the front of the top-most tubes.

When degassing is fast enough, there is enough nitrogen gas at the top of the downcomer to lower the level until the junctions with the cold legs. A partial draining starts about 18 to 25 min after the opening of the break and lasts for about 12 min, ending shortly after the closure of the accumulators (the accumulators close 25 to 35 min after the break opening). This nitrogen gas accumulates into the casings of the pump of the broken loop. In the case of the larger break size (2%), it also accumulates in the casing of the RCP of a loop connected to the pressurizer (loop 5). The level in the pump casing drops below the connection with the cold leg (broken loop) or in the front of this junction (loop 5). See Figure 5.7.

For these larger break sizes (and contrarily to the 1-% break), the flow is reversed, in the broken cold leg from the reactor pressure vessel towards the break. Unlike the cases calculated without nitrogen gas, this flow reversal in the broken loop lasts throughout the transient. The reason is a lower flow rate in the broken loop with nitrogen gas than without it. Then, the accumulation of nitrogen gas in the pump casing of the broken loop does not even

completely interrupt this circulation. But circulation is stopped in loop 5 and HPIS injection goes to steam generator 5 (1 h 10 min after the opening of the break).

Unlike the cases calculated without nitrogen gas, prolonged boiling occurs at the top of the core after the accumulators close: at the core outlet the temperature increases and reaches $T_{sat}(P_v)$. The steam produced accumulates at the top of the upper plenum. Simultaneously, the fast degassing in the upper plenum accumulates nitrogen gas as well. Eventually, about 10 min after the closure of the accumulators, the level in the upper plenum reaches the junctions with the hot legs and a mixture of steam + nitrogen gas circulates in the hot legs towards the steam generators (see Figure 5.7). The nitrogen gas goes to the break.

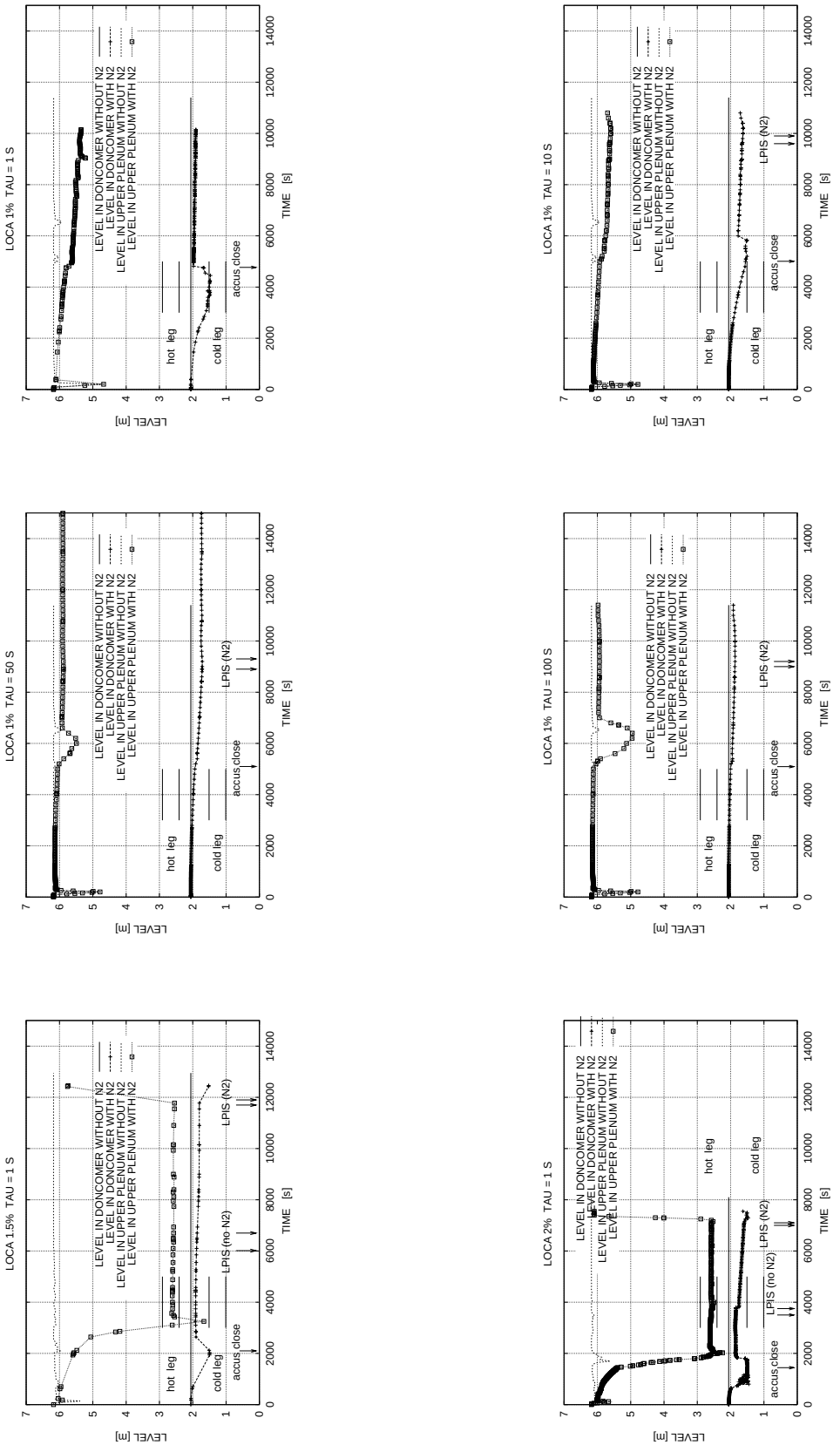

Figure 5.7. The levels in the downcomer and the upper plenum, with and without nitrogen gas, for the different cases.

In the loops where circulation was maintained: the broken loop and loops 3, 4 and 6 (1.5%) as well as loop 5 (2%), the primary tube bundle are completely uncovered when the level in the upper plenum drops and reaches the top of the connections to the cold legs.

Then (by manometric effect), the level re-increases in the reactor pressure vessel. The upper plenum refills until the junctions with the hot legs. This also causes a temporary refilling of the collectors in the remaining active intact loops (1.5%, loops 3,4 and 6), (2%, loop 5). Then, the water inventory in these SGs decreases completely after some minutes:

- break 1.5%: in loops 3,4 and 6, the liquid flow rate oscillates around a low value (few kg/s) until the water level definitively reaches the bottom of the collectors 1 h 10 min after the break opening, then liquid flow rate stops in these loops through the SGs,

- break 2%: the circulation stops only momentarily in the SG of loop 5, 40 min after the opening of the break. The circulation in the SG resumes when the level in the pump casing drops below the junction with the impeller 25 min later. The water of the HPIS flows towards the SG, refills it entirely and the flow goes to the core via the upper plenum.

Circulation is maintained in the broken loop. The liquid flow rate from the upper plenum goes into the SG. The level in the hot collector is maintained above the bottom-most layer. The boiling in the primary tubes fills the cold collector with steam. This steam also fills the loop seal of the cold leg and is expelled by the break.

The flow rate through the core drops when the level in the upper plenum reaches the elevation of the connections with the hot legs. Circulation is maintained owing to the water coming from the HPIS pumps of the intact loops. The average value of the flow rate (50 kg/s) is two to three times lower than in the corresponding cases calculated without nitrogen. It exhibits oscillations and reverses in the core bypass, and possibly in the bottom of the RPV and downcomer (see Figure 5.5).

Between 2 and 3 hours (2% and 1.5%, respectively) after the opening of the break, the pressure reaches the LPIS set point and the primary circuit refills. An earlier refilling corresponds to a larger break size. About 10 min after the start of the LPIS, subcooling at core outlet reaches 36^{o} C (respectively 18^{o} C) for a 1.5-% break (respectively 2%).

The remaining nitrogen gas in the primary circuit is mainly located at top of the downcomer, in the pump casing of the broken loop, and in the horizontal part the cold leg in the inlet of the RCP. There is also, to a lesser extent, nitrogen gas in the loops that have a loop seal connection: in the casings of the RCPs and in the hot leg loop seals (inclined section). In the case of the 2-% break, as seen before, there is also nitrogen gas in the casing of the RCP in loop 5. In this loop, the HPIS injection entrains nitrogen gas towards the cold collector where it stays trapped when the SG5 refills with water.

The fastest disappearance of nitrogen from the liquid or gas in the primary circuit corresponds to the largest break size.

5.5.4 Evolution of the N_2 Gas Quantities versus Time

Figure 5.4 shows the histories of the distribution of masses of nitrogen gas between the liquid and gaseous phases.
In all the cases, about 20% of the total amount of nitrogen dissolved in the accumulators before the transient is present in the liquid of the primary circuit for as long as the accumulators are opened. When the accumulators close, the concentration of dissolved nitrogen in the primary circuit naturally decreases. It disappears almost totally after an elapsed time that varies from 20 minutes (1.5-2%) to 1 hour (1%) after the closure of the accumulators. For a 1-% break, this value remains the same with every release time constant value.

In the case of larger break sizes, the amount of nitrogen gas present in the gaseous phase of the primary circuit falls radically when the flow rate at the break becomes two-phased between 30 min (2%) and 1 hour (1.5%) after the opening of the break. For the smallest break size, the amount of nitrogen gas present in the gaseous phase of the primary circuit increases regularly until the closure of the accumulators and then remains constant. The maximum amount of nitrogen gas present in the gaseous phase of the primary circuit varies between 10 and 70% of the total amount of nitrogen. This value decreases when τ increases and when the break size increases.

Break size 1%
About three hours after the opening of the break, 50-70% of the total amount of the nitrogen dissolved in the accumulators before the transient has been ejected through the break in the liquid phase; the remaining nitrogen is present in the primary circuit in the gaseous phase.

Break sizes 1.5-2%
About three hours after the opening of the break, 50-60% of the initial amount was ejected through the break in the gaseous phase. Of the remaining nitrogen, 30% was expelled in the liquid phase and 10-20% was present in the gaseous phase in the primary circuit.

Table 5.11 shows the distribution of nitrogen gas at stabilization:
- the ejected masses in the break,
- the masses and volumes present in primary circuit.

It also includes the calculation of
- the volumes that nitrogen gas would occupy at atmospheric pressure and for three different saturation margins ($\Delta T_{out\text{-}core,sat}$ = 10° C, 20° C, and 40° C).

The corresponding volumes occupied by the nitrogen gas in the primary circuit range from 65 m^3 to 15 m^3 for the different cases considered. The highest value corresponds to the smallest break size, the smallest value of the saturation margin and the fastest degassing.

Considering the reference case (break 1%, τ = 50 s), at a pressure of 0.1MPa and a saturation margin of 40° C, the nitrogen gas trapped in the primary circuit would occupy a volume equivalent to 39 m^3 which is about two thirds of the total volume of the primary side of the steam generators.

Table 5.11 The distribution of the nitrogen gas at stabilization: the ejected masses in the break and the masses and volumes in the primary circuit

break size	1%	1%	1%	1%	1.5%	2%
release time constant τ [s]	1	10	50	100	1	1
at time [s] P at core outlet [MPa] T at core outlet [^{o} C] $\Delta T_{out\text{-}core,sat}$ [^{o} C]	10000 0.80 161 9	10000 0.75 161 6	10000 0.83 154 18	10000 0.76 152 16	12300 0.51 106 46	7600 0.57 139 18
N_2 mass ejected at break (liquid phase) [kg]	65	77	89	92	41	40
N_2 mass ejected at break (gaseous phase) [kg]	0	0	0	0	67	73
N_2 mass present in primary (liquid phase) [kg]	3	2	0	1	1	0
N_2 mass present in primary (gaseous phase) [kg]	60	48	39	35	22	15
N_2 volume present in primary (gaseous phase) [m^3] at P, T	9.7	8.3	6.0	5.8	4.9	3.9
N_2 volume present in primary (gaseous phase) [m^3] at 0.1MPa, $\Delta T_{out\text{-}core,sat}$= 10^o C	64.7	51.8	42.1	37.8	23.7	16.2
N_2 volume present in primary (gaseous phase) [m^3] at 0.1MPa, $\Delta T_{out\text{-}core,sat}$= 20^o C	62.9	50.3	40.9	36.7	23.1	15.7
N_2 volume present in primary (gaseous phase) [m^3] at 0.1MPa, $\Delta T_{out\text{-}core,sat}$= 40^o C	59.4	47.5	38.6	34.6	21.8	14.8

During the intermediate break LOCA, it is mainly steam and not nitrogen gas that lowers the level in the upper plenum until the junctions with the hot legs. It is anticipated that in the IBLOCA transients calculated using the value of the release time constant, τ, equivalent to 50 s, the level in upper plenum will reach the junctions with the hot legs and the nitrogen gas will be expelled by the gaseous flow at the break, as happens in the IBLOCA calculated for a smaller value of τ. The amount of nitrogen gas expelled in the gaseous phase in the break will be certainly smaller than the value predicted for a fast degassing (2%, τ = 1 s), 73 kg.

5.5.5 Situation in the Steam Generators

Break size 1%

First, a more or less important degassing event occurs in the collectors, depending on the value of the release time constant. Simultaneously, when the primary pressure drops below the secondary pressure, boiling occurs in the top-most tubes. This boiling stops when the secondary pressure drops below the primary pressure. The closure of the accumulators induces a drop in the primary pressure, which initiates a sharp increase in the amount of nitrogen degassed, particularly in the collectors. Consequently, flashing is observed in the cold collectors. Flashing occurs when $T_{sat}(P_v)$ drops below the liquid temperature (T_l is higher in cold collectors than in the hot collectors), due to a sufficient concentration in the nitrogen gas in the gaseous phase in the cold collectors. An important amount of steam is produced, which lowers the water level in the steam generators. This amount is more important in the

case of slow degassing. This uncovers the primary tubes from the first layer (τ = 1s) to the third layer (τ = 50,100 s). Then, the nitrogen gas flows from the cold collectors to the hot collectors, more or less completely emptying the cold collectors from nitrogen gas. In the case of the fastest degassing, some nitrogen gas remains in the cold collectors. The partial pressure of the steam re-increases, $T_{sat}(P_v)$ increases, boiling stops, and condensation occurs. Then, the level re-increases in the steam generators, pushing the nitrogen present in the primary tubes in the collectors. Tstat(Pv) decreases below the liquid temperature in the cold collectors and boiling recommences. The oscillations stop only when the LPIS starts and the collectors refill.

Break sizes 1.5-2%

When there is enough nitrogen gas in the collectors of the SGs, the liquid temperature exceeds $T_{sat}(P_v)$ and boiling occurs. The levels in the SGs are lowered and the nitrogen flows towards the break.

For these larger break sizes, the low water inventory allows the nitrogen to circulate towards the break. There is almost no nitrogen gas trapped in the primary side of the steam generators; hence, there are no oscillations of the water levels in the SGs as in the case of the smaller break size.

Table 5.12 presents a summary of the location of nitrogen gas and steam in the Steam Generators when the LPIS starts for the studied cases.

Table 5.12 The location of steam – nitrogen gas in the SGs at the start of the LPIS

	without N_2	τ = 1 s	τ = 10 s	τ = 50-100 s
1% above water level in collectors:	(at 10 000 s) level in SG1-4,6 at top steam	(at 10 000 s) level in SG1,3-6 oscillates at the top-most layer level in SG2 at top N_2 gas + steam	level in SG1,3-6 oscillates in front of the three top-most layers level in SG2 above top-most layer N_2 gas + steam	level in SG1 above top-most layer level in SG2-6 oscillates in front of the three top-most layers N_2 gas + steam
1.5% above water level in collectors:	level in SG1,6 at top steam	level in hot collector in SG1 above bottom-most layer level steam	-	-
2% above water level in collectors:	level in SG1 at top steam	level in hot collector in SG1 above bottom-most layer level level in SG5 at top steam	-	-

5.6 Performance of Calculation

As mentioned in section 'Content of the CATHARE version' of the present chapter, the problems associated with calculations involving NC gases performed using the standard version of the code, were investigated by the code developers and solutions were found for correcting the anomalies. Although the corrections were introduced in the version of CATHARE that was used for the calculations involving nitrogen gas, unsolved problems remain in certain situations[12]. In the case of the fastest degassing, the calculation must be performed using small time steps (the average value is around 1 ms). This results in lengthy calculations and the intensive usage of CPU.

The simulation of 10 000 –12 000 seconds of transient time consumed between 3.10^5 and 8.10^7 seconds of CPU time on HP 9000/710 and SGI Origin 2000 computers (see Table 5.13).

The average time step ranged from 2.10^{-3} s to 6.10^{-3} s, and elementary time from 4.10^{-3} s/mesh/iteration to 3.10^{-2} s/mesh/iteration (on SGI Origin 2000).

Table 5.13 CPU time

	1.0%	1.0%	1.0%	1.0%	1.0%	1.5%	1.5%	2.0%	2.0%
	no N2	tau=1 s	tau=10 s	tau=50 s	tau=100 s	no N2	tau=1 s	no N2	tau=1 s
	HP 9000/71X	HP 9000/71X	SGI Origin 2000/300	SGI Origin 2000/300	SGI Origin 2000/300	SGI Power Challenge	HP 9000/71X	HP 9000/71X	DEC /COMPAQ Alpha 600
R Speed Ratio /HP 9000/71X	1.0	1.0	6.0	6.0	6.0	1.5	1.0	1.0	2.0
Mp nb meshes primary	661	661	661	661	661	661	661	661	661
Ms nb meshes secondary one loop	22	22	22	22	22	22	22	22	22
Texp experiment time simulated [s]	1.14E+04	1.02E+04	1.09E+04	1.65E+04	1.15E+04	1.30E+04	1.23E+04	8.14E+03	7.56E+03
Tcpu CPU time [s]	3.60E+05	9.09E+06	1.20E+06	3.83E+05	3.09E+05	9.75E+05	8.00E+07	3.71E+05	8.39E+06
N nb total iterations	3.25E+05	4.26E+06	1.71E+06	8.54E+05	6.31E+05	5.03E+05	2.40E+07	4.52E+05	9.96E+06
n nb total time steps	1.79E+05	1.99E+06	4.51E+05	2.56E+05	1.90E+05	2.73E+05	9.14E+06	1.95E+05	3.87E+06
N/n	1.8	2.1	3.8	3.3	3.3	1.8	2.6	2.3	2.6
Tcpu/Texp (Tcpu converted to SGI Origin 2000/300 time equivalent)	5	149	110	23	27	19	1082	8	370
Texp/n average time step size [s]	0.064	0.005	0.024	0.064	0.061	0.048	0.001	0.042	0.002
Tcpu/sigma(Mi*Ni) elementary time [s/mesh/iter]	0.0052	0.0054	0.0035	0.0036	0.0034	0.0070	0.0074	0.0033	0.0020

[12] Since then, more recent versions of the code have been improved regarding these problems.

5.7 Summary of the Results

The effect of the nitrogen gas released in the primary circuit on core cooling during the postulated LOCA accidents was studied for the VVER-440 geometry of the Loviisa NPP. Qualitative calculations indicate that at a pressure equal to 0.27 MPa and a typical saturation margin of 40^{o} C, the total amount of nitrogen gas dissolved in the accumulator water of the primary circuit would occupy a volume equivalent to the total active volume of the steam generators (6 x 10 m^{3}) (SGs). If the whole amount of nitrogen gas stays trapped in SGs, it would totally inactivate heat exchanges between the primary and secondary circuits. In the case of a small break, this may prevent the proper cooling of the core.

Small and intermediate break LOCA transients were calculated using the CATHARE code for a break situated in the cold leg at the bottom of the loop seal. Calculations were performed for different break sizes: 50 mm (the typical value of a hypothetical SBLOCA for the Loviisa NPP), 62 mm and 70 mm (1%, 1.5%, and 2% of the loop cross-section, respectively).

Version V1.3L Revision 5 of the CATHARE2 code was used, including the dissolution-release model and the standard interfacial friction coefficient which was validated for steam bubbles, but not for small nitrogen bubbles. As a consequence, the separation of nitrogen gas from the liquid may be overestimated in the hot and cold legs and the transportation of nitrogen gas to large vessels, such as the upper plenum, the top of downcomer, the casings of the RCPs and the collectors of the SGs may be underestimated. This 'too prompt' separation of nitrogen gas in hot and cold legs would force the flow rate to be larger than in reality – at least for the SBLOCA (see Figure 5.5) - and may lead to a non-conservative evaluation of the heat transfer phenomena.

A SBLOCA (1% of the cross-section in the cold leg loop seal) was calculated using a release time constant, τ, equivalent to 50 s as a reference case. This value of the release time constant corresponds to the value determined in Chapter 4 'Analysis of NC Gas Release Experiment'. When the LPIS set point is reached, at a pressure of 0.1 MPa and a saturation margin of 40^{o} C, the nitrogen trapped in primary circuit would occupy a volume that is about two thirds of the total volume of the primary side of the SGs. Nevertheless, this nitrogen is present not only in the collectors of the SGs but also in the top of the downcomer. The amount of nitrogen gas remaining in the primary circuit decreases when τ increases and when the break size increases.

In the case of a SBLOCA (calculated for τ = 1, 10, 50, 100 s), nitrogen gas is expelled to the break only under the liquid phase. A rather large proportion, 30% to 50%, of the nitrogen gas, initially dissolved in the water of the accumulators, remains in the gaseous phase at the top of the downcomer and in the collectors of the SGs. The presence of nitrogen gas in collectors of the SGs induces oscillatory behavior in the levels that stay in the front of the three top-most layers of the tubes. These oscillations cease at the initiation of the LPIS, and the collectors refill. At the actuation of the LPIS, the presence of nitrogen divides the saturation margin at the core outlet by a factor 2, when compared to the cases calculated without nitrogen gas: 10^{o} C. For fast degassing (τ = 1 s), the primary pressure stabilizes at 0.4 MPa above the LPIS set point.

In the case of IBLOCA (calculated for τ = 1 s), the nitrogen gas goes to the break when the boiling at the top of the core lowers the levels until the connections with the hot legs. Hence, at the actuation of the LPIS, 10 to 20% of the nitrogen gas, which is initially dissolved in the water of the accumulators, remains in the gaseous phase in the primary circuit. This nitrogen gas is mainly situated at the top of the downcomer, in the casings of the RCPs and their inlet of one or two loops. There is almost no nitrogen gas in the SGs. Compared to same cases calculated without nitrogen gas, the initiation of the LPIS is delayed from 1 – 1.75 h and the liquid flow rate in the core is divided by a factor of from 2 to 3.

At the moment of the actuation of the LPIS or in the late phase of the transient (for the 1-% break calculated with τ = 1 s), a sub-cooled regime was restored in the core in every case studied.

6 Conclusion

The study presented here is a result of the collaboration between CEA Grenoble, VTT, and LUT, particularly the investigation concerning the degassing of an NC gas dissolved in the primary coolant of an NPP (VVER-440).

Two effects of the presence of a NC gas in the primary circuit of a nuclear power plant (VVER-440 geometry) were examined.

Firstly, the impact of air on the steam condensation in the tubes of the steam generator were calculated for the first time in a horizontal geometry using the CATHARE2 V1.5a (Rev 6) code.

The initial and boundary conditions of the geometry parameters were derived from a preliminary experiment carried out on the Integral Effects Test PACTEL facility with air as the NC gas. A volume of air equivalent to the volume of the primary side of the SG was injected in the entrance of the hot collector at atmospheric pressure. The calculation shows that the air leaves the hot collector and stagnates in the second half-length of the primary tubes along the whole height of the tube bundle. The hot collector remains full of steam throughout the injection of the air, whereas the air fills the cold collector. The air is also present in the cold leg, mostly in the vertical parts (below the cold collector, at the inlet and outlet of the pump).

Future experiments performed on PACTEL with NC gas would provide a more reliable basis of data for the assessment of the CATHARE condensation models in horizontal tubes.

Secondly, the degassing of NC gas dissolved in the primary coolant of an NPP (VVER-440) was studied extensively using a model developed originally by CEA Grenoble.

The following results were obtained from this study:

- A model for the dissolution-release of a NC gas (nitrogen) was implemented in the thermal-hydraulic code, CATHARE2 V1.3L.

- An analytical experiment into the release of nitrogen gas at a high pressure was performed using some components of the PACTEL facility. The data reduction of the results provided estimations of
  - the release time constant of the nitrogen gas, 50 s, and
  - the bubble diameter of the nitrogen gas, 10^{-4} m.

- The postulated small and intermediate breaks LOCA in Loviisa NPP were calculated in such a way that the degassing of the nitrogen gas dissolved in the water of the accumulators was taken into account. The CATHARE2 V1.3L code, which included the dissolution-release model was used with the values of the release time constant ranging from 1 to 100 s.

- Not surprisingly, the amount of nitrogen gas trapped in the primary circuit increases when the break size decreases and the release time constant decreases.
- A significant proportion of this nitrogen gas accumulates in the steam generators in the case of small breaks but not in the case of intermediate breaks.
- The LPIS set point is reached in all the studied cases, except when the amount of nitrogen gas is the largest (SBLOCA and release time constant equal to 1 s); in the latter case, the primary pressure stabilizes 0.4 MPa above the LPIS set point (0.75 MPa).
- The primary circuit refills at the actuation of the LPIS.
- In all the considered cases, the total amount of nitrogen gas initially dissolved in the accumulators is released from the water when the pressure stabilizes or when the LPIS starts.

Interesting would be the validation of the CATHARE code by comparison with results obtained for such transients performed on the IET facility PACTEL without and with dissolved nitrogen gas in the water of the accumulators.

Applicability of the above obtained results to the actual safety conditions must necessarily take into account the real operating procedures in the nuclear power plant. Moreover, complete analysis must include a larger panel of transients, the already mentioned SGTR being among the first to be explored.

- A complete approach to the degassing problem of an NC gas, which would be handled using thermal-hydraulic codes, would include, besides the existing standard set of physical laws validated for steam bubbles, an additional set of physical laws specific to the characteristics of the NC gas bubbles. In the present state of the thermal-hydraulic codes, inserting such codes would be extremely difficult. This is the reason why such a model cannot be introduced in the standard versions before the above-mentioned problem is solved.

References

Alt, S., Fjodorov, A., Lischke, W., Steam condensation processes in horizontal tubes with presence of noncondensing gases. Proceedings of 5th International Conference on Nuclear Engineering, May 26-30, 1997, Nice, France, ICONE5-2435.

Aumiller, D., L., The implementation of non-condensable mass equations including a dissolved gas source term in WCOBRA/TRAC. Ph. D. Thesis, Pennsylvania State University, USA, May 1997.

Barré, F., Bestion, D., Validation of the CATHARE system code for nuclear reactor thermalhydraulics. ASME & JSME Fluid Engineering Conference, August 13-18, 1995, Hilton Head, South Carolina, USA.

Bestion, D., Physical Closure laws in CATHARE code (Rev 4), SETh/LEML-EM/89-161, CEA-Grenoble, 1989.

Bestion D., General description of CATHARE2 V1.3, V1.3E,V1.3U. CEA Report, STR/LML/EM/94-265, CEA-Grenoble, 1994.

Bestion, D., Coste, P., Barsotti, S., Study of condensation modeling in the CATHARE code with and without non condensible gas. Conference on New Trends in Nuclear System Thermohydraulics, Pisa, 30 May-2 June, 1994.

Bryce, W., First CATHARE2 version 1-4 Calculation of BETHSY test 6.9D. SMTH/LMDS/EM/99-006, CEA-Grenoble, 1999.

Chataing, T, Clement, P, Excoffon, J., Geffraye, G., A general correlation for steam condensation in case of wavy laminar flow along vertical tubes. Proceedings of 9th International Topical Meeting on Nuclear Reactor Thermal-Hydraulics (NURETH-9), San Francisco, California, October 3-8, 1999.

Chen, S. L., Gerner, F. M., Tien C. L., General Film Condensation Correlations. Int. Comm. Heat & Mass Transfer, vol. 20, pp. 265-277, 1993.

Cohen, P., 1980. Water coolant technology of power reactors. ANS.

Colburn, A. P., Hougen, O. A, Design of cooler condensers for mixtures of vapors with noncondensing gases. Industrial and Engineering Chemistry, 26, 1934, pp. 1178-1182.

Coste, P., Bestion, D., A simple modelling of mass diffusion effects on condensation with noncondensable gases for the CATHARE code. Proceedings of 7th International Meeting on Nuclear Reactor Thermal-Hydraulics (NURETH-7), September 10-15, 1995, Saratoga Springs, New York, USA.

Dehbi, A., A., Golay, M., W., Kazimi, M., S., The effects of noncondensable gases on the steam condensation under turbulent natural convection conditions. Report No. MIT-ANP-TR-004, June, 1990.

Dor, I., 1994. Cathare 2 V1.3. Description of the volume module Volume M2. STR/LML/EM/94-248, CEA-Grenoble.

Dreier, J., Aksan, N., Aubert, C., Fischer, O., Lomperski, S.,Huggenberger, M., Strassberger, H-J. Faluomi, V., Yadigaroglu, G., PANDA test results and code assessment for investigations of passive decay heat removal from the core of a BWR. Proceedings of ICONE 6463, 6th International Conference on Nuclear Engineering, May 10-15, 1998.

Farvacque, M., Sarrette, C., CATHARE2 V1.3, User manual, STR/LML/EM/91-61. CEA-Grenoble, 1991.

Farvacque, M., Sarrette, C., CATHARE2 V1.3E, Dictionary of operators and directives. STR/LML/EM/92-124, CEA-Grenoble, 1992.

FISA-99. Conference on EU Research in Reactor Safety. EC Luxembourg 29 November-1 December 1999, proceedings EUR 19532 EN.

Geffraye, G., Bestion, D., Kalitvianski, V., Chataing. T., Film condensation modelling in presence of non condensable gases. 40th European Two-Phase Flow Group meeting, KTH, Stockholm, June 10-13, 2002.

Haapalehto, T., 1995. Analysis of natural circulation in VVER-440 geometry with CATHARE2 V1.3U. Radiation and Nuclear Safety Authority, Helsinki, STUK-YTO-TR 89.

Hassan, Y, A; Banerjee, S, Implementation of a non-condensable model in RELAP5/MOD3. Nuclear-Engineering-and-Design. vol.162, no.2-3; p.281-300, 1996.

Hein, D., Rippel R., Weiss P., The distribution of gas in a U-tube heat exchanger and its influence on the condensation process. Proceedings of 7th International Heat Transfer Conference, Munich, West Germany, 1982.

Hicken, E. F., Verfondern, K., 'Investigation of the effectiveness of innovative passive safety systems for boiling water reactors', European BWR R&D Cluster for Innovative Passive Safety Systems – Final Report. Schriften des Forschungszentrums Jülich Reihe Energietechnik/Energy Technology, 11, ISSN 1433-5522, 2000.

Hyvärinen, J., Thermal-hydraulic safety impact of horizontal steam generators. Proceedings of Int. Seminar on Horizontal Steam Generator Modelling. Lappeenranta, March 11-14th, Finland, Research Papers 18, Vol 2, pp.327-340, 1991.

Hyvärinen, J., On the fundamentals of nuclear reactor safety assessment, Doctoral dissertation, Lappeenranta University of Technology, Finland, STUK-A 135, STUK, 1996.

Hänninen, M., Ylijoki, J., One-dimensional two-fluid model of APROS. HOHTI-2/92, Technical Research Centre of Finland, Nuclear Engineering Laboratory, 1992.

Ishii, M., Zuber, N., Drag coefficient and relative velocity in bubbly, droplet or particulate flows. AIChE Jul, Vol 25, No. 2, p 843, 1979.

Janicot, A., Qualification report Cathare Version 1.3 revision 5, COSI experiment. Volume Q11. STR/LML/EM/93-152, CEA-Grenoble, 1993.

Kadri, D., Etudes des propositions de W. Bryce pour l'amélioration du comportement physico-numérique de la version V1.4 - Introduction V1.5. SMTH/LMDS/EM/99-005, CEA-Grenoble, 1999.

Kang, S., W., Griffith, P., Pool heat transfer in a simulated PWR pressurizer. Trans. Am. Nuc. Soc., vol 46, p.845-847, 1984.

Karppinen, I., Tuomainen, M., Riikonen, V., Tuunanen, J., Kosonen, M. Cheung, Y. K., Analyses of the ESBWR passive containment cooling system (PCCS) performance with the APROS AND FLUENT CODES. Proceedings of ICONE 8, 8th International Conference on Nuclear Engineering, April 2-6, 2000, Baltimore, MD USA.

Korteniemi, V., Virtanen, E., Haapalehto, T., Kouhia, J., Analyses of the PACTEL loss of feed water experiments. Proceedings of 3rd International Seminar on Horizontal Steam Generator Modelling, October 18-20, 1994, Research Papers 43, p. 89-96, Lappeenranta, Finland.

Lischke, W., Fjodorow, A., Modellierung der Wärmeübergangsvorgänge bei der Dampfkondensation im Heizrohre liegender Dampferzeuger von WWER-Anlagen unter Störfallbedingungen. Jahrestagung Kerntechnik'96, Mannheim, 21-23 Mai 1996, Proceedings s.151-154.

Micaëlli, J.C., Barré, F., Bestion, D., CATHARE code development and assessment methodologies. Trans. of the ANS, Winter Meeting San Francisco, Oct. 29th- Nov. 2th, 1995, Vol. 73, pp. 509-510.

Nagasaka, H., Yamada, K., Katoh, M., Yokobori, S., Heat removal tests of isolation condenser applied as a passive containment cooling system, Proceedings of ICONE, International Conference on Nuclear Engineering, November 4-7, 1991 Vol. 1.

Narumo, T., Rajamäki, M., Dividing phases in two-phase flow and modeling of interfacial drag. OEDC/CSNI Workshop on Transient Thermal-Hydraulic and Neutronic Codes requirements, Annapolis, Md, USA, November 5-8, 1996.

Noel, B., Deruaz, R., Reflux condenser mode with non-condensible gas: assessment of CATHARE against BETHSY Test 7.2C. Nuclear Engineering and Design 149, pp. 291-298, 1994.

Noel, B., Dumont, D., Effect of non-condensible gas on steam generator condensation heat transfer: BETHSY Test 10.2. Proceedings of 5th International Conference on Nuclear Engineering, May 26-30, 1997, Nice, France, ICONE5-2536.

Noel, B., Dumont, D., Reflux condensation with non-condensible gas in SG U-tubes assessment of CATHARE against BETHSY experiment. Proceedings of 5th CATHARE International Seminar, Grenoble, France, December 3-5, 1997.

Perneczky, L., Ezsoel, G., Guba, A., Szabados, L., 15 years of The Hungarian integral type test facility: horizontal SG related PMK-2 experiments. Proceedings of 5th International Seminar on Horizontal Steam Generators, 20–22 March, 2001, Acta Universitatis Lappeenrantaensis 110, Lappeenranta, Finland.

Peterson, P., F., Schrock, V., E., Kageyama, T., Diffusion layer theory for turbulent vapor condensation with noncondensable gases. J. Heat Transfer, vol. 115, p. 998-1003, 1993.

Pilon, L., Geffraye, G., Chataing, T., Validation of the CATHARE film condensation model on COTURNE experiment. Proceedings of ICONE 6, 6th International Conference on Nuclear Engineering, May 10-14, 1998.

Pray, H. A., Shweickert, C. E. Minnich, B. H., Solubility of hydrogen, oxygen, nitrogen and helium in water at elevated temperatures. Industrial and Engineering Chemistry, Vol. 44, No. 5, pp. 1146-1151, 1952.

Purhonen, H., Kouhia, J., Holmström H., 1994, OECD/NEA/CSNI International Standard Problem No. 33 (ISP33), PACTEL natural circulation stepwise coolant inventory reduction experiment. Committee on the Safety of Nuclear Installations, OECD Nuclear Energy Agency, Comparison Report, Volume I, NEA/CSNI/R(94)24 Part I.

Purhonen, H., Kouhia, J., Kalli, H., ISP33 standard problem on the PACTEL facility. Proceedings of 7th International Topical Meeting on Nuclear Reactor Thermal-Hydraulics (NURETH-7), September 10-15, 1995, Saratoga Springs, USA.

Purhonen, H., Puustinen, M., Integral System and Horizontal Steam Generator Behavior in Noncondensable Gas Experiments with the PACTEL Facility, Fifth International Seminar on Horizontal Steam Generators, 20–22 March, 2001, Acta Universitatis Lappeenrantaensis 110, Lappeenranta, Finland.

RELAP5/MOD3 Code Manual, Vols. 1-6. Idaho National Engineering Laboratory Report, INEL-95/0174, US Nuclear Regulatory Commission Report, NUREG/CR-5535, 1995.

RELAP5/MOD3.3 Code Manual, Vol 4, December 2001.

Sarrette, C., Analysis of noncondensable effect during small break transient in VVER-440 geometry with CATHARE V1.3L, Preliminary results. Lappeenranta University of Technology, Department of Energy Technology. A Research Report 35, Lappeenranta, Finland, 1996.

Sarrette, C., Bestion, D., Analysis of non condensable gas effect during small break transient in VVER-440 geometry with CATHARE2 V1.3L. Proceedings of 8th International Topical Meeting on Nuclear Reactor Thermal-Hydraulics (NURETH-8), September 30-October 4, Kyoto, Japan, 1997.

Sarrette, C., Kouhia, J., Study on the release of dissolved noncondensable gas from water. VTT Energy, Technical Report, TEKOJA 6/98, 1998.

Sarrette, C., Puustinen M., Bestion D., Study of the effect of noncondensable gas on heat transfer phenomena in horizontal steam generator of PACTEL facility with CATHARE2 V1.5A. Proceedings of 5th International Seminar on Horizontal Steam Generators, 20-22 March, 2001, Acta Universitatis Lappeenrantaensis 110, Lappeenranta, Finland.

Sarrette, C., Bestion, D., Study of release of nitrogen gas dissolved in water during depressurisation - application to primary circuit of PWR, Nuclear Engineering and Design, to be published.

Schaffrath, A., Experimentelle und analytische Untersuchungen zur Wirksamkeit des Not-kondensators des SWR600, Final Report BMBF 15 NU 09485 Berechnung des passiven Notkondensators eines mit Naturumlauf arbeitenden, innovativen Siede-Wasserreaktors (SWR600) mit ATHLET, RUB ISR-01. University of Bochum (Germany), 1997.

Schaffrath, A., Dumaz, D., Post-test calculations of NOKO emergency condenser experiments. Proceedings of ICONE6, 6th International Conference on Nuclear Engineering, May 10-14, 1998.

Schaffrath, A., Krüssenberg, A. -K., Fjodorow, A., Gocht, U., Lischke, W., Modeling of condensation in horizontal tubes. Nuclear Engineering and Design 204 (2001) 251-265.

Shah, M. M., A general correlation for heat transfer during film condensation inside pipes. International Journal of Heat and Mass Transfer, vol. 22, pp. 547-556, 1979.

Schoen, B., Umminger, K., Heat transfer regimes in steam generators in presence of nitrogen during plant cooldown – experimental investigations in the PKL III test facility. Proceedings of 2nd International Symposium on Two-Phase Flow Modelling and Experimentation in Pisa, (Italy), May 23-25, 1999.

Serre, G., Qualification Report CATHARE 2 1.5 Qr6 on MIT NAGASAKA, COSI for Condensation with Non Condensable Gas. SMTH/LMDS/EM/98-002, CEA-Grenoble, 1998.

Serre, G., Bestion, D., 1999. Physical laws of CATHARE Revision 6. Pipe module. CEA Report, SMTH/LMDS/EM/98-038, Grenoble.

Siddique, M., Golay, M.W., Kazimi, M.S., 1992, The effects of noncondensible gases on steam condensation under forced convection conditions, Massachussetts Institute of Technology.

Sorjonen, J., Sarrette, C., Kalli, H., Bestion, D., D'Auria, F., Comparison of condensation correlations in CATHARE code for modelling isolation condenser experiment. Proceedings of ICONE5, 5th International Conference on Nuclear Engineering, Nice, France, May 26-30, 1997.

Teschendorff, V., Miro, J., Lerchl, G., ATHLET - ein fortschrittlicher Systemcode zur Analyse thermohydraulischer Prozesse. 12. GRS-Fachgespräch Forschung zur Erhörung der Reactorsicherheit, Köln, 3-4 November, 1988.

Tuunanen, J., Lahti, K., Analysis of Loviisa VVER-440 reactor pump trips with RELAP5/MOD1-Eur, RELAP5/MOD3 and CATHARE Codes. Proceedings of 6th International Topical Meeting on Nuclear Reactor Thermal-Hydraulics (NURETH-6), Grenoble, France, October 5-8, 1993.

Tuunanen, J., Kouhia, J., Purhonen, H., Riikonen, V., Puustinen, M., Semken, S.R., Partanen, H., Saure, I., Pylkkö, H., General description of the PACTEL test facility. VTT Research Notes 1929, Espoo, 1998.

Vanttola, T., 2000, Finnus national research programme on nuclear safety. Proceedings of 3rd Finnish-French colloquium on nuclear power plant safety, June 27–28, 2000, Acta Universitatis. Lappeenrantaensis. 100, Lappeenranta, Finland.
http://www.vtt.fi/ene/tutkimus/finnus/index.html

Vierow, K., M., Schrock, V., E., Condensation heat transfer in natural circulation with noncondensable gas. Report for General Electric Energy UCB-NE 4170, Department of Nuclear Engineering, University of California at Berkeley, May 1990.

Vierow, K., M., Schrock, V., E., Condensation in a natural circulation loop with noncondensable gases Part I - Heat Transfer. Proceeding of The International Conference on Multiphase Flows, '91- Tsukuba, September 24-27, 1991,Tsukuba, Japan.

Vihavainen, J., Coda-Zabetta, E., Tuunanen, J., Analysis of PACTEL experiment GDE-05 with CATHARE2 and RELAP5 codes. Proceedings of POST_Smirt 14 Seminar 'Passive Safety Features in Nuclear Installations', Aug. 25-27, 1997, Pisa, Italy.

Woon-Shing Yeung, W-S., Sundaram, R., Effect of nitrogen release from accumulators on PWR LOCA analysis. Proceedings of ICONE10, 10th International Conference on Nuclear Engineering Arlington, Virginia, USA, April 14-18, 2002.

Appendix A
The cross-section of the SG of PACTEL with the location of the thermocouples

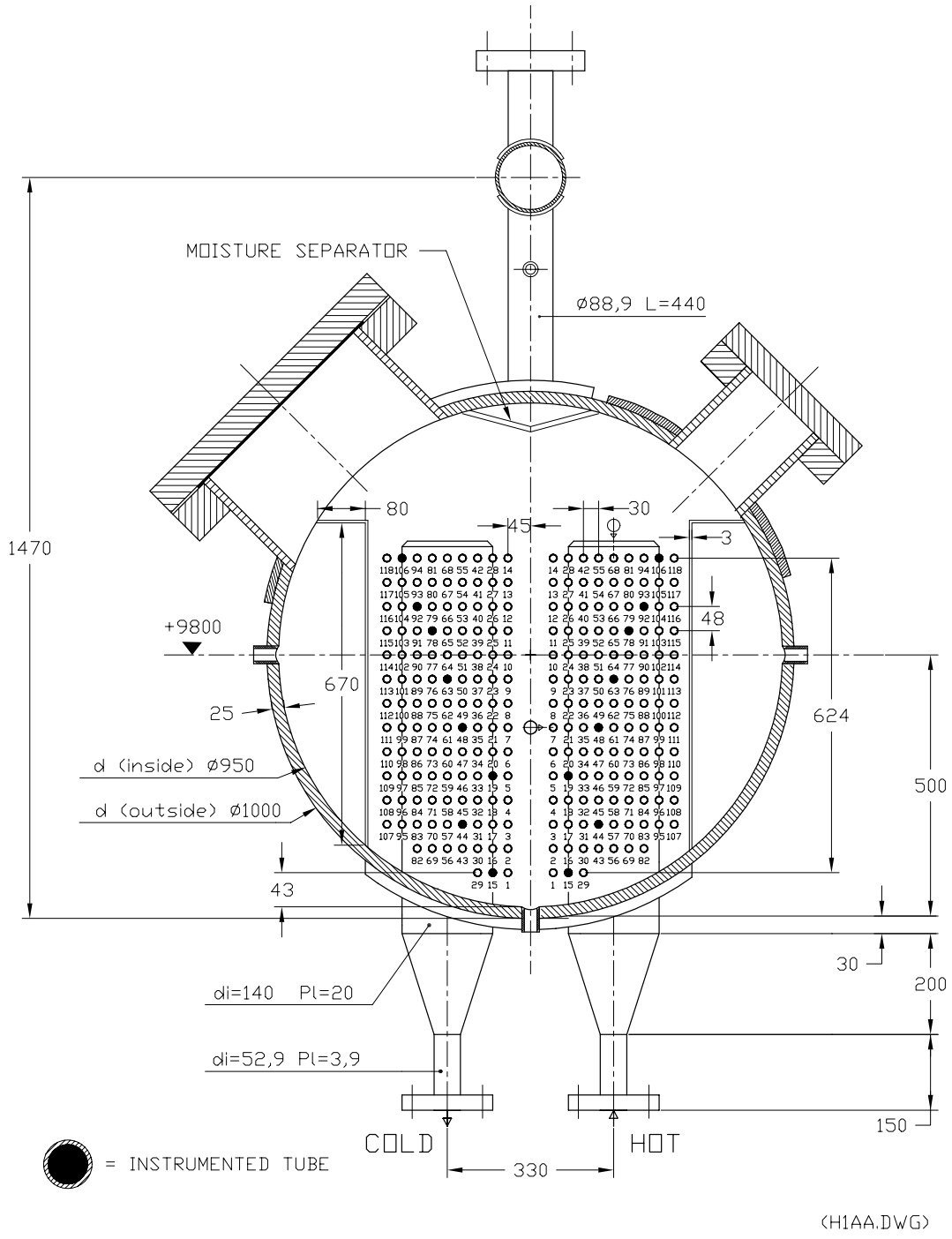

CROSS SECTION OF THE STEAM GENERATOR. LOOP 1.
PA0022_A 18.08.98

Appendix B
Versions used to calculate RUN-1 experiment

Calc N°	τ_{rel}	τ_{dis}	Degassing delay	τ_i
0	1 s	100 s	No	Standard τ_i (Eq. 4.17)
1	50 s	100 s	No	Standard τ_i (Eq. 4.17)
3	50 s	100 s	No	Constant Nb = 10^{10} during depressurization phases Standard τ_i between depressurization phases
3bis	50 s	100 s	No	Constant Nb = 10^{10} during depressurization phases Constant d = 10^{-4} for 787<t<1300
4	50 s	100 s	No	Constant Nb = 10^{10} during depressurization phases Constant d = 10^{-4} for 787<t<820 Constant d = 10^{-4} for 1360<t<1390
8	50 s	100 s	For 2nd depressurization only S_{ai} = 0 when Alfa < 1.6 10^{-3} and Xaleq<Xal<Xaleq+10^{-4}	Constant Nb = 10^{10} during depressurization phases Standard τ_i between depressurization phases

ACTA UNIVERSITATIS LAPPEENRANTAENSIS

105. VARIS, JUHA. A novel procedure for establishing clinching parameters for high strength steel sheet. 2000. 84 s., liitt. Diss.

106. PÄTÄRI, EERO. Essays on portfolio performance measurement. 2000. 201 s. Diss.

107. SANDSTRÖM, JAANA. Cost information in engineering design – potentials and limitations of activity-based costing. 2001. 143 s., liitt. Diss.

108. TOIVANEN, JOUKO. Balanced Scorecardin implementointi ja käytön nykytila Suomessa. 2001. 216 s. Väitösk.

109. PESONEN, MAUNO. Applying AHP and A´WOT to strategic planning and decision making: case studies in forestry and forest industry. 2001. U.s. Diss.

110. Proceedings of Fifth International Seminar on Horizontal Steam Generators. Ed. by Juhani Vihavainen. 2001. 255 s.

111. LAINE, PERTTI. Kohti vesiensuojelun aikaa: veden laadun muutokset eteläisellä Saimaalla. 2001. 264 s. Väitösk.

112. SILVENTOINEN, PERTTI. Electromagnetic compatibility and EMC-measurements in DC-voltage link converters. 2001. 115 s. Diss.

113. TERVONEN, ANTERO. Laadun kehittäminen suomalaisissa yrityksissä. 2001. 206 s. Väitösk.

114. SALMINEN, ANTTI. The effects of filler wire feed on the efficiency, parameters and tolerances of laser welding. 2001. 82 s., liitt. Diss.

115. HORTTANAINEN, MIKA. Propagation of the ignition front against airflow in packed beds of wood particles. 2001. U.s. Diss.

116. IKONEN, JOUNI. Improving distributed simulation in a workstation environment. 2001. U.s. Diss.

117. WU, HUAPENG. Analysis, design and control of a hydraulically driven parallel robot manipulator. 2001. U.s. Diss.

118. REUNANEN, ARTTU. Experimental and numerical analysis of different volutes in a centrifugal compressor. 2001. 150 s. Diss.

119. TAAVITSAINEN, VELI-MATTI. Strategies for combining soft and hard modelling in some physicochemical problems. 2001. U.s. Diss.

120. SAVOLAINEN, RAIJA. The use of branched ketene dimers in solving the deposit problems related to the internal sizing of uncoated fine paper. 2001. U.s. Diss.

121. SARAVIRTA, ALI. Project success through effective decisions: case studies on project goal setting, success evaluation and managerial decision making. 2001. 286 s. Diss.

122. BLOMQVIST, KIRSIMARJA. Partnering in the dynamic environment: the role of trust in asymmetric technology partnership formation. 2002. 296 s., liitt. Diss.

123. KARVONEN, VESA. Development of fiber recovery process. 2002. U.s. Diss.

124. KÄYHKÖ, JARI. The influence of process conditions on the deresination efficiency in mechanical pulp washing. 2002. 87 s., liitt. Diss.

125. SAVOLAINEN, PEKKA. Modeling of non-isothermal vapor membrane separation with thermodynamic models and generalized mass transfer equations. 2002. 179 s. Diss.

126. KÄRKKÄINEN, HANNU. Customer need assessment: Challenges and tools for product innovation in business-to-business organizations. 2002. U. s. Diss.

127. HÄMÄLÄINEN, MARKKU. Spray coating technique as a surface treatment for woodcontaining paper grades. 2002. 121 s. Diss.

128. RANTA, TAPIO. Logging residues from regeneration fellings for biofuel production – a GIS-based availability and supply cost analysis. 2002. 182 s. Diss.

129. KUOSA, MAUNU. Numerical and experimental modelling of gas flow and heat transfer in the air gap of an electric machine. 2002. 97 s. Diss.

130. LAITINEN, NIINA. Development of a ceramic membrane filtration equipment and its applicability for different wastewaters. 2002. U. s. Diss.

131. SUNDQVIST, SANNA. Market orientation in the international context: Antecedents, consequences and applicability. 2002. U. s. Diss.

132. TORKKELI, MARKO. Technology selection and group decision support systems: Case studies on supporting strategic technology selection processes. 2002. U.s. Diss.

133. KYRKI, VILLE. Local and global feature extraction for invariant object recognition. 2002. 115 s. Diss.

134. HEIKKILÄ, TANJA. Permanent magnet synchronous motor for industrial inverter applications – analysis and design. 2002. 109 s. Diss.

135. HUTTUNEN, PENTTI. Data-parallel computation in parallel and distributed environments. 2002. U.s. Diss.

136. LIU, YONG. On sliding mode control of hydraulic servo systems and a manipulator. 2002. U.s. Diss.

137. JUHANTILA, OLLI-PEKKA. Establishing intercompany relationships: Motives and methods for successful collaborative engagement. 2002. 281 s. Diss.

138. PREIS, SERGEI. Practical applications of a systematic approach to the chemical abatement of pollutants in water and air. 2002. 234 s. Diss.

139. TIIHONEN, JARI. Influence of stationary phase and eluent properties on chromatographic separation of carbohydrates. 2002. U. s. Diss.

140. KILKKI, JUHA. Automated formulation of optimisation models for steel beam structures. 2002. 85 s., liitt. Diss.

141. LENSU, LASSE. Photoelectric properties of bacteriorhodopsin films for photosensing and information processing. 2002. 114 s. Diss.

142. KAURANNE, TUOMO. Introducing parallel computers into operational weather forecasting. 2002. U.s. Diss.

143. PUUMALAINEN, KAISU. Global diffusion of innovations in telecommunications: Effects of data aggregation and market environment. 2002. 153 s. Diss.

145. SAARENKETO, SAMI. Born globals – internationalization of small and medium-sized knowledge-intensive firms. 2002. 247 s. Diss.

146. IKONEN, KIRSI. Metal surface and subsurface inspection using nondestructive optical methods. U.s. Diss.